The Astrophysical Journal, 653:1145–1171, 2006 December 20

GALACTIC CHEMICAL EVOLUTION: CARBON THROUGH ZINC

Chiaki Kobayashi,[1] Hideyuki Umeda,[2] Ken'ichi Nomoto,[2] Nozomu Tominaga,[2] and Takuya Ohkubo[2]

Received 2005 September 13; accepted 2006 August 30

ABSTRACT

We calculate the evolution of heavy-element abundances from C to Zn in the solar neighborhood, adopting our new nucleosynthesis yields. Our yields are calculated for wide ranges of metallicity ($Z = 0$–$Z_\odot$) and the explosion energy (normal supernovae and hypernovae), based on the light-curve and spectra fitting of individual supernovae. The elemental abundance ratios are in good agreement with observations. Among the α-elements, O, Mg, Si, S, and Ca show a plateau at $[\mathrm{Fe/H}] \lesssim -1$, while Ti is underabundant overall. The observed abundance of Zn ($[\mathrm{Zn/Fe}] \sim 0$) can be explained only by the high-energy explosion models, as it requires a large contribution of hypernovae. The observed decrease in the odd-Z elements (Na, Al, and Cu) toward low [Fe/H] is reproduced by the metallicity effect on nucleosynthesis. The iron-peak elements (Cr, Mn, Co, and Ni) are consistent with the observed mean values at $-2.5 \lesssim [\mathrm{Fe/H}] \lesssim -1$, and the observed trend at the lower metallicity can be explained by the energy effect. We also show the abundance ratios and the metallicity distribution functions of the Galactic bulge, halo, and thick disk. Our results suggest that the formation timescale of the thick disk is ~1–3 Gyr.

Subject headings: galaxies: abundances — galaxies: evolution — supernovae: general

Online material: machine-readable tables, color figures

1. INTRODUCTION

Elemental abundance ratios are the treasure house of information on star formation and galaxy formation because different types of supernovae produce different heavy elements with different timescales (e.g., Tinsley 1980; Pagel 1997; Matteucci 2001). High-resolution spectroscopy gives the elemental abundance patterns of individual stars in our Galaxy and nearby dwarf spheroidal galaxies, and of high-redshift quasar absorption line systems. These observations have shown different abundance patterns, which suggest different chemical enrichment histories of these objects and probably different initial mass functions (IMFs) depending on environment. The reionization of the universe at a very early epoch as suggested by the *Wilkinson Microwave Anisotropy Probe* (*WMAP*) result may require a different population for the first stars (e.g., Ciardi et al. 2003). However, to discuss these issues, nucleosynthesis yields have involved too many inconsistencies with recent observations.

There exist two distinct types of supernova explosions (e.g., Arnett 1996; Filippenko 1997). One is Type II supernovae (SNe II), which are the core-collapse–induced explosions of massive stars ($\gtrsim 8\ M_\odot$) with short lifetimes of 10^6–10^7 yr and produce more α-elements (O, Mg, Si, S, Ca, and Ti) relative to Fe with respect to the solar ratios (i.e., $[\alpha/\mathrm{Fe}] > 0$). The other is Type Ia supernovae (SNe Ia), which are the thermonuclear explosions of accreting white dwarfs (WDs) in close binaries and produce mostly Fe and little α-elements (e.g., Nomoto et al. 1994). Although the lifetime of SNe Ia has been estimated to be the order of billions of years from the chemical evolution of our Galaxy (e.g., Yoshii et al. 1996), the simulations of the SN Ia progenitor systems predict that the lifetime of the majority of SNe Ia is shorter than this (Hachisu et al. 1996; Kobayashi et al. 1998, hereafter K98). The metallicity effect of SNe Ia that is also predicted by the simulations can solve this problem (K98).

Following the development of observations of individual supernovae and elemental abundances, theory of stellar nucleosynthesis has been improved from Woosley & Weaver (1995) and Nomoto et al. (1997a, hereafter N97). From the light-curve and spectral fitting of individual supernovae, the mass of progenitor stars M, explosion energy E, and produced ^{56}Ni mass (which decayed to ^{56}Fe) have been obtained (e.g., Nomoto et al. 2004 for a review). There exist two distinct types of core-collapse supernovae. One is normal SNe II (including Ib and Ic), which have the explosion energy of $E_{51} \equiv E/10^{51}$ ergs ~ 1 and produce little iron relative to α-elements. Some SNe II with $M > 25\ M_\odot$ may have smaller energy ($E_{51} < 1$), which are called "faint SNe" (Turatto et al. 1998). The other is hypernovae (HNe), which have more than 10 times larger explosion energy ($E_{51} \gtrsim 10$) and produce a certain amount of iron. HNe may be related to gamma-ray bursts (Galama et al. 1998; Iwamoto et al. 1998).

Umeda & Nomoto (2002, 2005, hereafter UN05) updated the progenitor star models with a metallicity range of $Z = 0$–0.02 (see also Limongi & Chieffi 2003), and calculated the explosive nucleosynthesis yields for larger energies ($E_{51} > 1$). To meet the observed abundance patterns for extremely metal-poor (EMP) stars (Cayrel et al. 2004; Aoki et al. 2004; Beers & Christlieb 2005), they introduced the mixing and fallback mechanism. They then succeed in reproducing the observed abundance patterns of some EMP stars (Umeda & Nomoto 2003, hereafter UN03; UN05), based on the idea that the interstellar medium is not mixed and the EMP stars are enriched only by a single supernova (Audouse & Silk 1995). The trends of iron-peak element abundance patterns for the EMP stars (McWilliam et al. 1995; Ryan et al. 1996) have been explained by changing a parameter mass cut (Nakamura et al. 1999), while they were explained with the energy dependence: [(Zn, Co)/Fe] increases and [(Mn, Cr)/Fe] decreases for metal-poor stars because of higher energy and a larger amount of swept hydrogen mass (UN05).

In this paper, however, we focus on typical yields of core-collapse supernovae that are responsible for the plateau values of the $[\alpha/\mathrm{Fe}]$-[Fe/H] relations, which is important when we discuss the galaxy formation and evolution. Physical parameters in our

[1] Division of Theoretical Astronomy, National Astronomical Observatory of Japan, Mitaka-shi, Tokyo 181-8588, Japan; chiaki@th.nao.ac.jp.

[2] Department of Astronomy, School of Science, University of Tokyo, Bunkyo-ku, Tokyo 113-0033, Japan.

model are constrained from observations, i.e., the light curve and spectra of individual supernovae and the abundance patterns of metal-poor stars in the solar neighborhood. There may be a scatter in the observed mass-energy relation and [α/Fe]-[Fe/H] relations that arise from inhomogeneity of the explosion and of the mixing of the interstellar medium. However, at $-2.5 \lesssim$ [Fe/H] $\lesssim -1$, chemical enrichment of the interstellar medium proceed from many supernova explosions, and the average contribution of supernovae with different mass is imprinted in the [X/Fe]-[Fe/H] diagrams. First, we give a table set of nucleosynthesis yields both for SNe II and HNe as functions of progenitor mass and metallicity (§ 2). We then show the evolution of elemental abundance ratios from carbon to zinc in the solar neighborhood using a one-zone chemical evolution model (§ 3). In § 4 we construct models for the bulge, halo, and thick disk of the Milky Way Galaxy to meet their metallicity distribution functions, and show the age-metallicity relations. Showing the different evolution of elemental abundance ratios, we extend our discussion to the formation of the thick disk. Section 5 gives our conclusions.

2. NUCLEOSYNTHESIS YIELDS

2.1. *Nucleosynthesis Models*

Using the same calculation method as in Umeda & Nomoto (2002, 2005), we calculate stellar evolution, explosions, and nucleosynthesis for a wider ranges of metallicity and energy. The details of the calculations are described in Umeda et al. (2000) and Tominaga et al. (2006). The code is based on the Henyey-type stellar evolution code by Nomoto & Hashimoto (1988) and Umeda et al. (1999). We start calculations from the zero-age main sequence through core collapse including metallicity-dependent mass loss (de Jager et al. 1988; Kudritzki et al. 1989). This code runs a nuclear reaction network by Hix & Thielemann (1996) for nuclear energy generation and nucleosynthesis, including the neutron-capture processes. We adopt the Schwarzschild criterion for convective stability and diffusive convective mixing by Spruit (1992). In this work, a case for relatively fast mixing, $f_k = 0.3$, is adopted. The $^{12}C(\alpha,\gamma)^{16}O$ reaction rate, which is still uncertain (Fowler 1984), is chosen to be 1.3 times the value given in Caughlan & Fowler (1988).

For a given progenitor model, if the explosion mechanism is specified (or the procedure for the artificial explosion, as in Woosley & Weaver [1995] and Limongi & Chieffi [2003]), the remnant mass is uniquely determined as a function of the explosion energy. However, we do not specify the explosion mechanism and treat the mixing and fallback with free-parameters, especially because the precise explosion mechanism is unknown for hypernovae. Since we explode the progenitor model when the central density of 3×10^{10} g cm^{-3} is reached without calculating further collapse and bounce, our approach may be regarded as simulating a prompt explosion.

According to the constraint from the light-curve and spectral fitting (§ 1), we set two sequences of mass-energy relation; (1) $E_{51} = 1$ for all normal SNe II, and (2) $E_{51} = 10$, 10, 20, and 30 for the 20, 25, 30, and 40 $M_\odot$ HNe, respectively.

Using the presupernova models, we carry out one-dimensional hydrodynamical simulations of core-collapse explosions using the piecewise parabolic method (Colella & Woodward 1984) with the α-nuclear reaction network for the energy generation rate. Then, explosive nucleosynthesis is calculated as a postprocessing, using a larger reaction network of 300 isotopes. After the postprocess nucleosynthesis calculations, we obtain the final yields setting the mass cut for SNe II. The mass cuts are chosen to eject $M(\mathrm{Fe}) \simeq 0.07\ M_\odot$, which is constrained from the light curve and spectra of individual supernovae (e.g., Nomoto et al. 2004). For HNe we take account of the mixing-fallback mechanism. The Rayleigh-Taylor mixing and the amount of fallback both depend on, e.g., the stellar mass, presupernova density structure, explosion energy, and asphericity, so that its determination requires extremely high-resolution calculations. We thus determine the parameters involved in the mixing and fallback (UN05) to give [O/Fe] $\simeq 0.5$ according to the constraint from the abundance ratios of EMP stars (see §3.2).

The neutrino process is not included in our nucleosynthesis, but the number of electrons per nucleon, Y_e, depends on the neutrino process during the explosion (e.g., Liebendörfer et al. 2003; Janka et al. 2003). Therefore, Y_e in the incomplete Si-burning region is set to be 0.4997, independent of metallicity, while Y_e in the other region is kept constant, as in the presupernova model, where $Y_e \sim 0.5$ above the oxygen layer and decreases gradually toward the Fe core (UN05). The initial mass cut is determined to be located at the bottom of the $Y_e \simeq 0.5$ layer (Tominaga et al. 2006).

Tables 1 and 2 give the resulting nucleosynthesis yields in the ejecta in solar masses after radioactive decays, for SNe II and HNe as functions of the progenitor mass ($M = 13$, 15, 18, 20, 25, 30, and 40 $M_\odot$) and metallicity ($Z = 0$, 0.001, 0.004, and 0.02). The mass of the presupernova star, M_{final}, is larger for lower metallicity because of the metal-dependent stellar winds. The material inside the mass cut M_{cut} falls onto the remnant, and the rest ($M_{\mathrm{ejecta}} = M_{\mathrm{final}} - M_{\mathrm{cut}}$) is ejected by the supernova explosion.

Figures 1–4 show the abundance ratios relative to the solar abundance (Anders & Grevesse 1989) in the ejecta as a function of the progenitor mass for given metallicity. The solid and dashed lines show the SN II and HN yields, respectively. The yield masses of α-elements (O, Ne, Mg, Si, S, Ar, Ca, and Ti) are larger for more massive stars because of the larger mantle mass. Since the ejected Fe mass is $\simeq$0.07 $M_\odot$ for SNe II, being almost independent of the progenitors mass, the abundance ratio [α/Fe] is larger for more massive stars. This mass dependence of [α/Fe] is smaller in the present yields than in N97, because N97 adopted a larger ejected Fe mass (0.15 $M_\odot$ for 13–15 $M_\odot$) from the supernova observations around the early 1980s, while the present study adopt the smaller Fe mass from the modeling of the recent well-observed supernova light curves. For HNe, although the Fe mass is larger for more massive stars because of the higher energy, the mass of α-elements is also larger, and thus [α/Fe] is almost constant independent of the stellar mass.

In the present yields, the abundance ratios of iron-peak elements (Cr, Mn, Co, and Ni) are almost constant with respect to the progenitor mass. The differences from N97 are due to the new implementation of the mixing-fallback. Zn and Cu yields are much larger than N97. This is because the neutron-capture processes enhance the neutron-rich Zn and Cu abundances for $Z \geq 0.004$. For smaller Z the larger Zn production is due to the larger energy and larger electron fraction Y_e in the present explosion models. It might be possible to reduce Zn production for high- or low-mass stars and explain the observed [Zn/Fe] trend by mass sequence, but then the average Zn abundance would be much smaller than observed. The smaller [Mn/Fe] is also due to large $Y_e \sim 0.5$.

2.2. *IMF-Weighted Yields*

The mass-energy relation has been obtained from the light-curve and spectral fitting for individual supernovae. However, there is currently no constraint on the energy distribution function because of the poor statistics. Therefore, in the chemical evolution model, we should introduce one important parameter to describe the fraction of hypernovae, ϵ_{HN}, which may depend

TABLE 1

NUCLEOSYNTHESIS YIELDS FOR THE TYPE II SUPERNOVAE IN THE EJECTA

ELEMENT	YIELDS (in $M_\odot$) FOR M =						
	13	15	18	20	25	30	40
				$Z = 0$			
$M_{\rm final}$	13.00	15.00	18.00	20.00	25.00	30.00	40.00
$M_{\rm cut}$	1.57	1.48	1.65	1.66	1.92	2.07	2.89
p	6.60E+00	7.58E+00	8.43E+00	8.77E+00	1.06E+01	1.17E+01	1.40E+01
D	1.49E−16	1.69E−16	1.28E−16	8.66E−17	2.02E−16	1.34E−16	3.46E−16
^{3}He	4.12E−05	4.09E−05	3.33E−05	4.76E−05	2.11E−04	2.06E−04	2.57E−05
^{4}He	4.01E+00	4.40E+00	5.42E+00	5.94E+00	8.03E+00	9.52E+00	1.19E+01
^{6}Li	3.65E−23	1.11E−22	4.37E−23	3.65E−21	2.69E−21	1.13E−22	7.54E−22
^{7}Li	2.18E−10	2.94E−10	7.34E−11	2.79E−10	5.68E−09	2.36E−08	3.76E−11
^{9}Be	1.77E−20	3.22E−22	1.05E−22	4.49E−23	1.24E−17	1.26E−20	5.33E−20
^{10}B	2.92E−21	8.30E−20	3.92E−21	1.57E−19	2.87E−18	5.18E−20	2.37E−17
^{11}B	2.94E−16	3.30E−16	7.14E−16	6.55E−17	9.46E−16	3.27E−15	3.07E−14
^{12}C	7.41E−02	1.72E−01	2.19E−01	2.11E−01	2.94E−01	3.38E−01	4.29E−01
^{13}C	8.39E−08	6.21E−08	2.63E−09	1.14E−08	1.47E−08	1.02E−08	3.22E−09
^{14}N	1.83E−03	1.86E−03	1.89E−04	5.42E−05	5.91E−04	1.64E−06	5.89E−07
^{15}N	6.39E−08	6.86E−08	2.40E−08	1.13E−08	1.18E−07	1.68E−08	6.29E−07
^{16}O	4.50E−01	7.73E−01	1.38E+00	2.11E+00	2.79E+00	4.81E+00	8.38E+00
^{17}O	1.69E−06	1.57E−06	2.79E−07	6.83E−08	1.49E−06	1.88E−08	1.42E−09
^{18}O	5.79E−08	4.89E−06	4.63E−06	2.53E−08	6.75E−07	2.07E−09	2.13E−07
^{19}F	1.17E−10	1.97E−09	7.91E−09	1.62E−09	1.71E−09	8.94E−10	2.38E−10
^{20}Ne	1.53E−02	3.27E−01	4.94E−01	9.12E−01	5.33E−01	8.51E−01	3.07E−01
^{21}Ne	5.42E−07	3.76E−05	9.12E−05	4.30E−05	1.33E−05	5.51E−05	1.08E−05
^{22}Ne	1.99E−07	1.61E−05	2.57E−05	6.92E−05	2.02E−05	8.57E−05	6.75E−06
^{23}Na	1.44E−04	2.45E−03	2.08E−03	2.90E−03	1.03E−03	1.42E−03	1.84E−04
^{24}Mg	8.62E−02	6.82E−02	1.57E−01	1.50E−01	1.20E−01	2.27E−01	4.78E−01
^{25}Mg	1.56E−04	2.98E−04	5.83E−04	1.16E−04	3.97E−05	2.44E−04	4.28E−04
^{26}Mg	7.17E−05	3.99E−04	8.77E−04	2.38E−04	5.09E−05	1.32E−04	1.26E−04
^{27}Al	3.78E−03	1.37E−03	3.14E−03	1.37E−03	8.08E−04	2.63E−03	1.47E−02
^{28}Si	8.04E−02	7.32E−02	1.16E−01	9.94E−02	3.51E−01	2.48E−01	1.03E+00
^{29}Si	7.50E−04	2.39E−04	4.42E−04	1.82E−04	2.71E−04	5.88E−04	2.60E−03
^{30}Si	1.42E−03	1.49E−04	3.45E−04	1.10E−04	7.54E−05	2.55E−04	4.06E−03
^{31}P	4.88E−04	5.63E−05	1.32E−04	8.01E−05	8.47E−05	1.17E−04	1.60E−03
^{32}S	2.37E−02	3.20E−02	4.07E−02	5.31E−02	1.85E−01	1.16E−01	3.73E−01
^{33}S	8.98E−05	7.55E−05	1.03E−04	1.98E−04	2.74E−04	1.65E−04	8.10E−04
^{34}S	2.79E−04	2.02E−04	2.85E−04	4.90E−04	4.24E−04	8.42E−05	1.59E−03
^{36}S	1.48E−08	1.43E−09	5.34E−09	2.56E−09	3.42E−10	7.04E−10	3.19E−08
^{35}Cl	5.48E−05	1.47E−05	2.64E−05	6.88E−05	5.42E−05	2.30E−05	2.16E−04
^{37}Cl	3.04E−06	5.83E−06	9.12E−06	3.86E−05	6.12E−05	1.54E−05	9.66E−05
^{36}Ar	3.24E−03	5.28E−03	5.67E−03	9.67E−03	3.10E−02	1.97E−02	4.87E−02
^{38}Ar	5.23E−05	6.23E−05	1.70E−04	3.86E−04	3.59E−04	3.48E−05	1.11E−03
^{40}Ar	8.01E−11	1.78E−11	3.96E−11	1.06E−10	1.77E−11	4.66E−12	1.30E−10
^{39}K	5.02E−06	7.86E−06	1.93E−05	4.40E−05	6.30E−05	1.31E−05	1.18E−04
^{40}K	1.14E−09	9.10E−10	1.96E−09	1.30E−08	8.04E−09	9.94E−10	1.04E−08
^{41}K	3.54E−07	8.05E−07	1.72E−06	9.47E−06	2.08E−05	3.39E−06	2.80E−05
^{40}Ca	2.92E−03	4.41E−03	4.40E−03	6.22E−03	2.48E−02	1.74E−02	3.73E−02
^{42}Ca	9.77E−07	1.23E−06	3.62E−06	1.28E−05	7.46E−06	8.62E−07	2.17E−05
^{43}Ca	6.46E−08	4.93E−08	3.39E−08	7.43E−08	1.58E−08	1.93E−09	9.65E−09
^{44}Ca	1.68E−05	2.21E−05	1.45E−05	1.45E−05	9.79E−06	5.44E−06	8.71E−06
^{46}Ca	1.07E−12	1.76E−12	9.27E−12	1.30E−10	2.78E−11	6.05E−13	5.20E−12
^{48}Ca	1.55E−17	4.21E−14	4.12E−16	4.40E−16	1.26E−11	3.55E−16	1.30E−17
^{45}Sc	2.12E−08	4.03E−08	5.54E−08	2.55E−07	6.16E−07	1.51E−07	5.81E−07
^{46}Ti	6.28E−06	2.71E−06	4.06E−06	5.98E−06	3.18E−06	5.28E−07	1.08E−05
^{47}Ti	8.76E−06	3.86E−06	5.30E−06	4.26E−06	5.90E−08	3.80E−08	9.30E−08
^{48}Ti	6.34E−05	8.39E−05	7.65E−05	8.86E−05	1.55E−04	1.81E−04	2.45E−04
^{49}Ti	2.27E−06	3.32E−06	3.00E−06	3.94E−06	7.04E−06	8.84E−06	1.20E−05
^{50}Ti	1.18E−12	9.55E−13	1.72E−12	1.83E−12	2.24E−12	4.59E−14	9.41E−12
^{50}V	1.36E−11	1.05E−11	4.61E−11	1.36E−10	1.17E−10	2.64E−12	6.53E−10
^{51}V	1.65E−05	1.08E−05	1.24E−05	1.10E−05	9.01E−06	1.06E−05	1.76E−05
^{50}Cr	1.04E−05	1.55E−05	2.64E−05	2.22E−05	4.88E−05	3.82E−05	1.78E−04
^{52}Cr	8.80E−04	1.09E−03	1.13E−03	1.36E−03	2.77E−03	3.12E−03	3.95E−03
^{53}Cr	4.96E−05	6.76E−05	6.43E−05	8.28E−05	1.50E−04	1.82E−04	2.61E−04
^{54}Cr	2.35E−10	4.13E−10	3.25E−09	3.18E−09	9.32E−09	1.72E−10	8.59E−08
^{55}Mn	1.33E−04	1.86E−04	1.74E−04	2.26E−04	4.30E−04	5.16E−04	7.15E−04

TABLE 1—*Continued*

Element	Yields (in $M_\odot$) for M = 13	15	18	20	25	30	40
^{54}Fe	7.29E−04	1.24E−03	1.40E−03	1.42E−03	3.31E−03	4.09E−03	9.30E−03
^{56}Fe	7.00E−02	7.00E−02	7.00E−02	7.00E−02	7.00E−02	7.00E−02	7.02E−02
^{57}Fe	9.97E−04	1.14E−03	8.78E−04	8.67E−04	4.67E−04	4.83E−04	5.01E−04
^{58}Fe	5.67E−11	1.76E−10	8.07E−10	1.05E−09	2.31E−09	2.26E−10	1.41E−08
^{59}Co	1.76E−04	1.32E−04	1.61E−04	1.50E−04	1.57E−05	2.47E−06	1.88E−06
^{58}Ni	3.85E−04	4.14E−04	3.83E−04	3.78E−04	2.93E−04	3.82E−04	5.74E−04
^{60}Ni	2.12E−03	1.62E−03	1.57E−03	1.34E−03	1.48E−04	3.60E−06	4.38E−06
^{61}Ni	3.61E−05	3.14E−05	2.12E−05	1.85E−05	5.77E−07	6.04E−09	1.32E−09
^{62}Ni	1.94E−05	1.51E−05	1.35E−05	1.19E−05	3.88E−07	1.64E−09	5.36E−10
^{64}Ni	3.83E−15	9.97E−14	1.09E−14	6.10E−14	3.27E−12	3.26E−14	7.71E−15
^{63}Cu	4.89E−06	3.54E−06	3.92E−06	3.44E−06	1.23E−07	2.37E−10	2.06E−11
^{65}Cu	2.14E−07	2.42E−07	1.63E−07	1.42E−07	7.79E−09	1.03E−12	1.30E−13
^{64}Zn	1.25E−04	1.22E−04	9.50E−05	8.29E−05	2.54E−06	3.02E−10	4.36E−11
^{66}Zn	6.84E−07	1.07E−06	5.05E−07	4.24E−07	1.59E−08	3.53E−12	5.14E−13
^{67}Zn	1.62E−08	2.33E−08	1.30E−08	1.05E−08	2.16E−10	6.31E−13	8.47E−14
^{68}Zn	2.94E−08	3.25E−08	4.02E−08	3.43E−08	8.05E−10	1.30E−12	2.62E−13
^{70}Zn	6.94E−16	3.59E−14	6.59E−15	2.51E−14	3.97E−14	1.86E−14	4.45E−16
^{69}Ga	7.81E−09	5.62E−09	6.10E−09	4.93E−09	8.74E−11	5.06E−13	4.26E−15
^{71}Ga	8.53E−15	1.12E−13	1.84E−14	9.21E−14	2.24E−13	2.34E−14	1.36E−15
^{70}Ge	8.99E−09	6.57E−09	4.80E−09	3.93E−09	6.84E−12	2.19E−12	1.89E−12
^{72}Ge	1.73E−14	8.02E−13	5.74E−13	3.33E−13	1.30E−13	8.32E−13	4.61E−14
^{73}Ge	1.56E−14	1.19E−13	1.09E−13	1.66E−13	1.39E−13	9.13E−14	2.94E−15
^{74}Ge	4.13E−15	1.20E−13	4.87E−14	1.00E−13	2.55E−13	2.97E−14	8.35E−16
			Z = 0.001				
$M_{\rm final}$	12.93	14.92	17.84	19.72	24.42	29.05	37.81
$M_{\rm cut}$	1.65	1.53	1.70	1.85	1.91	2.06	3.17
p	6.44E+00	7.45E+00	8.46E+00	8.43E+00	9.80E+00	1.11E+01	1.29E+01
D	7.19E−15	3.38E−12	3.07E−15	4.35E−16	4.47E−16	5.03E−16	7.03E−14
^{3}He	1.43E−04	1.53E−04	1.57E−04	1.60E−04	1.26E−04	1.44E−04	1.21E−04
^{4}He	3.86E+00	5.16E+00	6.54E+00	5.94E+00	6.97E+00	8.38E+00	1.09E+01
^{6}Li	2.37E−17	1.11E−17	8.84E−18	2.40E−23	2.35E−21	2.75E−23	2.29E−16
^{7}Li	6.34E−10	3.76E−13	5.83E−13	8.47E−11	9.12E−13	1.12E−12	6.68E−12
^{9}Be	2.33E−17	9.06E−16	9.32E−17	1.43E−23	2.05E−25	0.00E+00	4.06E−16
^{10}B	1.15E−11	6.01E−12	6.57E−12	2.37E−12	7.60E−12	2.25E−12	2.01E−12
^{11}B	5.11E−11	2.68E−11	2.94E−11	1.03E−11	3.42E−11	1.01E−11	7.02E−12
^{12}C	1.07E−01	8.50E−02	1.30E−01	1.28E−01	2.15E−01	1.21E−01	7.37E−02
^{13}C	1.67E−04	5.38E−05	7.20E−05	1.96E−05	9.81E−05	8.20E−05	2.82E−04
^{14}N	9.07E−03	3.58E−03	4.47E−03	1.29E−02	9.20E−03	6.19E−03	8.69E−03
^{15}N	7.57E−06	8.59E−07	9.21E−07	1.37E−06	7.24E−06	3.79E−07	2.45E−06
^{16}O	5.04E−01	2.94E−01	4.22E−01	2.18E+00	3.82E+00	5.33E+00	8.37E+00
^{17}O	6.96E−05	2.56E−05	2.42E−05	2.18E−05	2.79E−05	4.87E−05	2.86E−05
^{18}O	1.81E−03	3.66E−04	3.06E−04	8.09E−06	7.05E−05	2.69E−05	2.63E−05
^{19}F	3.07E−06	1.98E−07	3.32E−07	2.81E−06	6.12E−07	2.39E−06	4.47E−06
^{20}Ne	6.60E−02	1.90E−01	1.77E−01	6.27E−01	1.22E+00	1.45E+00	2.87E−01
^{21}Ne	1.85E−04	6.75E−05	8.76E−05	1.37E−04	5.09E−04	6.11E−04	1.11E−04
^{22}Ne	1.33E−03	2.74E−04	4.75E−04	1.18E−03	1.47E−03	1.56E−03	8.76E−04
^{23}Na	5.41E−04	1.96E−03	2.09E−03	1.81E−03	8.09E−03	6.86E−03	9.00E−04
^{24}Mg	6.36E−02	6.37E−02	5.93E−02	2.42E−01	1.79E−01	2.86E−01	7.04E−01
^{25}Mg	1.40E−03	8.80E−04	9.46E−04	2.40E−03	1.74E−03	3.55E−03	2.21E−03
^{26}Mg	8.34E−04	1.14E−03	9.27E−04	2.44E−03	1.99E−03	4.27E−03	1.11E−03
^{27}Al	3.57E−03	2.35E−03	2.31E−03	6.98E−03	5.05E−03	8.73E−03	3.01E−02
^{28}Si	8.99E−02	4.29E−02	1.53E−01	1.28E−01	1.20E−01	1.65E−01	8.81E−01
^{29}Si	1.42E−03	3.82E−04	6.01E−04	1.11E−03	4.40E−04	1.03E−03	6.04E−03
^{30}Si	1.85E−03	4.25E−04	5.34E−04	7.76E−04	2.75E−04	7.09E−04	1.01E−02
^{31}P	5.31E−04	8.12E−05	1.87E−04	1.97E−04	1.07E−04	2.04E−04	3.48E−03
^{32}S	3.70E−02	1.64E−02	7.88E−02	5.62E−02	5.51E−02	7.80E−02	3.29E−01
^{33}S	1.96E−04	4.76E−05	3.01E−04	9.91E−05	8.12E−05	1.39E−04	8.37E−04
^{34}S	9.22E−04	2.39E−04	6.37E−04	3.10E−04	1.79E−04	3.68E−04	2.12E−03
^{36}S	7.49E−07	1.55E−07	3.20E−07	4.05E−07	6.53E−07	9.04E−07	5.56E−07
^{35}Cl	8.16E−05	8.10E−06	8.16E−05	2.33E−05	2.10E−05	3.35E−05	3.52E−04
^{37}Cl	1.44E−05	2.63E−06	4.13E−05	1.02E−05	1.29E−05	1.92E−05	6.31E−05
^{36}Ar	5.69E−03	2.46E−03	1.22E−02	1.01E−02	9.29E−03	1.35E−02	4.56E−02
^{38}Ar	2.68E−04	2.26E−05	4.12E−04	1.07E−04	8.25E−05	1.63E−04	8.37E−04

TABLE 1—*Continued*

Element	Yields (in $M_\odot$) for M = 13	15	18	20	25	30	40
^{40}Ar	1.76E−07	4.90E−08	1.03E−07	5.43E−08	9.81E−08	1.19E−07	6.83E−08
^{39}K	2.51E−05	4.15E−06	5.69E−05	1.39E−05	1.53E−05	2.37E−05	1.11E−04
^{40}K	2.66E−08	1.95E−09	3.92E−08	7.57E−09	9.91E−09	9.51E−09	2.38E−08
^{41}K	2.41E−06	3.13E−07	1.09E−05	2.07E−06	2.22E−06	3.98E−06	1.52E−05
^{40}Ca	4.73E−03	1.73E−03	8.06E−03	9.20E−03	7.94E−03	1.17E−02	3.66E−02
^{42}Ca	6.62E−06	4.05E−07	1.35E−05	2.79E−06	2.49E−06	4.64E−06	2.29E−05
^{43}Ca	4.15E−07	3.35E−07	2.45E−07	1.91E−07	2.90E−07	3.55E−07	2.81E−07
^{44}Ca	2.48E−05	2.07E−05	1.87E−05	4.88E−06	7.96E−06	6.44E−06	1.10E−05
^{46}Ca	6.65E−08	1.41E−08	2.55E−08	3.35E−08	3.02E−08	7.10E−08	1.22E−07
^{48}Ca	3.16E−07	9.66E−08	1.22E−07	1.25E−07	1.57E−07	1.86E−07	2.17E−07
^{45}Sc	2.52E−07	5.08E−08	3.55E−07	2.16E−07	3.24E−07	4.22E−07	9.92E−07
^{46}Ti	3.99E−06	1.24E−05	5.11E−06	1.36E−06	1.31E−06	2.15E−06	9.99E−06
^{47}Ti	2.55E−06	1.28E−05	1.50E−06	4.30E−07	3.36E−07	4.50E−07	6.35E−07
^{48}Ti	9.68E−05	5.19E−05	9.98E−05	1.37E−04	1.17E−04	1.67E−04	2.53E−04
^{49}Ti	3.85E−06	1.94E−06	4.13E−06	6.78E−06	5.68E−06	8.43E−06	1.40E−05
^{50}Ti	6.32E−07	1.62E−07	1.86E−07	5.05E−07	8.49E−07	1.14E−06	1.16E−06
^{50}V	1.10E−08	1.12E−09	1.81E−09	8.49E−09	1.31E−08	2.06E−08	9.25E−08
^{51}V	8.95E−06	1.62E−05	7.56E−06	8.23E−06	7.52E−06	9.95E−06	1.94E−05
^{50}Cr	2.10E−05	1.33E−05	2.99E−05	2.37E−05	2.75E−05	3.51E−05	1.35E−04
^{52}Cr	1.20E−03	3.03E−04	1.52E−03	2.22E−03	2.18E−03	2.92E−03	3.94E−03
^{53}Cr	7.43E−05	2.82E−05	9.07E−05	1.37E−04	1.11E−04	1.77E−04	2.56E−04
^{54}Cr	1.87E−06	4.80E−07	5.96E−07	1.41E−06	2.19E−06	2.74E−06	2.84E−06
^{55}Mn	2.27E−04	8.01E−05	2.81E−04	3.80E−04	2.99E−04	5.01E−04	7.86E−04
^{54}Fe	1.53E−03	7.07E−04	2.06E−03	2.37E−03	2.25E−03	3.31E−03	1.04E−02
^{56}Fe	7.26E−02	7.08E−02	7.11E−02	7.09E−02	7.11E−02	7.12E−02	7.15E−02
^{57}Fe	1.41E−03	1.75E−03	1.27E−03	7.21E−04	5.30E−04	5.83E−04	5.75E−04
^{58}Fe	5.68E−05	1.31E−05	1.55E−05	4.99E−05	7.78E−05	9.28E−05	1.02E−04
^{59}Co	8.91E−05	2.32E−04	6.30E−05	6.21E−05	3.42E−05	5.39E−05	4.42E−05
^{58}Ni	5.09E−04	9.11E−04	1.76E−03	3.54E−04	2.51E−04	3.79E−04	7.80E−04
^{60}Ni	1.62E−03	2.57E−03	1.17E−03	2.95E−04	6.57E−05	1.94E−04	1.01E−04
^{61}Ni	5.05E−05	6.92E−05	4.63E−05	1.22E−05	1.57E−05	2.10E−05	2.06E−05
^{62}Ni	1.01E−04	1.87E−04	2.97E−04	2.54E−05	3.71E−05	5.15E−05	7.60E−05
^{64}Ni	1.62E−05	1.83E−06	2.30E−06	2.37E−05	4.32E−05	6.46E−05	7.83E−05
^{63}Cu	8.05E−06	5.47E−06	2.78E−06	9.64E−06	1.44E−05	1.97E−05	1.40E−05
^{65}Cu	4.86E−06	8.85E−07	1.14E−06	8.05E−06	1.50E−05	2.23E−05	2.90E−05
^{64}Zn	7.15E−05	6.50E−05	5.32E−05	1.17E−05	9.03E−06	1.61E−05	1.29E−05
^{66}Zn	9.89E−06	3.96E−06	7.73E−06	1.12E−05	1.93E−05	3.09E−05	4.78E−05
^{67}Zn	1.04E−06	1.41E−07	1.87E−07	2.04E−06	3.86E−06	6.06E−06	4.18E−06
^{68}Zn	6.87E−06	5.82E−07	7.86E−07	9.86E−06	1.86E−05	3.15E−05	4.63E−05
^{70}Zn	2.29E−07	1.05E−08	1.75E−08	2.86E−08	2.35E−08	7.37E−08	1.39E−07
^{69}Ga	7.11E−07	7.43E−08	1.13E−07	1.24E−06	2.33E−06	3.73E−06	4.73E−06
^{71}Ga	6.34E−07	5.13E−08	7.70E−08	1.09E−06	2.01E−06	3.84E−06	5.46E−06
^{70}Ge	8.84E−07	1.01E−07	1.46E−07	1.99E−06	3.78E−06	6.48E−06	8.61E−06
^{72}Ge	1.57E−06	9.80E−08	1.37E−07	2.00E−06	4.12E−06	7.28E−06	1.39E−05
^{73}Ge	2.40E−07	2.18E−08	3.05E−08	3.91E−07	7.25E−07	1.40E−06	6.61E−07
^{74}Ge	2.86E−06	1.89E−07	2.62E−07	4.12E−06	9.16E−06	1.77E−05	2.63E−05
			Z = 0.004				
$M_{\rm final}$	12.86	14.39	16.59	19.52	24.03	27.56	32.93
$M_{\rm cut}$	1.61	1.50	1.61	1.76	1.68	2.56	2.81
p	6.37E+00	7.11E+00	7.47E+00	8.95E+00	1.02E+01	1.01E+01	1.03E+01
D	1.07E−14	1.99E−14	4.58E−14	8.80E−14	3.23E−16	6.93E−14	2.64E−16
^{3}He	1.70E−04	1.59E−04	2.24E−04	1.75E−04	1.85E−04	1.84E−04	1.80E−04
^{4}He	4.04E+00	4.95E+00	6.06E+00	7.03E+00	8.48E+00	7.92E+00	8.12E+00
^{6}Li	3.44E−17	6.50E−17	1.50E−16	2.90E−16	5.19E−23	2.23E−16	2.14E−20
^{7}Li	3.15E−15	7.20E−14	5.04E−13	1.56E−12	1.02E−13	8.01E−13	4.71E−12
^{9}Be	1.07E−16	1.08E−16	1.58E−16	5.51E−16	4.88E−24	3.78E−16	6.00E−22
^{10}B	2.55E−11	2.55E−11	1.55E−10	2.92E−11	3.09E−11	3.04E−11	6.57E−12
^{11}B	1.15E−10	1.15E−10	6.97E−10	4.60E−08	1.39E−10	1.37E−10	2.80E−11
^{12}C	8.78E−02	8.81E−02	1.05E−01	9.74E−02	1.32E−01	1.82E−01	4.58E−01
^{13}C	1.88E−04	2.09E−04	6.03E−02	2.92E−04	3.83E−04	3.39E−04	3.68E−04
^{14}N	9.08E−03	1.29E−02	7.27E−02	1.84E−02	3.15E−02	2.01E−02	2.60E−02
^{15}N	6.84E−06	8.70E−06	5.35E−02	2.78E−05	9.53E−05	4.98E−06	5.01E−06
^{16}O	3.85E−01	2.92E−01	5.21E−01	9.94E−01	2.20E+00	4.79E+00	7.96E+00

TABLE 1—*Continued*

Element	Yields (in $M_\odot$) for M = 13	15	18	20	25	30	40
^{17}O	8.75E−05	8.66E−05	1.11E−03	1.04E−04	1.12E−04	1.20E−04	1.59E−04
^{18}O	1.95E−03	9.68E−04	5.20E−02	1.28E−03	8.48E−04	4.35E−05	8.37E−04
^{19}F	1.98E−06	2.13E−06	1.21E−05	5.36E−06	8.50E−05	1.16E−05	1.04E−06
^{20}Ne	1.32E−01	1.25E−01	2.00E−01	2.77E−01	8.20E−01	9.37E−01	1.88E+00
^{21}Ne	1.85E−04	1.43E−04	1.00E−03	2.58E−04	3.83E−04	7.21E−04	1.17E−03
^{22}Ne	1.05E−03	7.54E−04	4.17E−03	2.16E−03	4.57E−03	6.18E−03	2.87E−03
^{23}Na	1.50E−03	8.19E−04	6.63E−03	4.07E−03	6.25E−03	1.41E−02	2.61E−02
^{24}Mg	4.38E−02	7.46E−02	6.93E−02	9.65E−02	2.33E−01	2.18E−01	3.79E−01
^{25}Mg	1.38E−03	1.95E−03	8.20E−03	2.20E−03	6.04E−03	7.09E−03	1.20E−02
^{26}Mg	1.24E−03	1.93E−03	6.46E−03	1.88E−03	6.71E−03	7.08E−03	1.33E−02
^{27}Al	2.21E−03	3.31E−03	6.29E−03	5.13E−03	1.12E−02	1.69E−02	3.04E−02
^{28}Si	6.11E−02	1.03E−01	9.41E−02	1.24E−01	1.19E−01	3.95E−01	5.23E−01
^{29}Si	5.41E−04	1.12E−03	2.70E−03	1.27E−03	1.93E−03	3.37E−03	4.55E−03
^{30}Si	6.56E−04	1.29E−03	3.89E−03	1.61E−03	1.58E−03	4.82E−03	6.50E−03
^{31}P	1.50E−04	2.74E−04	7.36E−04	3.87E−04	3.86E−04	1.02E−03	1.48E−03
^{32}S	2.68E−02	3.44E−02	4.07E−02	5.15E−02	3.48E−02	1.90E−01	2.26E−01
^{33}S	9.09E−05	1.83E−04	2.62E−04	1.89E−04	1.66E−04	4.34E−04	4.55E−04
^{34}S	4.27E−04	9.56E−04	2.38E−03	9.12E−04	7.22E−04	2.03E−03	2.35E−03
^{36}S	7.10E−07	9.91E−07	7.79E−06	1.36E−06	2.68E−06	6.10E−06	1.19E−05
^{35}Cl	2.66E−05	5.21E−05	1.09E−04	5.46E−05	5.30E−05	1.23E−04	1.56E−04
^{37}Cl	1.01E−05	1.65E−05	4.60E−05	2.05E−05	3.03E−05	7.79E−05	1.13E−04
^{36}Ar	4.50E−03	4.31E−03	6.96E−03	7.99E−03	4.73E−03	3.09E−02	3.48E−02
^{38}Ar	1.66E−04	4.94E−04	7.43E−04	3.06E−04	2.67E−04	9.77E−04	1.14E−03
^{40}Ar	2.30E−07	3.74E−07	2.55E−06	3.30E−07	3.57E−07	9.25E−07	1.15E−06
^{39}K	1.78E−05	3.20E−05	7.20E−05	3.12E−05	2.64E−05	1.02E−04	9.93E−05
^{40}K	7.79E−09	9.13E−09	6.68E−08	1.85E−08	3.34E−08	7.91E−08	7.41E−08
^{41}K	1.87E−06	2.46E−06	7.11E−06	3.13E−06	3.43E−06	1.30E−05	1.35E−05
^{40}Ca	3.91E−03	3.08E−03	6.12E−03	6.50E−03	3.77E−03	2.59E−02	2.83E−02
^{42}Ca	4.16E−06	9.59E−06	1.81E−05	7.31E−06	6.00E−06	2.65E−05	2.98E−05
^{43}Ca	3.41E−07	3.60E−07	1.93E−06	5.23E−07	7.95E−07	9.89E−07	1.43E−06
^{44}Ca	2.07E−05	2.30E−05	3.40E−05	2.09E−05	2.65E−05	1.52E−05	1.88E−05
^{46}Ca	7.37E−08	1.18E−07	6.81E−07	1.10E−07	1.28E−07	1.97E−07	3.24E−07
^{48}Ca	3.22E−07	4.02E−07	2.37E−06	5.02E−07	6.19E−07	6.48E−07	7.80E−07
^{45}Sc	2.16E−07	2.48E−07	1.35E−06	3.61E−07	5.30E−07	1.09E−06	1.64E−06
^{46}Ti	5.16E−06	6.10E−06	8.19E−06	3.54E−06	5.14E−06	1.22E−05	1.40E−05
^{47}Ti	5.40E−06	3.40E−06	4.65E−06	1.34E−06	6.46E−06	1.46E−06	2.04E−06
^{48}Ti	8.17E−05	7.41E−05	1.37E−04	1.14E−04	8.94E−05	2.33E−04	2.69E−04
^{49}Ti	3.49E−06	2.81E−06	7.25E−06	5.20E−06	4.09E−06	1.36E−05	1.72E−05
^{50}Ti	5.85E−07	5.61E−07	3.72E−06	1.08E−06	2.25E−06	4.10E−06	7.70E−06
^{50}V	4.61E−09	4.94E−09	4.06E−08	1.01E−08	1.98E−08	5.38E−08	9.68E−08
^{51}V	1.31E−05	9.56E−06	1.23E−05	8.01E−06	1.41E−05	1.77E−05	2.20E−05
^{50}Cr	1.75E−05	2.71E−05	3.34E−05	3.06E−05	2.47E−05	8.56E−05	1.21E−04
^{52}Cr	1.11E−03	9.63E−04	1.81E−03	1.66E−03	1.24E−03	3.73E−03	4.08E−03
^{53}Cr	6.78E−05	5.90E−05	1.23E−04	1.04E−04	7.21E−05	2.43E−04	2.76E−04
^{54}Cr	1.75E−06	1.84E−06	1.07E−05	3.11E−06	5.79E−06	8.65E−06	1.39E−05
^{55}Mn	2.00E−04	1.71E−04	4.68E−04	3.29E−04	2.34E−04	7.62E−04	8.38E−04
^{54}Fe	1.24E−03	1.23E−03	2.63E−03	2.37E−03	1.41E−03	7.09E−03	9.39E−03
^{56}Fe	7.26E−02	7.30E−02	8.72E−02	7.40E−02	7.47E−02	7.46E−02	7.47E−02
^{57}Fe	1.05E−03	1.13E−03	4.00E−03	1.22E−03	1.05E−03	7.15E−04	7.31E−04
^{58}Fe	4.77E−05	4.89E−05	2.66E−04	9.17E−05	1.85E−04	2.89E−04	4.34E−04
^{59}Co	1.96E−04	1.31E−04	2.69E−04	6.21E−05	2.17E−04	1.29E−04	1.91E−04
^{58}Ni	5.14E−04	4.64E−04	2.25E−02	4.93E−04	5.44E−04	7.14E−04	8.27E−04
^{60}Ni	1.80E−03	1.67E−03	1.37E−03	1.29E−03	1.80E−03	2.63E−04	3.80E−04
^{61}Ni	4.25E−05	4.99E−05	2.66E−04	5.67E−05	6.09E−05	5.55E−05	9.80E−05
^{62}Ni	3.55E−05	2.40E−05	3.08E−03	9.09E−05	1.09E−04	1.75E−04	3.01E−04
^{64}Ni	1.09E−05	3.62E−06	6.69E−05	2.79E−05	9.88E−05	1.95E−04	4.25E−04
^{63}Cu	1.05E−05	5.37E−06	3.62E−05	1.35E−05	4.27E−05	5.23E−05	1.04E−04
^{65}Cu	3.81E−06	1.51E−06	2.12E−05	1.02E−05	3.17E−05	6.94E−05	1.45E−04
^{64}Zn	1.14E−04	1.16E−04	2.31E−05	6.04E−05	1.29E−04	2.98E−05	5.80E−05
^{66}Zn	6.72E−06	4.66E−06	8.57E−05	1.71E−05	4.58E−05	1.06E−04	2.18E−04
^{67}Zn	7.89E−07	3.21E−07	5.78E−06	2.25E−06	8.56E−06	1.82E−05	4.11E−05
^{68}Zn	3.52E−06	1.52E−06	2.86E−05	1.17E−05	4.38E−05	1.20E−04	2.65E−04
^{70}Zn	1.13E−07	8.93E−08	1.06E−06	9.23E−08	1.66E−07	4.58E−07	5.82E−07
^{69}Ga	5.06E−07	1.74E−07	2.88E−06	1.55E−06	5.59E−06	1.60E−05	3.37E−05
^{71}Ga	3.05E−07	2.05E−07	2.89E−06	1.17E−06	4.72E−06	1.33E−05	2.92E−05

TABLE 1—*Continued*

Element	Yields (in $M_\odot$) for M = 13	15	18	20	25	30	40
^{70}Ge	6.23E−07	2.08E−07	3.42E−06	2.13E−06	8.24E−06	2.38E−05	5.16E−05
^{72}Ge	6.71E−07	2.88E−07	4.82E−06	2.43E−06	9.76E−06	4.18E−05	8.41E−05
^{73}Ge	1.52E−07	7.93E−08	1.08E−06	4.30E−07	1.98E−06	6.05E−06	1.37E−05
^{74}Ge	1.03E−06	5.17E−07	1.08E−05	4.55E−06	2.17E−05	1.22E−04	2.49E−04
			Z = 0.02				
$M_{\rm final}$	12.73	14.14	16.76	18.36	21.63	24.58	21.83
$M_{\rm cut}$	1.60	1.50	1.58	1.55	1.69	2.10	2.21
p	6.16E+00	6.79E+00	7.53E+00	7.93E+00	8.41E+00	8.75E+00	3.55E+00
D	8.34E−15	1.02E−14	4.16E−16	1.20E−15	9.87E−16	1.08E−15	7.71E−17
^{3}He	1.96E−04	2.18E−04	2.30E−04	2.38E−04	2.21E−04	2.12E−04	5.05E−05
^{4}He	4.30E+00	5.25E+00	6.11E+00	6.76E+00	7.24E+00	8.36E+00	4.71E+00
^{6}Li	1.32E−17	3.17E−17	2.78E−19	1.09E−22	9.53E−23	5.90E−23	3.47E−22
^{7}Li	5.63E−11	7.09E−13	2.80E−13	4.32E−12	6.93E−13	4.33E−13	5.72E−13
^{9}Be	4.61E−19	1.55E−18	7.56E−18	4.72E−23	2.23E−20	4.92E−23	7.03E−23
^{10}B	1.12E−10	1.36E−10	1.42E−10	1.47E−10	1.51E−10	1.55E−10	6.96E−14
^{11}B	4.28E−10	6.02E−10	6.41E−10	6.54E−10	6.77E−10	6.92E−10	3.22E−14
^{12}C	1.07E−01	6.51E−02	1.36E−01	2.45E−01	1.52E−01	2.50E−01	5.96E−01
^{13}C	1.00E−03	1.15E−03	1.38E−03	1.45E−03	6.66E−02	1.92E−03	4.31E−04
^{14}N	4.80E−02	6.15E−02	6.61E−02	7.19E−02	8.43E−02	1.02E−01	5.81E−02
^{15}N	4.09E−05	5.97E−05	1.53E−05	2.24E−04	4.63E−02	6.56E−06	5.72E−06
^{16}O	2.18E−01	1.62E−01	7.70E−01	1.05E+00	2.35E+00	3.22E+00	7.33E+00
^{17}O	8.68E−04	8.12E−04	8.76E−04	9.51E−04	1.34E−03	1.69E−03	9.72E−04
^{18}O	3.50E−03	2.54E−03	1.17E−02	5.22E−03	8.43E−02	6.18E−03	1.23E−02
^{19}F	1.42E−05	1.64E−05	4.47E−06	6.05E−05	1.19E−04	7.81E−06	5.26E−06
^{20}Ne	3.47E−02	3.39E−02	1.49E−01	3.94E−01	8.53E−01	9.37E−01	2.21E+00
^{21}Ne	2.25E−04	1.30E−04	2.02E−04	1.81E−03	1.59E−03	2.97E−03	4.97E−03
^{22}Ne	4.52E−03	1.72E−03	6.63E−03	9.04E−03	1.68E−02	1.86E−02	1.09E−02
^{23}Na	9.25E−04	1.06E−03	2.93E−03	1.68E−02	1.86E−02	3.47E−02	7.76E−02
^{24}Mg	2.52E−02	3.79E−02	1.03E−01	7.16E−02	2.18E−01	1.88E−01	3.10E−01
^{25}Mg	2.56E−03	1.47E−03	7.08E−03	1.44E−02	3.13E−02	3.12E−02	7.28E−02
^{26}Mg	2.18E−03	1.73E−03	5.90E−03	8.87E−03	2.73E−02	2.80E−02	7.34E−02
^{27}Al	1.50E−03	2.44E−03	1.00E−02	9.90E−03	2.70E−02	3.41E−02	8.30E−02
^{28}Si	7.48E−02	8.38E−02	1.01E−01	6.32E−02	1.28E−01	2.40E−01	2.41E−01
^{29}Si	1.49E−03	2.20E−03	6.96E−03	2.04E−03	7.06E−03	7.38E−03	9.99E−03
^{30}Si	1.55E−03	2.75E−03	6.82E−03	2.44E−03	6.19E−03	1.06E−02	9.76E−03
^{31}P	3.75E−04	7.06E−04	1.74E−03	6.58E−04	1.50E−03	2.56E−03	3.53E−03
^{32}S	3.73E−02	3.47E−02	3.69E−02	2.81E−02	4.99E−02	1.08E−01	1.09E−01
^{33}S	2.00E−04	2.44E−04	3.51E−04	2.26E−04	3.25E−04	4.81E−04	4.81E−04
^{34}S	1.64E−03	1.53E−03	2.19E−03	1.70E−03	2.26E−03	3.76E−03	3.42E−03
^{36}S	5.37E−06	2.54E−06	1.20E−05	9.19E−06	2.42E−05	5.09E−05	9.40E−05
^{35}Cl	1.15E−04	1.37E−04	1.75E−04	1.25E−04	1.62E−04	2.33E−04	2.76E−04
^{37}Cl	3.03E−05	2.49E−05	5.65E−05	8.42E−05	1.70E−04	2.63E−04	5.64E−04
^{36}Ar	6.29E−03	4.90E−03	5.48E−03	4.66E−03	7.92E−03	1.81E−02	1.81E−02
^{38}Ar	6.86E−04	6.51E−04	7.83E−04	6.74E−04	8.98E−04	1.64E−03	1.65E−03
^{40}Ar	8.96E−07	1.06E−06	1.30E−06	1.42E−06	2.68E−06	7.41E−06	5.67E−06
^{39}K	5.02E−05	7.00E−05	7.67E−05	7.39E−05	8.83E−05	1.29E−04	1.14E−04
^{40}K	1.28E−07	6.43E−08	1.38E−07	9.30E−08	2.00E−07	2.94E−07	4.05E−07
^{41}K	4.68E−06	5.85E−06	7.75E−06	9.03E−06	1.39E−05	1.97E−05	4.52E−05
^{40}Ca	4.93E−03	4.01E−03	4.54E−03	3.74E−03	6.55E−03	1.57E−02	1.56E−02
^{42}Ca	1.39E−05	1.75E−05	2.07E−05	1.74E−05	2.47E−05	4.15E−05	4.48E−05
^{43}Ca	1.36E−06	1.50E−06	2.12E−06	2.52E−06	3.42E−06	2.97E−06	4.93E−06
^{44}Ca	3.52E−05	3.55E−05	5.45E−05	5.79E−05	5.11E−05	4.04E−05	4.67E−05
^{46}Ca	2.12E−07	3.33E−07	7.83E−07	6.15E−07	1.19E−06	1.18E−06	2.86E−06
^{48}Ca	1.58E−06	1.86E−06	2.73E−06	2.35E−06	2.73E−06	1.42E−05	2.43E−06
^{45}Sc	7.29E−07	9.30E−07	1.26E−06	1.30E−06	2.80E−06	2.58E−06	6.15E−06
^{46}Ti	6.01E−06	8.64E−06	9.50E−06	8.53E−06	1.14E−05	1.86E−05	2.11E−05
^{47}Ti	4.41E−06	3.44E−06	5.34E−06	6.55E−06	5.59E−06	8.81E−06	6.75E−06
^{48}Ti	8.13E−05	1.07E−04	1.32E−04	1.15E−04	1.53E−04	2.53E−04	2.44E−04
^{49}Ti	4.74E−06	5.07E−06	6.11E−06	6.37E−06	1.10E−05	1.92E−05	2.42E−05
^{50}Ti	2.33E−06	2.41E−06	3.91E−06	5.82E−06	1.23E−05	9.91E−06	3.81E−05
^{50}V	2.03E−08	2.66E−08	6.60E−08	3.89E−08	9.61E−08	2.49E−07	1.87E−07
^{51}V	1.18E−05	9.96E−06	1.14E−05	1.33E−05	1.44E−05	2.50E−05	2.24E−05
^{50}Cr	2.24E−05	3.95E−05	3.68E−05	3.10E−05	5.22E−05	7.71E−05	9.21E−05

TABLE 1—*Continued*

Element	Yields (in $M_\odot$) for M = 13	15	18	20	25	30	40
^{52}Cr	6.48E−04	1.27E−03	1.28E−03	1.08E−03	2.04E−03	3.76E−03	3.78E−03
^{53}Cr	6.24E−05	9.27E−05	9.62E−05	8.28E−05	1.41E−04	2.74E−04	2.50E−04
^{54}Cr	6.55E−06	6.80E−06	1.52E−05	1.66E−05	2.77E−05	5.12E−05	5.67E−05
^{55}Mn	2.81E−04	3.80E−04	4.05E−04	3.60E−04	5.50E−04	1.04E−03	8.28E−04
^{54}Fe	1.92E−03	2.46E−03	2.49E−03	2.22E−03	3.84E−03	6.87E−03	6.42E−03
^{56}Fe	8.32E−02	8.52E−02	8.72E−02	8.87E−02	9.01E−02	9.18E−02	8.08E−02
^{57}Fe	2.22E−03	1.99E−03	2.67E−03	2.34E−03	1.87E−03	2.82E−03	9.75E−04
^{58}Fe	1.21E−04	1.10E−04	5.86E−04	4.96E−04	8.37E−04	2.39E−03	1.48E−03
^{59}Co	1.41E−04	9.00E−05	1.82E−04	2.92E−04	3.89E−04	5.39E−04	6.95E−04
^{58}Ni	2.23E−03	1.15E−03	2.70E−03	1.84E−03	1.56E−03	1.55E−03	8.83E−04
^{60}Ni	2.13E−03	1.87E−03	2.13E−03	2.49E−03	1.81E−03	6.12E−04	1.20E−03
^{61}Ni	8.21E−05	1.24E−04	1.04E−04	1.49E−04	2.16E−04	1.10E−04	3.91E−04
^{62}Ni	2.28E−04	1.64E−04	4.64E−04	3.86E−04	6.61E−04	2.22E−04	1.17E−03
^{64}Ni	3.35E−05	1.72E−05	2.99E−05	1.87E−04	6.16E−04	7.11E−05	2.22E−03
^{63}Cu	1.83E−05	1.30E−05	1.90E−05	1.28E−04	2.94E−04	8.56E−05	6.85E−04
^{65}Cu	1.03E−05	7.18E−06	7.63E−06	4.40E−05	1.46E−04	1.30E−05	6.49E−04
^{64}Zn	9.67E−05	6.77E−05	5.74E−05	1.20E−04	5.37E−05	1.87E−05	1.68E−04
^{66}Zn	1.74E−05	1.78E−05	2.17E−05	6.26E−05	2.39E−04	1.55E−05	1.07E−03
^{67}Zn	2.88E−06	1.78E−06	2.03E−06	1.29E−05	5.26E−05	2.73E−06	2.48E−04
^{68}Zn	1.32E−05	7.49E−06	1.17E−05	6.03E−05	3.14E−04	1.27E−05	1.55E−03
^{70}Zn	1.83E−06	5.59E−07	5.13E−07	1.62E−06	8.43E−06	3.69E−07	2.65E−05
^{69}Ga	1.67E−06	8.45E−07	9.10E−07	6.66E−06	2.74E−05	1.38E−06	1.75E−04
^{71}Ga	1.48E−06	7.96E−07	1.06E−06	5.15E−06	2.79E−05	1.11E−06	1.32E−04
^{70}Ge	1.10E−06	8.38E−07	1.08E−06	9.18E−06	4.34E−05	2.04E−06	2.79E−04
^{72}Ge	2.10E−06	1.24E−06	1.83E−06	1.17E−05	7.17E−05	4.08E−06	4.67E−04
^{73}Ge	1.06E−06	3.51E−07	4.45E−07	2.73E−06	1.69E−05	8.12E−07	1.06E−04
^{74}Ge	4.34E−06	2.31E−06	7.07E−06	2.45E−05	1.99E−04	4.98E−05	1.56E−03

Note.—The value of E_{51} for all M values is 1. Table 1 is also available in machine-readable form in the electronic edition of the *Astrophysical Journal*.

on metallicity, and may be constrained by the gamma-ray burst rate. Here, we adopt $\epsilon_{\rm HN} = 0.5$, independent of the mass and metallicity. This gives a good agreement with the $[\alpha/{\rm Fe}]$ plateau against [Fe/H] as shown in §3.2. Such large $\epsilon_{\rm HN}$ is required from the observed $[{\rm Zn/Fe}] \sim 0$, especially for low metallicity.

Table 3 gives the IMF-weighted yields as a function of metallicity, and also the SN Ia yields (W7 model from Nomoto et al. 1984, 1997b) for comparison. We adopt a Salpeter IMF, i.e., a power-law mass spectrum with a slope of $x = 1.35$ and a mass range from $M_l = 0.07\ M_\odot$ to $M_u = 50\ M_\odot$. We should note that the abundance ratios depend on x, and more strongly on M_u. Figure 5 shows the metallicity dependence of the SN II+HN yields. In the metal-free stellar evolution, because of the lack of initial CNO elements, the CNO cycle dose not operate until the star contracts to a much higher central temperature ($\sim 10^8$ K) than Population II stars, where the 3α reaction produces a tiny fraction of ^{12}C ($\sim 10^{-10}$ in mass fraction). However, the late core evolution and the resulting Fe core masses of metal-free stars are not much different from metal-rich stars. Therefore, the $[\alpha/{\rm Fe}]$ ratio is larger by only a fraction of $\sim$0.2 dex and the abundance ratios of the iron-peak elements are not so different from metal-rich stars, except for Mn. On the other hand, the CNO cycle produces only a small amount of ^{14}N, which is transformed into ^{22}Ne during He-burning. The surplus of neutrons in ^{22}Ne increases the abundances of odd-Z elements (Na, Al, P,...). Therefore, the metallicity effect is realized for odd-Z elements and the inverse ratio of α-elements and their isotopes (e.g., $^{13}{\rm C}/^{12}{\rm C}$). [Na/Fe] and [Al/Fe] of metal-free stars are smaller by $\sim$1.0 and 0.7 dex, respectively, than solar abundance stars, which are consistent with the observed trends (§3.2).

Among α-elements, it has been reported that Ca is underabundant relative to the other α-elements in elliptical galaxies (Thomas et al. 2003). Although dependencies of [Ca/Fe] on the mass, metallicity, and energy are not clearly seen in our yields, [Ca/Fe] tends to be smaller for more massive and more metal-rich supernovae. In the case of a flat IMF with rapid chemical enrichment, i.e., in elliptical galaxies, [Ca/O] could be small.

3. CHEMICAL EVOLUTION OF THE SOLAR NEIGHBORHOOD

3.1. *Chemical Evolution Model*

Using the one-zone chemical evolution model, we compare our nucleosynthesis yields with the observed elemental abundance ratios in the solar neighborhood. Here, the instantaneous recycling approximation is not applied, i.e., the mass dependence of yields (i.e., the stellar lifetime dependence) is taken into account, and the contributions of HNe, SNe II, and SNe Ia are included, while those of low- and intermediate-mass stars are not. For the solar neighborhood, we use a model that allows the infall of primordial gas from outside the disk region (see Kobayashi et al. [2000, hereafter K00] for the formulation). For the infall rate, we adopt a formula that is proportional to $t\exp(-t/\tau_i)$ (Pagel 1989; Yoshii et al. 1996) with an infall timescale of $\tau_i = 5$ Gyr. The Galactic age is assumed to be 13 Gyr, which corresponds to the formation redshift $z_f \sim 9$ for the *WMAP* cosmology ($h = 0.7$, $\Omega_0 = 0.3$, $\lambda_0 = 0.7$). In K98 we assumed 15 Gyr, and the following parameters are slightly updated to meet the metallicity distribution function (MDF). The star formation rate (SFR) is assumed to be proportional to the gas fraction as $\psi \equiv (1/\tau_s) f_g$

TABLE 2

NUCLEOSYNTHESIS YIELDS FOR HYPERNOVAE IN EJECTA

ELEMENT	YIELDS (in $M_\odot$) FOR M = 20	25	30	40
E_{51}	10	10	20	30
		$Z = 0$		
$M_{\rm final}$	20.00	25.00	30.00	40.00
$M_{\rm cut}$	1.88	2.80	3.27	5.53
p	8.77E+00	1.06E+01	1.17E+01	1.40E+01
D	8.66E−17	2.06E−16	1.09E−14	1.66E−14
^{3}He	4.76E−05	2.11E−04	2.06E−04	2.57E−05
^{4}He	5.96E+00	8.03E+00	9.54E+00	1.18E+01
^{6}Li	1.53E−22	3.22E−20	3.50E−17	5.39E−17
^{7}Li	2.79E−10	5.68E−09	2.36E−08	3.42E−11
^{9}Be	4.83E−20	3.69E−17	3.09E−18	9.03E−18
^{10}B	1.95E−19	7.45E−14	1.05E−14	9.41E−15
^{11}B	1.09E−15	1.28E−12	9.53E−14	9.41E−13
^{12}C	1.90E−01	2.67E−01	3.16E−01	3.72E−01
^{13}C	1.18E−08	6.94E−08	6.32E−08	8.19E−08
^{14}N	5.43E−05	5.96E−04	4.18E−05	3.39E−06
^{15}N	2.95E−08	1.75E−07	2.20E−07	6.54E−07
^{16}O	2.03E+00	2.38E+00	3.92E+00	6.32E+00
^{17}O	7.13E−08	1.49E−06	3.81E−08	1.23E−08
^{18}O	2.33E−08	3.87E−07	5.03E−07	2.93E−07
^{19}F	2.12E−09	1.67E−09	7.88E−09	1.17E−07
^{20}Ne	7.49E−01	2.85E−01	5.20E−01	2.64E−01
^{21}Ne	3.58E−05	1.22E−05	3.51E−05	1.41E−05
^{22}Ne	5.51E−05	8.62E−06	3.52E−05	1.66E−05
^{23}Na	2.31E−03	4.42E−04	7.36E−04	3.28E−04
^{24}Mg	1.65E−01	1.53E−01	2.17E−01	3.37E−01
^{25}Mg	1.07E−04	4.57E−05	1.45E−04	5.95E−04
^{26}Mg	2.10E−04	4.02E−05	8.29E−05	1.07E−04
^{27}Al	1.50E−03	8.93E−04	1.55E−03	7.52E−03
^{28}Si	1.03E−01	2.31E−01	2.47E−01	7.20E−01
^{29}Si	2.95E−04	5.38E−04	8.85E−04	3.73E−03
^{30}Si	1.13E−04	6.35E−05	1.47E−04	2.82E−03
^{31}P	7.67E−05	5.91E−05	1.16E−04	1.01E−03
^{32}S	4.27E−02	9.16E−02	8.49E−02	2.59E−01
^{33}S	1.44E−04	2.31E−04	3.02E−04	8.45E−04
^{34}S	1.84E−04	1.26E−04	2.70E−04	2.09E−03
^{36}S	8.33E−10	5.78E−11	1.41E−09	5.04E−08
^{35}Cl	3.95E−05	3.23E−05	4.48E−05	1.80E−04
^{37}Cl	1.88E−05	2.89E−05	2.39E−05	7.96E−05
^{36}Ar	6.80E−03	1.36E−02	1.15E−02	3.55E−02
^{38}Ar	1.27E−04	1.70E−04	9.07E−05	7.83E−04
^{40}Ar	3.79E−11	1.16E−11	1.87E−11	2.68E−10
^{39}K	2.31E−05	3.76E−05	2.05E−05	1.31E−04
^{40}K	4.40E−09	1.40E−09	2.52E−09	1.18E−08
^{41}K	3.73E−06	6.48E−06	3.66E−06	2.13E−05
^{40}Ca	4.77E−03	1.02E−02	8.22E−03	2.86E−02
^{42}Ca	3.41E−06	5.15E−06	1.62E−06	1.97E−05
^{43}Ca	2.60E−07	7.25E−08	1.71E−07	1.40E−07
^{44}Ca	1.26E−04	7.04E−05	1.82E−04	1.75E−04
^{46}Ca	1.15E−11	1.47E−11	9.25E−12	3.69E−11
^{48}Ca	3.74E−15	1.17E−11	8.16E−13	1.27E−11
^{45}Sc	1.85E−07	2.20E−07	6.95E−08	6.28E−07
^{46}Ti	6.54E−06	5.22E−06	6.23E−06	1.11E−05
^{47}Ti	9.65E−06	9.45E−06	2.08E−05	2.59E−05
^{48}Ti	1.57E−04	1.36E−04	2.81E−04	3.43E−04
^{49}Ti	2.75E−06	3.62E−06	5.70E−06	6.92E−06
^{50}Ti	7.64E−13	6.12E−12	2.49E−12	3.37E−11
^{50}V	2.62E−11	2.79E−11	9.03E−12	1.20E−10
^{51}V	2.42E−05	1.86E−05	3.71E−05	3.48E−05
^{50}Cr	1.68E−05	2.56E−05	1.90E−05	4.13E−05
^{52}Cr	6.58E−04	1.21E−03	1.51E−03	2.70E−03
^{53}Cr	3.33E−05	7.24E−05	9.03E−05	1.31E−04
^{54}Cr	2.61E−09	5.72E−09	9.64E−11	3.52E−09
^{55}Mn	8.22E−05	2.02E−04	2.47E−04	3.68E−04
^{54}Fe	7.18E−04	1.80E−03	1.74E−03	3.30E−03
^{56}Fe	8.24E−02	9.60E−02	1.59E−01	2.56E−01
^{57}Fe	1.78E−03	1.63E−03	3.10E−03	4.24E−03
^{58}Fe	1.28E−09	2.60E−09	9.19E−11	3.31E−09
^{59}Co	3.70E−04	2.38E−04	5.19E−04	5.19E−04
^{58}Ni	8.75E−04	6.72E−04	1.27E−03	1.43E−03
^{60}Ni	2.99E−03	2.80E−03	5.49E−03	8.37E−03
^{61}Ni	6.29E−05	4.34E−05	8.63E−05	9.87E−05
^{62}Ni	4.19E−05	2.86E−05	5.74E−05	6.74E−05
^{64}Ni	9.55E−14	1.56E−11	3.38E−12	2.46E−11
^{63}Cu	1.18E−05	8.19E−06	1.72E−05	2.06E−05
^{65}Cu	7.24E−07	6.01E−07	1.39E−06	1.86E−06
^{64}Zn	3.80E−04	2.64E−04	5.83E−04	6.88E−04
^{66}Zn	5.06E−06	2.59E−06	7.05E−06	6.90E−06
^{67}Zn	1.95E−07	6.07E−08	1.91E−07	1.18E−07
^{68}Zn	8.96E−08	1.21E−07	2.69E−07	4.87E−07
^{70}Zn	8.31E−14	1.95E−12	8.49E−13	1.95E−11
^{69}Ga	1.77E−08	2.11E−08	4.08E−08	8.95E−08
^{71}Ga	1.54E−12	2.17E−11	3.79E−12	1.57E−10
^{70}Ge	2.42E−08	1.44E−08	2.95E−08	3.75E−08
^{72}Ge	6.38E−12	1.69E−11	7.43E−12	7.11E−11
^{73}Ge	1.86E−12	2.64E−11	6.59E−12	9.15E−11
^{74}Ge	2.44E−13	1.32E−11	2.47E−12	4.28E−11
		$Z = 0.001$		
$M_{\rm final}$	19.71	24.45	29.05	37.82
$M_{\rm cut}$	2.24	2.15	2.57	5.52
p	8.43E+00	9.80E+00	1.11E+01	1.29E+01
D	4.10E−16	4.47E−16	1.53E−13	2.66E−15
^{3}He	1.60E−04	1.26E−04	1.44E−04	1.21E−04
^{4}He	5.96E+00	7.00E+00	8.43E+00	1.08E+01
^{6}Li	9.37E−22	4.74E−21	5.08E−16	7.65E−18
^{7}Li	8.42E−11	9.12E−13	1.12E−12	1.91E−12
^{9}Be	1.72E−21	2.54E−25	2.59E−16	1.35E−18
^{10}B	2.37E−12	7.60E−12	2.25E−12	2.02E−12
^{11}B	1.05E−11	3.42E−11	1.01E−11	8.36E−12
^{12}C	1.24E−01	1.94E−01	1.05E−01	5.08E−02
^{13}C	1.96E−05	9.81E−05	8.20E−05	2.82E−04
^{14}N	1.29E−02	9.20E−03	6.19E−03	8.53E−03
^{15}N	1.37E−06	7.24E−06	9.07E−07	3.17E−06
^{16}O	2.00E+00	3.70E+00	4.95E+00	6.42E+00
^{17}O	2.18E−05	2.79E−05	4.87E−05	2.83E−05
^{18}O	8.10E−06	7.05E−05	1.99E−05	1.76E−04
^{19}F	2.81E−06	6.07E−07	2.04E−06	1.65E−06
^{20}Ne	4.56E−01	1.05E+00	1.05E+00	1.83E−01
^{21}Ne	9.70E−05	4.23E−04	4.43E−04	2.16E−05
^{22}Ne	1.17E−03	1.44E−03	1.26E−03	1.25E−04
^{23}Na	1.29E−03	6.76E−03	4.68E−03	6.04E−04
^{24}Mg	2.30E−01	1.93E−01	3.11E−01	5.20E−01
^{25}Mg	1.74E−03	1.52E−03	2.79E−03	1.64E−03
^{26}Mg	1.75E−03	1.76E−03	3.21E−03	9.18E−04
^{27}Al	6.32E−03	5.17E−03	8.70E−03	1.96E−02
^{28}Si	1.14E−01	1.12E−01	2.36E−01	7.14E−01
^{29}Si	1.28E−03	7.80E−04	1.69E−03	6.22E−03
^{30}Si	1.07E−03	4.86E−04	1.24E−03	8.00E−03
^{31}P	2.71E−04	1.84E−04	3.95E−04	2.67E−03
^{32}S	3.63E−02	4.25E−02	9.25E−02	2.80E−01
^{33}S	1.80E−04	2.13E−04	4.11E−04	1.20E−03
^{34}S	5.11E−04	4.16E−04	1.02E−03	3.74E−03
^{36}S	3.31E−07	5.67E−07	9.40E−07	9.90E−07
^{35}Cl	3.80E−05	5.36E−05	1.01E−04	3.55E−04
^{37}Cl	1.38E−05	1.92E−05	3.75E−05	8.89E−05
^{36}Ar	5.55E−03	6.86E−03	1.40E−02	3.67E−02

TABLE 2—*Continued*

TABLE 2—*Continued*

Element	Yields (in $M_\odot$) for M = 20	25	30	40
^{38}Ar	1.43E−04	1.18E−04	3.61E−04	1.24E−03
^{40}Ar	4.53E−08	8.65E−08	2.54E−07	3.89E−07
^{39}K	2.05E−05	1.76E−05	5.43E−05	1.61E−04
^{40}K	6.87E−09	1.10E−08	1.23E−08	3.11E−08
^{41}K	2.64E−06	2.25E−06	7.08E−06	2.06E−05
^{40}Ca	4.49E−03	5.46E−03	1.10E−02	2.93E−02
^{42}Ca	3.70E−06	2.18E−06	8.11E−06	3.10E−05
^{43}Ca	3.78E−07	4.93E−07	6.45E−07	4.08E−07
^{44}Ca	1.30E−04	1.33E−04	2.44E−04	1.57E−04
^{46}Ca	2.46E−08	2.66E−08	1.10E−07	1.90E−07
^{48}Ca	1.19E−07	1.51E−07	1.81E−07	2.14E−07
^{45}Sc	2.13E−07	3.18E−07	5.55E−07	1.04E−06
^{46}Ti	3.79E−06	1.34E−05	1.30E−05	1.52E−05
^{47}Ti	4.83E−06	2.80E−05	3.27E−05	1.93E−05
^{48}Ti	1.65E−04	1.80E−04	3.25E−04	3.33E−04
^{49}Ti	2.70E−06	2.74E−06	5.41E−06	8.76E−06
^{50}Ti	4.09E−07	7.50E−07	9.05E−07	7.63E−07
^{50}V	7.18E−09	1.23E−08	1.72E−08	5.05E−08
^{51}V	1.19E−05	5.45E−05	4.73E−05	2.75E−05
^{50}Cr	1.24E−05	2.01E−05	2.68E−05	5.49E−05
^{52}Cr	7.39E−04	8.99E−04	1.53E−03	2.97E−03
^{53}Cr	3.97E−05	3.81E−05	7.11E−05	1.63E−04
^{54}Cr	1.15E−06	1.95E−06	2.28E−06	1.97E−06
^{55}Mn	1.09E−04	1.12E−04	1.96E−04	4.66E−04
^{54}Fe	8.40E−04	1.18E−03	1.94E−03	4.06E−03
^{56}Fe	8.06E−02	1.50E−01	2.00E−01	2.59E−01
^{57}Fe	2.05E−03	2.79E−03	3.83E−03	4.21E−03
^{58}Fe	3.93E−05	6.84E−05	7.77E−05	6.60E−05
^{59}Co	1.55E−04	6.60E−04	7.86E−04	4.49E−04
^{58}Ni	5.66E−04	1.10E−03	1.69E−03	1.39E−03
^{60}Ni	2.75E−03	6.17E−03	7.02E−03	7.93E−03
^{61}Ni	8.43E−05	1.15E−04	1.31E−04	1.31E−04
^{62}Ni	5.49E−05	1.03E−04	1.16E−04	1.17E−04
^{64}Ni	1.82E−05	3.78E−05	4.87E−05	4.48E−05
^{63}Cu	1.46E−05	3.36E−05	3.88E−05	2.62E−05
^{65}Cu	7.79E−06	1.45E−05	2.08E−05	2.17E−05
^{64}Zn	3.34E−04	5.24E−04	7.85E−04	6.51E−04
^{66}Zn	1.72E−05	2.46E−05	4.11E−05	4.89E−05
^{67}Zn	1.68E−06	3.50E−06	4.84E−06	2.55E−06
^{68}Zn	7.85E−06	1.67E−05	2.49E−05	2.89E−05
^{70}Zn	2.42E−08	2.37E−08	1.08E−07	1.90E−07
^{69}Ga	1.21E−06	2.16E−06	3.84E−06	4.16E−06
^{71}Ga	8.48E−07	1.80E−06	3.02E−06	3.40E−06
^{70}Ge	2.17E−06	4.35E−06	7.57E−06	7.74E−06
^{72}Ge	1.71E−06	3.75E−06	6.13E−06	9.92E−06
^{73}Ge	3.14E−07	6.35E−07	1.15E−06	5.08E−07
^{74}Ge	3.18E−06	8.03E−06	1.34E−05	1.54E−05
	Z = 0.004			
$M_{\rm final}$	19.51	24.02	27.55	32.93
$M_{\rm cut}$	2.23	1.97	4.05	4.51
p	8.95E+00	1.02E+01	1.01E+01	1.03E+01
D	1.84E−13	2.01E−13	2.89E−13	3.88E−14
^{3}He	1.75E−04	1.85E−04	1.84E−04	1.80E−04
^{4}He	7.03E+00	8.49E+00	7.93E+00	8.12E+00
^{6}Li	6.12E−16	6.65E−16	9.58E−16	1.29E−16
^{7}Li	4.31E−13	1.02E−13	8.01E−13	4.62E−12
^{9}Be	6.27E−16	3.94E−16	1.88E−16	9.49E−18
^{10}B	2.91E−11	3.09E−11	3.04E−11	6.57E−12
^{11}B	2.79E−09	1.39E−10	1.37E−10	2.83E−11
^{12}C	8.32E−02	1.28E−01	1.36E−01	3.73E−01
^{13}C	2.91E−04	3.83E−04	3.39E−04	3.68E−04
^{14}N	1.84E−02	3.15E−02	2.01E−02	2.52E−02
^{15}N	2.74E−05	9.45E−05	5.59E−06	1.35E−05

TABLE 2—*Continued*

Element	Yields (in $M_\odot$) for M = 20	25	30	40
^{16}O	7.88E−01	2.07E+00	3.82E+00	6.80E+00
^{17}O	1.03E−04	1.12E−04	1.20E−04	1.57E−04
^{18}O	6.68E−04	7.80E−04	4.38E−05	6.51E−04
^{19}F	4.87E−06	8.48E−05	5.57E−06	8.50E−06
^{20}Ne	1.42E−01	6.35E−01	4.92E−01	1.15E+00
^{21}Ne	3.12E−04	3.57E−04	4.13E−04	8.62E−04
^{22}Ne	1.42E−03	4.54E−03	3.00E−03	7.99E−04
^{23}Na	2.05E−03	4.68E−03	6.56E−03	1.32E−02
^{24}Mg	8.10E−02	2.27E−01	1.91E−01	4.01E−01
^{25}Mg	1.64E−03	4.78E−03	4.94E−03	9.65E−03
^{26}Mg	1.70E−03	5.27E−03	5.64E−03	1.02E−02
^{27}Al	3.64E−03	1.04E−02	1.18E−02	2.29E−02
^{28}Si	1.04E−01	1.22E−01	3.56E−01	5.74E−01
^{29}Si	1.78E−03	2.27E−03	4.86E−03	6.63E−03
^{30}Si	1.99E−03	2.32E−03	4.83E−03	7.37E−03
^{31}P	4.68E−04	5.29E−04	1.35E−03	2.00E−03
^{32}S	3.30E−02	4.02E−02	1.54E−01	2.30E−01
^{33}S	2.93E−04	3.05E−04	1.05E−03	1.52E−03
^{34}S	1.39E−03	1.25E−03	4.80E−03	7.22E−03
^{36}S	5.15E−06	2.32E−06	8.75E−06	1.23E−05
^{35}Cl	7.46E−05	8.11E−05	2.90E−04	4.16E−04
^{37}Cl	2.39E−05	3.41E−05	1.06E−04	1.58E−04
^{36}Ar	4.40E−03	6.02E−03	2.28E−02	3.40E−02
^{38}Ar	4.28E−04	3.78E−04	1.78E−03	2.48E−03
^{40}Ar	1.46E−06	3.81E−07	2.87E−06	1.93E−06
^{39}K	4.32E−05	4.15E−05	1.72E−04	2.15E−04
^{40}K	2.25E−08	3.29E−08	8.55E−08	1.08E−07
^{41}K	4.38E−06	4.66E−06	1.90E−05	2.33E−05
^{40}Ca	3.07E−03	4.69E−03	1.67E−02	2.55E−02
^{42}Ca	1.09E−05	9.19E−06	4.44E−05	5.81E−05
^{43}Ca	1.09E−06	9.55E−07	1.12E−06	2.18E−06
^{44}Ca	2.86E−05	1.06E−04	1.12E−04	2.26E−04
^{46}Ca	2.35E−07	1.43E−07	6.94E−07	4.28E−07
^{48}Ca	1.07E−06	6.03E−07	9.78E−07	1.36E−06
^{45}Sc	6.09E−07	6.12E−07	1.52E−06	1.79E−06
^{46}Ti	4.52E−06	7.87E−06	1.99E−05	2.55E−05
^{47}Ti	1.57E−06	8.80E−06	1.23E−05	1.24E−05
^{48}Ti	4.89E−05	1.59E−04	2.30E−04	4.30E−04
^{49}Ti	1.49E−06	4.46E−06	6.49E−06	1.16E−05
^{50}Ti	8.29E−07	1.96E−06	2.54E−06	4.85E−06
^{50}V	1.02E−08	2.02E−08	4.10E−08	7.58E−08
^{51}V	3.17E−06	2.26E−05	2.18E−05	2.74E−05
^{50}Cr	1.49E−05	2.05E−05	5.69E−05	8.03E−05
^{52}Cr	2.69E−04	8.48E−04	1.71E−03	3.28E−03
^{53}Cr	2.14E−05	5.36E−05	1.06E−04	1.99E−04
^{54}Cr	2.34E−06	5.15E−06	5.76E−06	9.29E−06
^{55}Mn	9.05E−05	1.67E−04	3.26E−04	5.81E−04
^{54}Fe	8.16E−04	1.17E−03	3.00E−03	4.98E−03
^{56}Fe	3.11E−02	8.33E−02	1.53E−01	2.74E−01
^{57}Fe	9.93E−04	1.93E−03	3.31E−03	6.26E−03
^{58}Fe	5.48E−05	1.62E−04	1.77E−04	2.84E−04
^{59}Co	4.90E−05	3.67E−04	3.31E−04	4.47E−04
^{58}Ni	3.00E−04	9.15E−04	9.42E−04	1.51E−03
^{60}Ni	1.01E−03	2.98E−03	4.92E−03	8.28E−03
^{61}Ni	1.50E−04	9.23E−05	2.93E−04	3.60E−04
^{62}Ni	1.23E−04	1.72E−04	2.78E−04	6.21E−04
^{64}Ni	1.66E−05	8.07E−05	1.10E−04	2.66E−04
^{63}Cu	8.84E−06	4.24E−05	4.77E−05	9.13E−05
^{65}Cu	7.52E−06	2.84E−05	4.86E−05	1.12E−04
^{64}Zn	3.63E−05	3.19E−04	3.56E−04	5.84E−04
^{66}Zn	2.10E−05	4.85E−05	1.08E−04	2.13E−04
^{67}Zn	1.45E−06	7.12E−06	1.14E−05	2.81E−05
^{68}Zn	7.86E−06	3.70E−05	7.55E−05	1.84E−04
^{70}Zn	2.39E−07	1.97E−07	1.33E−06	2.98E−06
^{69}Ga	1.36E−06	5.39E−06	1.49E−05	3.43E−05

TABLE 2—*Continued*

Element	Yields (in $M_\odot$) for M = 20	25	30	40
^{71}Ga	1.10E−06	3.95E−06	9.36E−06	2.16E−05
^{70}Ge	1.92E−06	8.33E−06	2.37E−05	4.98E−05
^{72}Ge	1.75E−06	8.88E−06	2.69E−05	6.24E−05
^{73}Ge	3.19E−07	1.67E−06	4.28E−06	1.08E−05
^{74}Ge	2.58E−06	1.77E−05	7.00E−05	1.56E−04
	Z = 0.02			
M_{final}	18.36	21.63	24.58	21.84
M_{cut}	1.77	2.09	3.05	2.67
p	7.93E+00	8.41E+00	8.75E+00	3.55E+00
D	2.47E−13	1.97E−13	7.25E−13	1.43E−12
^{3}He	2.38E−04	2.21E−04	2.12E−04	5.05E−05
^{4}He	6.76E+00	7.25E+00	8.37E+00	4.78E+00
^{6}Li	8.22E−16	6.56E−16	2.41E−15	4.75E−15
^{7}Li	3.57E−12	5.29E−13	1.56E−14	5.72E−13
^{9}Be	1.21E−16	1.85E−16	6.98E−16	2.43E−15
^{10}B	1.47E−10	1.51E−10	1.55E−10	7.44E−14
^{11}B	6.62E−10	6.79E−10	6.96E−10	3.80E−13
^{12}C	2.09E−01	1.44E−01	1.79E−01	4.90E−01
^{13}C	1.45E−03	6.66E−02	1.92E−03	4.31E−04
^{14}N	7.19E−02	8.43E−02	1.02E−01	5.81E−02
^{15}N	2.53E−04	4.63E−02	1.54E−05	4.26E−05
^{16}O	9.80E−01	2.18E+00	2.74E+00	7.05E+00
^{17}O	9.49E−04	1.34E−03	1.68E−03	9.69E−04
^{18}O	3.98E−03	8.37E−02	2.79E−03	1.04E−02
^{19}F	6.92E−05	1.18E−04	9.33E−06	9.84E−06
^{20}Ne	2.92E−01	6.47E−01	5.41E−01	1.74E+00
^{21}Ne	1.98E−03	1.70E−03	2.57E−03	5.19E−03
^{22}Ne	8.81E−03	1.66E−02	1.13E−02	1.07E−02
^{23}Na	1.20E−02	1.41E−02	1.81E−02	5.76E−02
^{24}Mg	6.88E−02	2.08E−01	1.68E−01	3.29E−01
^{25}Mg	1.12E−02	2.42E−02	2.18E−02	5.82E−02
^{26}Mg	7.52E−03	2.12E−02	2.37E−02	5.94E−02
^{27}Al	8.56E−03	2.34E−02	2.37E−02	7.20E−02
^{28}Si	9.41E−02	1.24E−01	2.67E−01	3.28E−01
^{29}Si	2.95E−03	8.30E−03	1.08E−02	1.70E−02
^{30}Si	3.49E−03	1.10E−02	1.50E−02	1.97E−02
^{31}P	9.79E−04	1.99E−03	3.65E−03	5.43E−03
^{32}S	4.75E−02	4.35E−02	1.08E−01	1.40E−01
^{33}S	5.28E−04	6.07E−04	1.42E−03	1.73E−03
^{34}S	3.77E−03	4.36E−03	1.41E−02	1.69E−02
^{36}S	1.30E−05	2.23E−05	5.90E−05	8.41E−05
^{35}Cl	2.68E−04	1.58E−04	6.05E−04	8.23E−04
^{37}Cl	9.70E−05	1.40E−04	2.33E−04	5.21E−04
^{36}Ar	7.36E−03	6.63E−03	1.41E−02	1.98E−02
^{38}Ar	1.22E−03	5.80E−04	4.51E−03	5.14E−03
^{40}Ar	3.19E−06	3.30E−06	1.36E−05	8.04E−06
^{39}K	1.37E−04	6.78E−05	2.58E−04	2.56E−04
^{40}K	1.79E−07	2.25E−07	5.09E−07	9.26E−07
^{41}K	1.37E−05	1.11E−05	2.65E−05	4.65E−05
^{40}Ca	4.99E−03	5.67E−03	9.29E−03	1.42E−02
^{42}Ca	3.53E−05	1.34E−05	1.12E−04	1.24E−04
^{43}Ca	2.84E−06	3.57E−06	6.10E−06	7.56E−06
^{44}Ca	5.12E−05	9.93E−05	1.28E−04	4.13E−04
^{46}Ca	9.08E−07	1.33E−06	2.39E−06	3.71E−06
^{48}Ca	2.95E−06	2.77E−06	1.23E−05	2.69E−06
^{45}Sc	1.83E−06	2.71E−06	4.44E−06	6.81E−06
^{46}Ti	1.66E−05	7.32E−06	4.58E−05	5.62E−05
^{47}Ti	5.70E−06	8.09E−06	1.28E−05	3.99E−05
^{48}Ti	7.37E−05	1.66E−04	2.27E−04	5.93E−04
^{49}Ti	4.41E−06	8.24E−06	1.17E−05	1.84E−05
^{50}Ti	5.21E−06	1.06E−05	8.54E−06	3.31E−05
^{50}V	5.94E−08	1.40E−07	3.68E−07	3.69E−07
^{51}V	1.09E−05	1.55E−05	2.48E−05	6.58E−05

TABLE 2—*Continued*

Element	Yields (in $M_\odot$) for M = 20	25	30	40
^{50}Cr	7.07E−05	2.02E−05	9.87E−05	1.21E−04
^{52}Cr	4.11E−04	9.25E−04	1.45E−03	2.47E−03
^{53}Cr	5.54E−05	7.52E−05	1.34E−04	1.44E−04
^{54}Cr	1.48E−05	2.42E−05	3.72E−05	4.99E−05
^{55}Mn	3.18E−04	3.53E−04	5.85E−04	4.94E−04
^{54}Fe	3.79E−03	2.12E−03	4.03E−03	5.89E−03
^{56}Fe	3.57E−02	8.87E−02	1.04E−01	2.77E−01
^{57}Fe	1.22E−03	2.83E−03	4.11E−03	8.90E−03
^{58}Fe	4.24E−04	7.36E−04	1.77E−03	1.36E−03
^{59}Co	2.43E−04	4.22E−04	6.60E−04	1.42E−03
^{58}Ni	1.52E−03	2.12E−03	3.38E−03	7.14E−03
^{60}Ni	1.20E−03	3.14E−03	3.33E−03	1.12E−02
^{61}Ni	2.43E−04	2.97E−04	9.10E−04	8.55E−04
^{62}Ni	3.69E−04	8.87E−04	8.34E−04	2.97E−03
^{64}Ni	1.60E−04	5.10E−04	6.97E−05	1.95E−03
^{63}Cu	9.89E−05	2.32E−04	6.14E−05	5.85E−04
^{65}Cu	4.15E−05	1.34E−04	2.02E−05	5.70E−04
^{64}Zn	5.27E−05	1.35E−04	8.32E−05	6.38E−04
^{66}Zn	7.13E−05	2.35E−04	7.40E−05	1.02E−03
^{67}Zn	1.17E−05	4.38E−05	3.01E−06	2.31E−04
^{68}Zn	5.33E−05	2.75E−04	1.19E−05	1.43E−03
^{70}Zn	2.45E−06	8.48E−06	5.89E−07	5.62E−05
^{69}Ga	6.82E−06	2.69E−05	1.27E−06	1.61E−04
^{71}Ga	4.95E−06	2.39E−05	2.26E−06	1.29E−04
^{70}Ge	8.72E−06	3.81E−05	2.04E−06	2.40E−04
^{72}Ge	9.95E−06	6.93E−05	4.13E−06	4.09E−04
^{73}Ge	2.48E−06	1.36E−05	7.62E−07	9.51E−05
^{74}Ge	2.08E−05	1.65E−04	3.19E−05	1.38E−03

NOTE.—Table 2 is also available in machine-readable form in the electronic edition of the *Astrophysical Journal*.

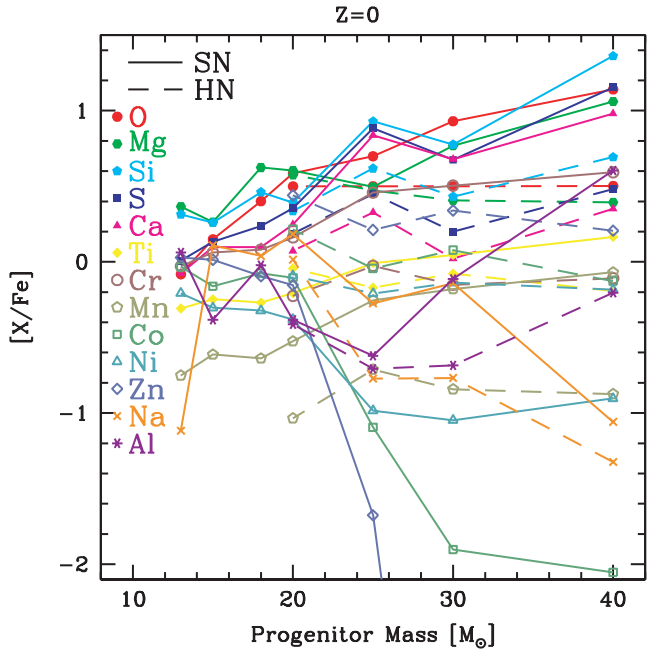

FIG. 1.—Relative abundance ratios as a function of the progenitor mass with $Z = 0$. The solid and dashed lines show normal SNe II with $E_{51} = 1$ and HNe, respectively.

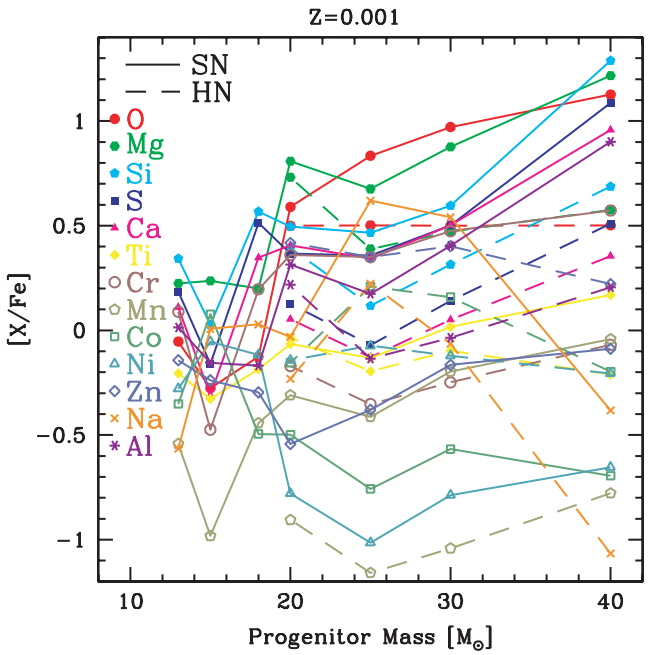

FIG. 2.—Same as Fig. 1, but for $Z = 0.001$.

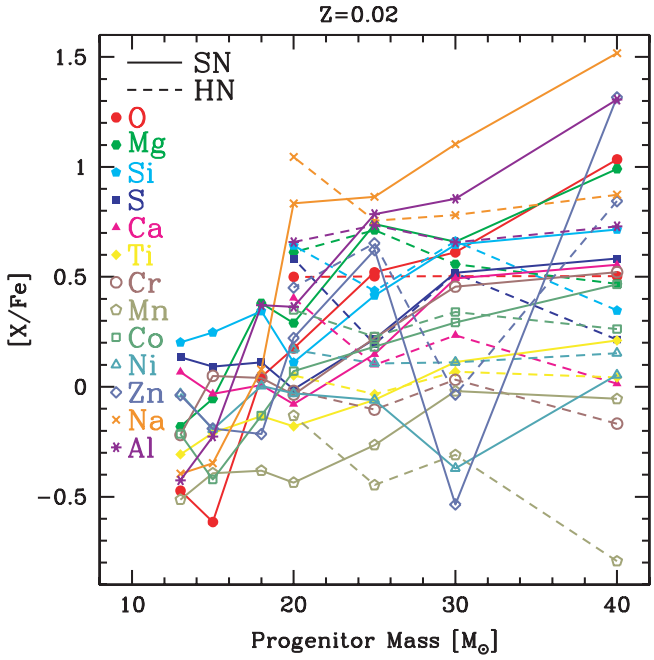

FIG. 4.—Same as Fig. 1, but for $Z = 0.02$.

with a timescale of 2.2 Gyr, which is constrained from the present gas fraction $f_g = 0.15$. The metallicity-dependent main-sequence lifetime is taken from Kodama & Arimoto (1997).

The treatment of SNe Ia is the same as in K98 and K00. The lifetime distribution is given by the mass ranges of companion stars in WD binary systems, which are constrained from the binary evolution (Hachisu et al. 1996, 1999a, 1999b). The fraction of primary stars that eventually produce SNe Ia is given by the parameters $b_{\rm RG}$ and $b_{\rm MS}$, respectively, for the main-sequence (MS) and red-giant (RG) companions, that are constrained from the [O/Fe]-[Fe/H] relation. The smaller values ($b_{\rm RG} = 0.02$, $b_{\rm MS} = 0.04$) than K98 and K00 are adopted for the WD+RG and the WD+MS systems, respectively, because more Fe is produced by HNe. The metallicity effect of SNe Ia (K98) is also taken into account. To produce SNe Ia, optically thick winds should be brown from the accreting WDs in the binary systems, which requires a large enough Fe opacity. If [Fe/H] < -1.1, no SN Ia can occur from these binary systems.

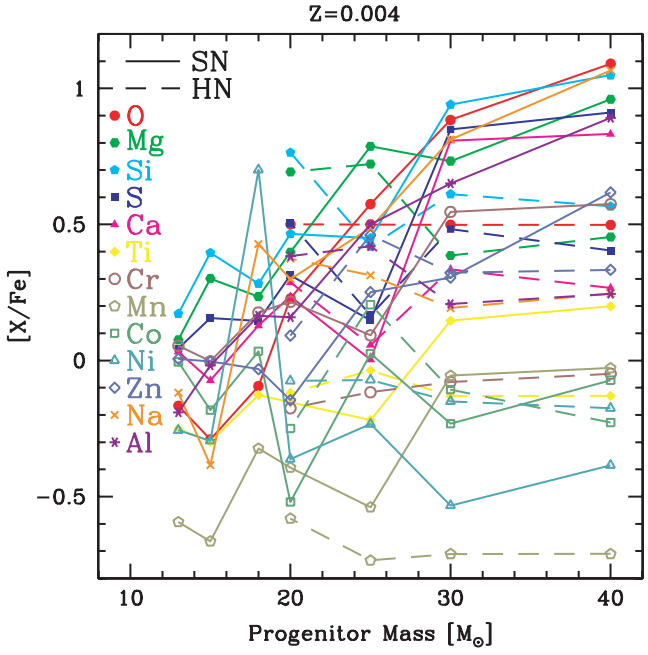

FIG. 3.—Same as Fig. 1, but for $Z = 0.004$.

These parameters are constrained from the chemical evolution of the solar neighborhood, and are determined as follows. Figure 6*a* shows the SFR, Figure 6*b* shows the age-metallicity relation, and Figure 6*c* shows the MDF in the solar neighborhood. The solid and dashed lines show the results of this work and K98 model with N97 yields, respectively. Our SFRs peak at ~8 Gyr (Fig. 6*a*), which is later than previous models (Chiappini et al. 1997; Fenner & Gibson 2003). The sources of this difference may be as follows. (1) We adopt the time-dependent infall rate, while others adopted the double-infall rate. (2) The adopted parameters such as the star formation timescale are different, because these parameters are chosen in order to reproduce the present gas fraction and the MDF for different set of the adopted SN Ia model, nucleosynthesis yields, IMF, and the Galactic age. As a result, these models can give an identical MDF, and the resulting [X/Fe]-[Fe/H] relations do not differ at all.

The iron abundance (Fig. 6*b*) increases quickly by SNe II and HNe at $t \lesssim 3$ Gyr to reach [Fe/H] ~ -1, and then gradually by SNe Ia. [Fe/H] reaches 0 at ~12 Gyr in our models, which is consistent with the average of the observational data (Edvardsson et al. 1993; Nordström et al. 2004). This means that the solar system has formed in a relatively metal-enhanced region. At $t \lesssim 3$ Gyr, our [Fe/H] looks lower than the observations, but this is because there are many stars with unreasonably old ages in the observational data, owing to the difficulty of the age estimate. The slow accretion and slow star formation are required from the lack of metal-poor stars in the MDF (Fig. 6*c*). The observed MDF (Edvardsson et al. 1993; Wyse & Gilmore 1995) is reproduced with our model by adopting a 0.15 dex convolution that corresponds to an observational error. Recently, Nordström et al. (2004) showed a narrower MDF. We find that our model with 0.1 dex convolution is nearly consistent with this new MDF.

TABLE 3

IMF-weighted Yields with $x = 1.35$, $M_l = 0.07\ M_\odot$, and $M_u = 50\ M_\odot$

Element	SN II + HN for Z = 0	0.001	0.004	0.02	SN Ia
p	3.28E−02	3.14E−02	2.96E−02	2.45E−02	0.00E+00
D	5.76E−18	2.21E−15	1.97E−16	5.34E−16	0.00E+00
^{3}He	2.51E−07	5.24E−07	6.52E−07	7.06E−07	0.00E+00
^{4}He	2.30E−02	2.26E−02	2.22E−02	2.05E−02	5.66E−03
^{6}Li	1.70E−20	1.52E−19	6.49E−19	1.76E−18	0.00E+00
^{7}Li	8.67E−12	6.67E−13	3.14E−15	5.85E−14	0.00E+00
^{9}Be	1.25E−20	7.74E−19	6.54E−19	7.26E−19	0.00E+00
^{10}B	1.86E−17	2.38E−14	1.47E−13	4.25E−13	0.00E+00
^{11}B	5.00E−16	1.05E−13	1.12E−11	1.83E−12	0.00E+00
^{12}C	7.51E−04	4.14E−04	5.17E−04	6.75E−04	4.83E−02
^{13}C	1.75E−10	4.33E−07	2.80E−05	3.06E−05	1.40E−06
^{14}N	3.36E−06	2.82E−05	8.77E−05	2.35E−04	1.16E−06
^{15}N	5.17E−10	1.35E−08	2.41E−05	1.90E−05	1.32E−09
^{16}O	8.03E−03	8.05E−03	6.58E−03	6.14E−03	1.43E−01
^{17}O	3.45E−09	1.42E−07	8.36E−07	3.60E−06	3.54E−08
^{18}O	5.69E−09	2.24E−06	2.70E−05	5.29E−05	8.25E−10
^{19}F	3.49E−11	6.76E−09	4.98E−08	1.08E−07	5.67E−10
^{20}Ne	1.28E−03	1.38E−03	1.57E−03	1.68E−03	2.02E−03
^{21}Ne	1.05E−07	6.66E−07	1.62E−06	4.95E−06	8.46E−06
^{22}Ne	7.53E−08	3.39E−06	8.01E−06	2.79E−05	2.49E−03
^{23}Na	4.46E−06	8.18E−06	2.03E−05	5.41E−05	6.32E−05
^{24}Na	5.69E−04	6.69E−04	4.88E−04	4.06E−04	8.50E−03
^{25}Mg	9.62E−07	5.62E−06	1.59E−05	6.08E−05	4.05E−05
^{26}Mg	9.19E−07	5.04E−06	1.57E−05	5.68E−05	3.18E−05
^{27}Al	1.27E−05	2.49E−05	2.95E−05	6.53E−05	9.86E−04
^{28}Si	8.11E−04	7.09E−04	6.17E−04	4.55E−04	1.50E−01
^{29}Si	3.03E−06	5.90E−06	7.62E−06	1.88E−05	8.61E−04
^{30}Si	3.40E−06	7.40E−06	9.24E−06	2.12E−05	1.74E−03
^{31}P	1.28E−06	2.34E−06	2.14E−06	5.54E−06	4.18E−04
^{32}S	3.12E−04	2.86E−04	2.50E−04	1.96E−04	8.41E−02
^{33}S	8.06E−07	1.03E−06	1.17E−06	1.62E−06	4.50E−04
^{34}S	1.70E−06	3.20E−06	6.09E−06	1.31E−05	1.90E−03
^{36}S	3.84E−11	1.98E−09	1.48E−08	8.19E−08	3.15E−07
^{35}Cl	2.18E−07	3.34E−07	3.49E−07	7.91E−07	1.34E−04
^{37}Cl	8.78E−08	8.89E−08	1.50E−07	4.89E−07	3.98E−05
^{36}Ar	4.54E−05	4.21E−05	3.80E−05	3.03E−05	1.49E−02
^{38}Ar	8.47E−07	1.11E−06	2.29E−06	4.51E−06	1.06E−03
^{40}Ar	2.42E−13	4.64E−10	3.34E−09	1.02E−08	1.26E−08
^{39}K	1.16E−07	1.41E−07	2.08E−07	3.41E−07	8.52E−05
^{40}K	1.39E−11	6.81E−11	1.29E−10	7.86E−10	0.00E+00
^{41}K	2.25E−08	1.92E−08	2.25E−08	4.91E−08	7.44E−06
^{40}Ca	3.58E−05	3.34E−05	3.02E−05	2.39E−05	1.23E−02
^{42}Ca	1.95E−08	2.95E−08	5.48E−08	1.12E−07	3.52E−05
^{43}Ca	2.58E−10	1.30E−09	3.25E−09	9.89E−09	1.03E−07
^{44}Ca	1.50E−07	1.74E−07	1.61E−07	2.65E−07	8.86E−06
^{46}Ca	5.69E−14	2.06E−10	8.71E−10	3.60E−09	1.99E−09
^{48}Ca	8.04E−15	6.91E−10	2.93E−09	1.07E−08	7.10E−12
^{45}Sc	6.48E−10	1.26E−09	2.55E−09	7.59E−09	2.47E−07
^{46}Ti	2.02E−08	2.61E−08	3.03E−08	5.11E−08	1.71E−05
^{47}Ti	2.71E−08	2.70E−08	1.84E−08	2.80E−08	6.04E−07
^{48}Ti	4.58E−07	4.98E−07	4.97E−07	5.70E−07	2.03E−04
^{49}Ti	1.56E−08	1.77E−08	2.09E−08	3.07E−08	1.69E−05
^{50}Ti	1.52E−14	2.04E−09	7.64E−09	3.16E−08	1.26E−05
^{50}V	2.88E−13	5.92E−11	9.07E−11	3.42E−10	8.28E−09
^{51}V	6.03E−08	5.76E−08	5.09E−08	6.13E−08	5.15E−05
^{50}Cr	1.14E−07	1.12E−07	1.33E−07	1.72E−07	2.71E−04
^{52}Cr	5.45E−06	5.51E−06	5.76E−06	5.06E−06	5.15E−03
^{53}Cr	3.17E−07	3.30E−07	3.68E−07	3.81E−07	7.85E−04
^{54}Cr	2.73E−11	5.57E−09	1.84E−08	7.09E−08	1.90E−04
^{55}Mn	8.72E−07	9.72E−07	1.16E−06	1.54E−06	8.23E−03
^{54}Fe	7.32E−06	8.34E−06	9.03E−06	1.13E−05	1.04E−01
^{56}Fe	3.17E−04	3.38E−04	3.22E−04	3.48E−04	6.13E−01
^{57}Fe	4.66E−06	6.03E−06	6.79E−06	9.57E−06	2.55E−02
^{58}Fe	6.15E−12	1.81E−07	5.26E−07	2.15E−06	9.63E−04
^{59}Co	6.82E−07	6.72E−07	7.47E−07	1.20E−06	1.02E−03
^{58}Ni	1.96E−06	3.12E−06	1.22E−05	8.12E−06	1.28E−01
^{60}Ni	8.03E−06	8.48E−06	7.61E−06	9.46E−06	1.05E−02
^{61}Ni	1.26E−07	2.17E−07	4.20E−07	8.15E−07	2.51E−04
^{62}Ni	7.54E−08	4.66E−07	1.81E−06	2.12E−06	2.66E−03
^{64}Ni	1.01E−14	8.66E−08	2.89E−07	1.36E−06	1.31E−06
^{63}Cu	2.08E−08	4.44E−08	1.10E−07	5.07E−07	1.79E−06
^{65}Cu	1.36E−09	3.25E−08	1.05E−07	3.84E−07	6.83E−07
^{64}Zn	6.32E−07	5.74E−07	5.07E−07	4.43E−07	1.22E−05
^{66}Zn	5.80E−09	6.24E−08	2.03E−07	6.65E−07	2.12E−05
^{67}Zn	1.45E−10	6.43E−09	2.75E−08	1.43E−07	1.34E−08
^{68}Zn	2.67E−10	4.31E−08	1.67E−07	8.69E−07	1.02E−08
^{70}Zn	5.14E−15	3.62E−10	1.85E−09	2.63E−08	0.00E+00
^{69}Ga	4.93E−11	5.26E−09	2.45E−08	9.57E−08	0.00E+00
^{71}Ga	4.22E−14	4.81E−09	1.87E−08	7.68E−08	0.00E+00
^{70}Ge	3.67E−11	9.13E−09	3.62E−08	1.45E−07	0.00E+00
^{72}Ge	2.34E−14	1.13E−08	5.05E−08	2.44E−07	0.00E+00
^{73}Ge	2.83E−14	1.28E−09	8.59E−09	5.62E−08	0.00E+00
^{74}Ge	1.33E−14	2.18E−08	1.35E−07	7.93E−07	0.00E+00

Note.—Table 3 is also available in machine-readable form in the electronic edition of the *Astrophysical Journal*.

The peak metallicity of the MDF strongly depends on the slope x of the IMF. Under the above assumptions of x and M_u, the combination of M_l and $b_{\rm RG}$ is constrained from the high-metallicity edge of the MDF. We choose b parameters to give better agreement with the [O/Fe]-[Fe/H] evolutionary trend at [Fe/H] $\gtrsim -1$.

3.2. *Evolution of* [X/Fe] *against* [Fe/H]

Figures 7–28 show the evolutions of heavy-element abundance ratios [X/Fe] against [Fe/H]. Our model with new yields (*solid line*) are in much better agreement with the observational data

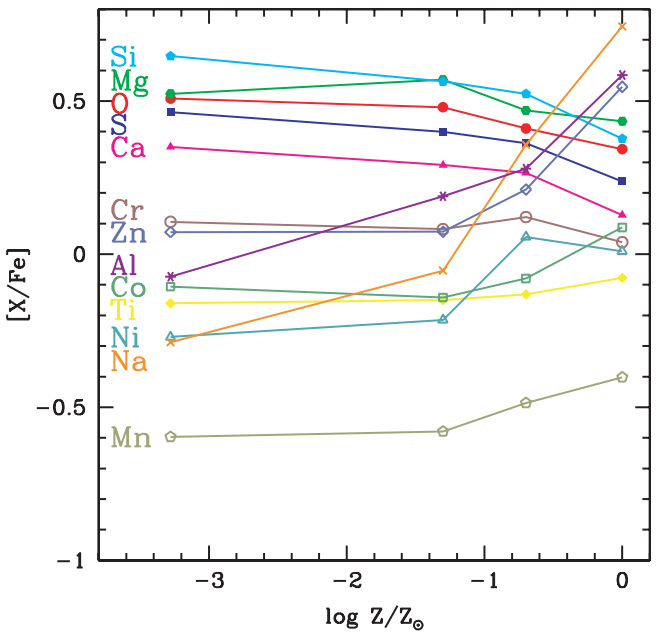

Fig. 5.—IMF-weighted abundance ratios as a function of metallicity of progenitors, where the HN fraction $\epsilon_{\rm HN} = 0.5$ is adopted. The $Z = 0$ results are plotted at $\log Z = -5$.

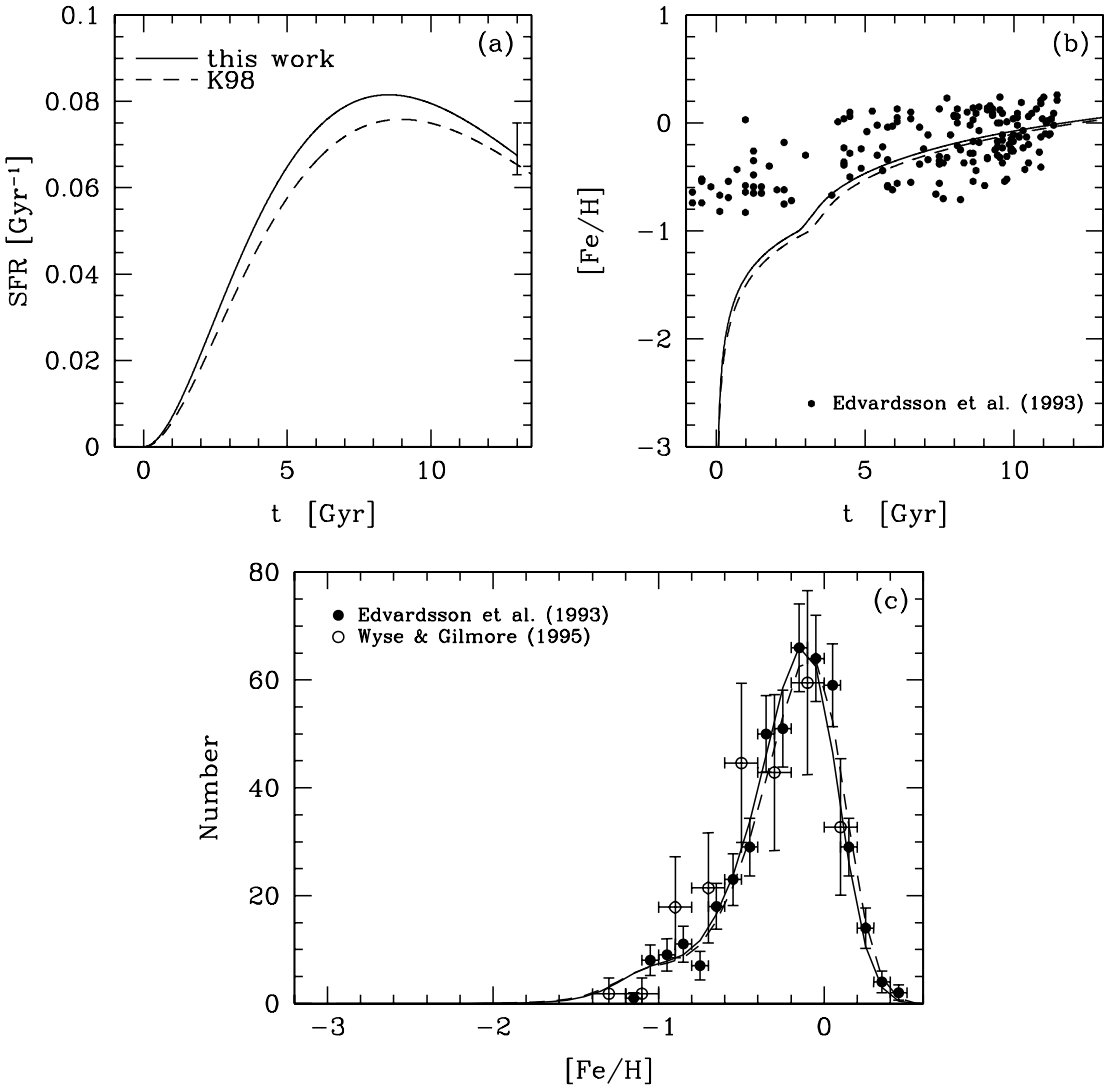

FIG. 6.—Chemical evolution of the solar neighborhood: (*a*) star formation rate, (*b*) age-metallicity relation, and (*c*) metallicity distribution function for the model with our yields (*solid line*) and K98 model with N97 yields (*dashed line*). Observational data sources are Matteucci (1997; *error bar*) in (*a*); Edvardsson et al. (1993; *filled circles*) in (*b*) and (*c*); and Wyse & Gilmore (1995; *open circles*) in (*c*).

than K98 model with N97 yields (*dashed line*), especially for Al, Na, Ca, and Zn. As the time goes, the iron abundance increases, and the abundance ratio for many elements stays constant with a plateau value at $[\mathrm{Fe/H}] \lesssim -1$, which is determined only by SNe II and HNe. From $[\mathrm{Fe/H}] \sim -1$, SNe Ia start to occur (see K98 for SN Ia models) producing more Fe than α-elements, and thus, $[\alpha/\mathrm{Fe}]$ decreases toward the solar abundance. In §§ 3.2.1–3.2.9, we discuss the details for each element.

3.2.1. *Oxygen*

Oxygen is the most abundant heavy element, which covers one-half of the metallicity for the solar abundance and is one of the best-described elements in nucleosynthesis. However, the observation has been debated. (1) The abundances determined from the forbidden line [O I] at 6300 Å in giants show a plateau, with $[\mathrm{O/Fe}] \sim 0.4$–0.5. (2) Those from the near-infrared (IR) triplet O I at 7774 Å in unevolved subdwarfs suggest that [O/Fe] gradually increases with decreasing [Fe/H] to reach $[\mathrm{O/Fe}] \sim 0.8$ at $[\mathrm{Fe/H}] \sim -3$. 3) Those from the OH line in the near-ultraviolet (UV) of unevolved stars show a monotonic increase with a steeper slope from $[\mathrm{Fe/H}] \sim [\mathrm{O/Fe}] \sim 0$ to $[\mathrm{Fe/H}] \sim -3$ and $[\mathrm{O/Fe}] \sim 1$ (Israelian et al. 1998, 2001; Boesgaard et al. 1999). However, when a suitable temperature scale is adopted and the non–local thermodynamic equilibrium (NLTE) and three-dimensional effects are taken into account, [O I], O I, and IR OH lines give consistent results. A plateau of $[\mathrm{O/Fe}] \sim 0.3$–0.45 is seen at $-2 \lesssim [\mathrm{Fe/H}] \lesssim -1$, e.g., $[\mathrm{O/Fe}] \sim 0.45$ (Carretta et al. 2000), 0.35 (Melendez & Barbuy 2002), and 0.3 with a three-dimensional correction (Nissen et al. 2002). At $[\mathrm{Fe/H}] \sim -3$, a gentle increase in $[\mathrm{O/Fe}] \sim 0.5$–0.6 is seen, e.g., 0.47 with three-dimensional correction (Cayrel et al. 2004).

C, N, O, Ne, and Mg are mainly produced in the hydrostatic burning phase, so their yields depend mainly on the presupernova model. In our model, [O/Fe] is 0.42 at $[\mathrm{Fe/H}] = -1$ and slightly increases to 0.57 at $[\mathrm{Fe/H}] = -3$, being consistent with the observations (except for UV OH results), as shown in Figure 7. The gradual increase in [O/Fe] with decreasing [Fe/H] stems from larger [O/Fe] in the more massive SNe II, more metal-poor SNe II, and HNe. The metallicity dependence is as small as 0.15 dex between $Z = Z_{\odot}$ and $Z = 0$ (Fig. 5). The mass dependence is large for normal SNe II ($[\mathrm{O/Fe}] \sim -0.5$ to 1 for $Z = Z_{\odot}$; see Figs. 1–4), but such a dependence is weakened by the HN

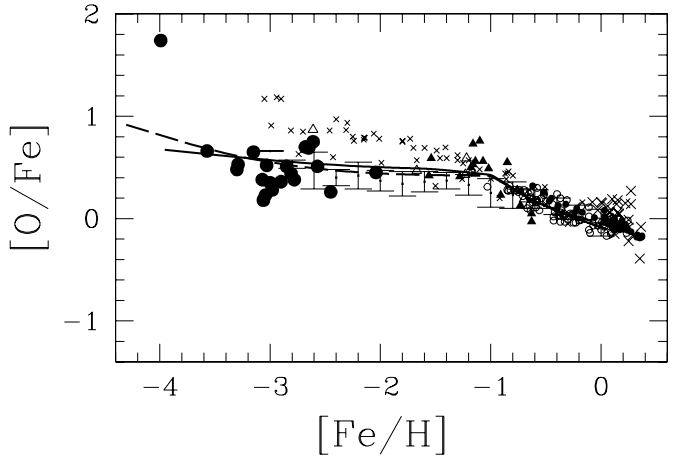

FIG. 7.—[O/Fe]-[Fe/H] relation for the model with our yields (*solid line*) and K98 model with N97 yield (*dashed line*). Observational data sources for disk stars are Edvardsson et al. (1993; *small open circles*), Feltzing & Gustafsson (1998; *crosses*), thin disk stars in Bensby et al. (2004a; *small filled circles*), and the dissipative (*filled triangles*) and accretion (*open triangles*) components in Gratton et al. (2003). Data source for halo stars is Cayrel et al. (2004; *large filled circles*). UV OH observation is shown with small crosses (Israelian et al. 1998 2001) and plus signs (Boesgaard et al. 1999). The error bars show the average taken with [O I] from Melendez & Barbuy (2002). [*See the electronic edition of the Journal for a color version of this figure.*]

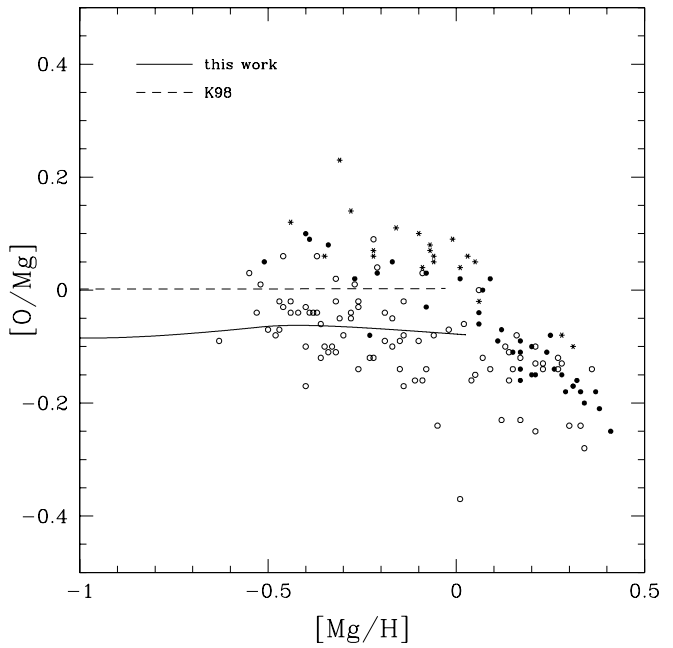

FIG. 9.—[O/Mg] vs. [Mg/H] for the model with our yields (*solid line*) and K98 model with N97 yields (*dashed line*). The observational data are shown with open circles (Edvardsson et al. 1993), and with filled circles and asterisks, respectively, for the thin and thick disk stars (Bensby et al. 2004a).

contribution, because HNe produce more Fe and give constant [O/Fe]. From [Fe/H] ~ -1, [O/Fe] decreases quickly due to a large amount of Fe production by SNe Ia.

Low $[\alpha/\mathrm{Fe}]$ is often used to discuss the formation timescale under the assumption that the SN Ia lifetime is 1.5 Gyr. We note, however, this approach would be misleading if the following effects are not taken into account: the lifetime distribution and the metallicity effect of SNe Ia, the mass and energy dependences of the nucleosynthesis yields of SNe II and HNe, and an uncertainty of the IMF. (1) The enrichment by SNe Ia results in low $[\alpha/\mathrm{Fe}]$. The shortest lifetime of SNe Ia depends on the SN Ia model: $\sim$0.1 Gyr for the double-degenerate (Tutukov & Yungelson 1994), $\sim$0.3 Gyr for the Matteucci & Recchi (2001) model, and $\sim$0.5 Gyr for our single-degenerate model (K98). (2) Some anomalous stars (e.g., Nissen & Schuster 1997) have [O/Fe] ~ 0 at [Fe/H] $\lesssim -1$. Such small [O/Fe] can be explained by the low-mass 13–15 $M_\odot$ SNe II, where the O yield is smaller than in massive stars (K00). The abundance patterns in the dwarf spheroidal galaxies can also be explained by these SNe II (Tolstoy et al. 2003; Travaglio et al. 2004). (3) HNe may produce an even larger amount of Fe due to a smaller fallback mass or a larger energy than the typical HNe in our yields. (4) SNe I.5, which are the SN Ia–like explosions of metal-poor asymptotic giant branch (AGB) stars, have also been suggested by Nomoto et al. (2003; see also Tsujimoto 2006).

On the other hand, very large [O/Fe] (>1) could be explained by the small Fe production, namely by either (1) massive SNe II with $E_{51} \leq 1$ or (2) HNe with a larger mass cut (i.e., a large black hole mass). In such stars other α-elements should show the same trend, especially Mg, Si, and S. The difference between these

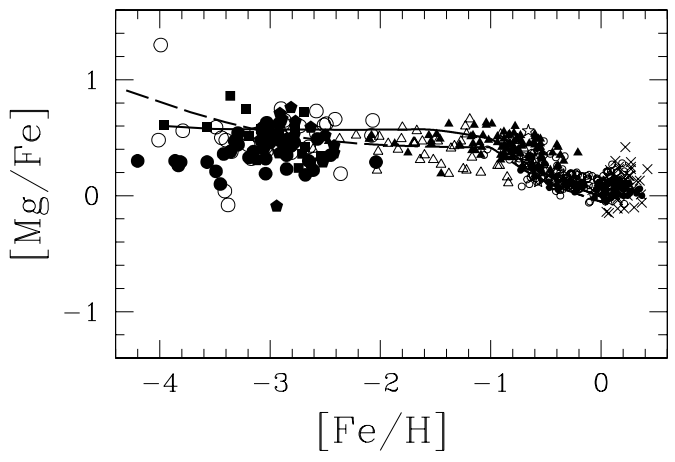

FIG. 8.—[Mg/Fe]-[Fe/H] relation for the model with our yields (*solid line*) and the K98 model with N97 yields (*dashed line*). Observational data sources for disk stars are Edvardsson et al. (1993; *small open circles*), Feltzing & Gustafsson (1998; *crosses*), thin disk stars in Bensby et al. (2003; *small filled circles*); and the thin disk (*stars*), dissipative (*filled triangles*), and accretion (*open triangles*) components in Gratton et al. (2003). Data source for halo stars are McWilliam et al. (1995; *large open circles*), Ryan et al. (1996; *filled squares*), Cayrel et al. (2004; *large filled circles*), and Honda et al. (2004; *filled pentagons*). [*See the electronic edition of the Journal for a color version of this figure.*]

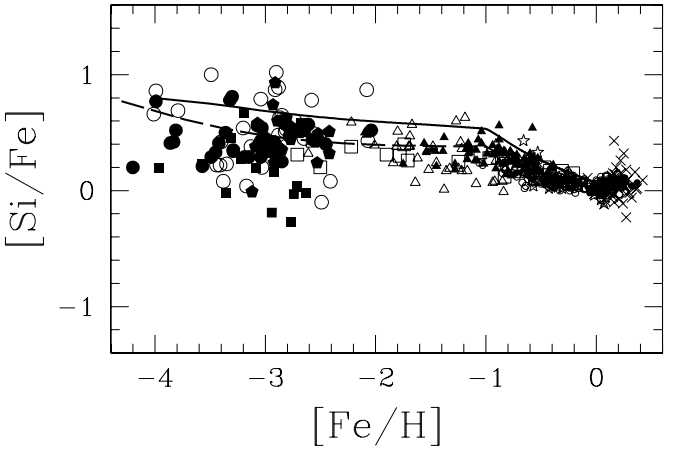

FIG. 10.—Same as Fig. 8, but for [Si/Fe]-[Fe/H] relation. Data sources for halo stars also include Gratton & Sneden (1991; *open squares*). [*See the electronic edition of the Journal for a color version of this figure.*]

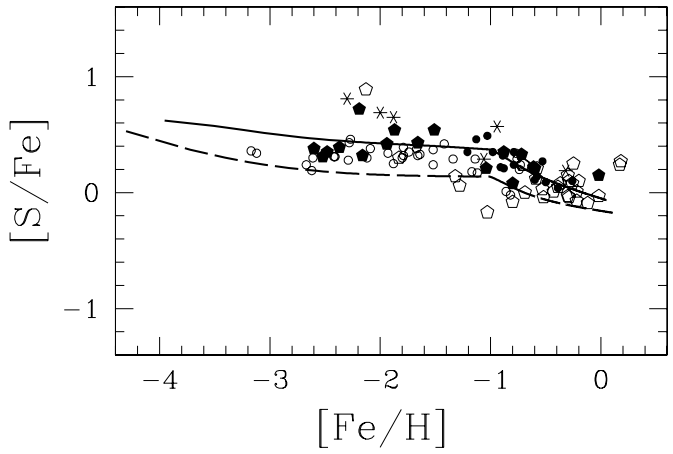

FIG. 11.—[S/Fe]-[Fe/H] relation. Observational data sources are Israelian & Reboro (2001; *asterisks*); Takada-Hidai et al. (2002; *open pentagons*); Chen et al. (2002; *filled circles*); Nissen et al. (2004; *open circles*); and Takada-Hidai et al. (2005; *filled pentagons*). [*See the electronic edition of the Journal for a color version of this figure*.]

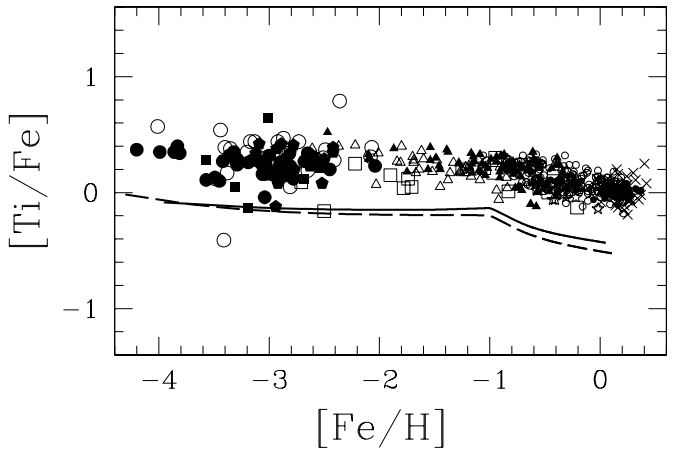

FIG. 13.—Same as Fig. 10, but for [Ti/Fe]-[Fe/H] relation. [*See the electronic edition of the Journal for a color version of this figure*.]

two possibilities appears in the abundance ratios among the iron-peak elements, especially large [(Zn, Co)/Fe]. BPS CS 22949−037, with [O/Fe] ~ 2 at [Fe/H] ~ -4 in Figure 7, has large [Mg/Fe] ($\sim$1.6), normal [(Ca, Ti)/Fe] ($\sim$0.35), and large [(Zn, Co)/Fe], which are explained with a HN model (UN05). The low-energy explosion with $E_{51} = 0.4$ in Tsujimoto & Shigeyama (2003) also gives large [O/Fe] but cannot explain the large [(Zn, Co)/Fe].

3.2.2. *Magnesium*

Mg is one of the best-observed elements with several lines and little NLTE effect. Cayrel et al. (2004, hereafter C04) claimed that [(Mg, Si, Ca, Ti)/Fe] is constant as $\sim$0.2–0.3 with a very small dispersion of $\sim$0.1 dex. In our chemical evolution model [Mg/Fe] is 0.49 at [Fe/H] ~ -1 and slightly increases to 0.57 at [Fe/H] ~ -3, which is larger than 0.27 in C04, but in good agreement with the observational data over the wide range of [Fe/H] as shown in Figure 8. We note that the overall agreement of the [Mg/Fe]-[Fe/H] relation is due to our assumptions of the mixing-fallback, the HN fraction $\epsilon_{\rm HN} = 0.5$, the upper mass limit $M_u = 50\ M_\odot$, and the time- and metallicity-independent IMF. SNe II typically provide [Mg/Fe] ~ 0.5, varying between -0.2 ($Z = Z_\odot$, 18 $M_\odot$) and 1 (40 $M_\odot$). For HNe, [Mg/Fe] ~ 0.5, despite the large progenitor masses ($M \geq 20\ M_\odot$), because the iron yield is as large as the yields of α-elements. Therefore, the scatter of [Mg/Fe] can be small, independent of the mixing process of the interstellar medium (Tominaga et al. 2006; Nomoto et al. 2006).

[O/Mg] is $\sim$0, independent of [Fe/H] in N97 yields, while it is in a range from ~ -0.08 to -0.06 in our new yields. Compared with the Edvardsson et al. (1993) data for [Fe/H] $\gtrsim -1$, there was a 0.1 dex offset in [O/Mg] with N97 yields; this problem is solved with our yields (Fig. 9). Recently, however, Bensby et al. (2004a) showed a 0.1 dex larger [O/Mg] for [Mg/H] $\lesssim 0$ and decreasing trend for high metallicity. With our model the iron abundance does not reach such high metallicity, and we do not calculate the nucleosynthesis yields for $Z > Z_\odot$ yet. Such a decrease in O/Mg would require some additional effects that are not included in our stellar evolution models, such as strong stellar winds or a process that causes the change in the C/O ratio.

3.2.3. *Silicon, Sulfur, Calcium, and Titanium*

The observed Si abundance is represented by only two lines and affected by the contamination of CH and Hδ lines. These may arise larger scatter than Mg. The [Si/Fe] is 0.53–0.68 at $-3 \lesssim$ [Fe/H] $\lesssim -1$ in our model, which is a bit larger than the value of 0.37 in C04 and other observations (Fig. 10).

For S, because of the hardness of observation, the plateau value has not been established. Some observations (Israelian & Reboro

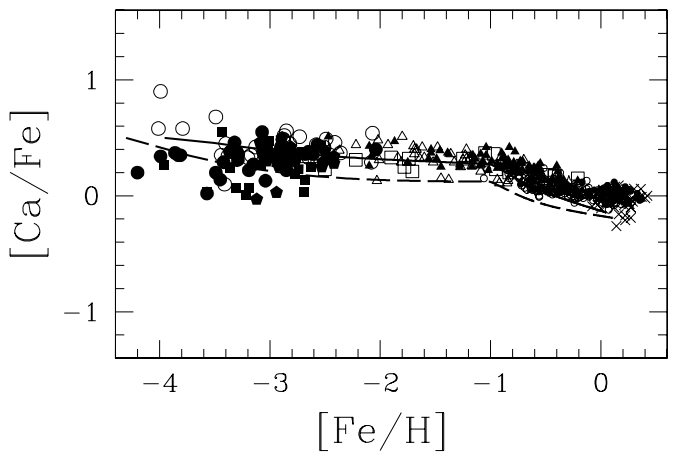

FIG. 12.—Same as Fig. 10, but for [Ca/Fe]-[Fe/H] relation. [*See the electronic edition of the Journal for a color version of this figure*.]

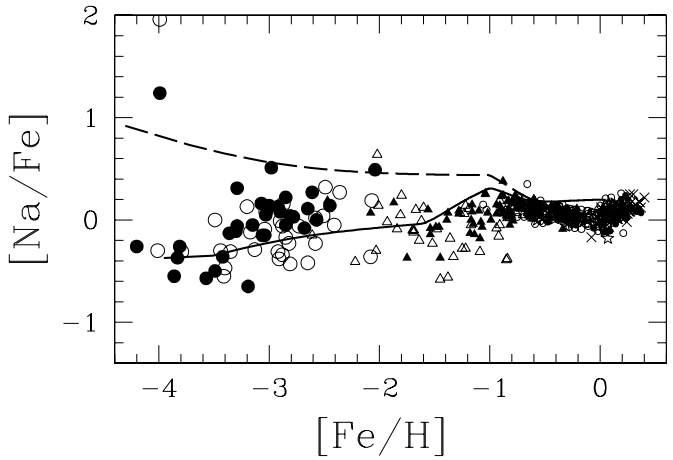

FIG. 14.—Same as Fig. 8, but for [Na/Fe]-[Fe/H] relation. [*See the electronic edition of the Journal for a color version of this figure*.]

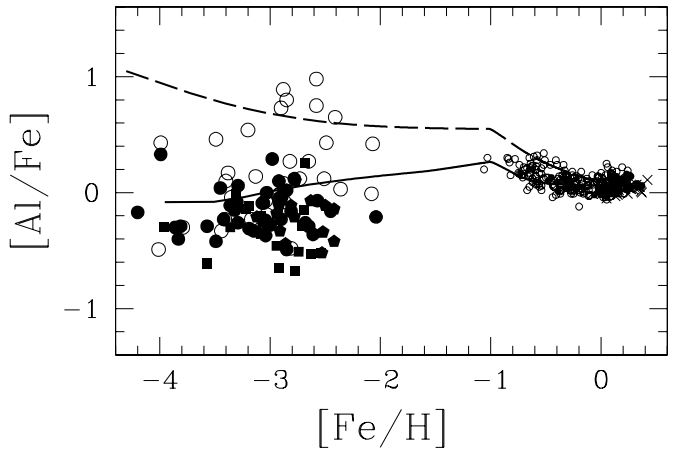

FIG. 15.—Same as Fig. 8, but for [Al/Fe]-[Fe/H] relation. [*See the electronic edition of the Journal for a color version of this figure.*]

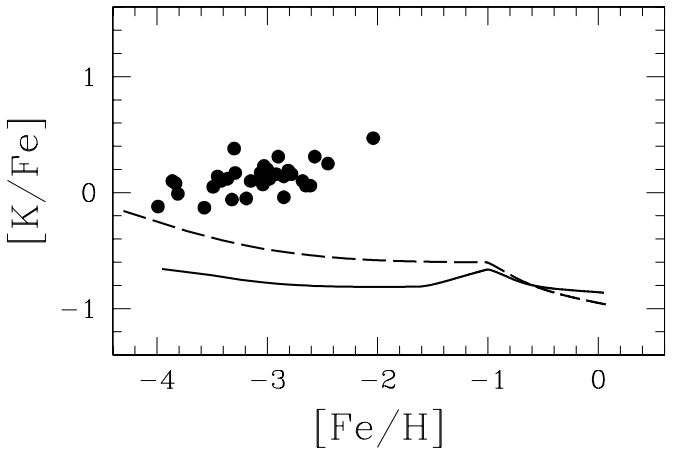

FIG. 17.—Same as Fig. 8, but for [K/Fe]-[Fe/H] relation. [*See the electronic edition of the Journal for a color version of this figure.*]

2001; Takada-Hidai et al. 2002) suggest a sharp increase in [S/Fe] with decreasing [Fe/H], like the UV OH result, where SI (6) lines at ∼8694 Å are used. Takada-Hidai et al. (2002) adopted a NLTE model and actually commented that the very high [S/Fe] at [Fe/H] ~ -2.1 could be smaller with different temperature. So the S trend is uncertain. Other recent observations (Nissen et al. 2004; Takada-Hidai et al. 2005) using SI (1) lines at ∼9200 Å with LTE models provided plateau values of ∼0.3 and 0.46, respectively. These are consistent with our prediction of [S/Fe] = 0.37–0.50 at $-3 \lesssim$ [Fe/H] $\lesssim -1$ (Fig. 11).

Ca is a well-observed element, and our model succeeds in reproducing the observed plateau [Ca/Fe] $\sim$ 0.27–0.39, which is larger by ∼0.2 dex than the N97 model (Fig. 12). However, [Ti/Fe] is ∼0.4 dex underabundant overall, which cannot be improved by changing our parameters (Fig. 13). A possible model that enhances Ti is a jetlike explosion with high entropy (Maeda & Nomoto 2003).

3.2.4. *Sodium, Aluminum, and Copper*

As shown in Figure 5, the abundances of the odd-*Z* elements show a strong metallicity dependence. The odd-*Z* elements are enhanced by the surplus of neutrons in ^{22}Ne, and ^{22}Ne is transformed from ^{14}N by the CNO cycle during He-burning. Thus, smaller amounts of CNO elements result in smaller amounts of the odd-*Z* elements. With our one-zone model, the decreasing trend of [(Na, Al, Cu)/Fe] toward lower [Fe/H] is seen more weakly because of the mass dependence, and the resulting trends are in excellent agreement with the observations (Figs. 14, 15, and 16). Observationally, the NLTE effect for Na and Al is large for metal-poor stars, and the observational data at [Fe/H] $\lesssim -2$ (McWilliam et al. 1995; Ryan et al. 1996; Cayrel et al. 2004; Honda et al. 2004) in Figures 14 and 15 are shifted by a constant of −0.2 and +0.5, respectively (Frebel et al. 2005; Asplund 2005). The McWilliam et al. (1995) data show significant offset with higher [Al/Fe], of which reason is unclear (Ryan et al. 1996).

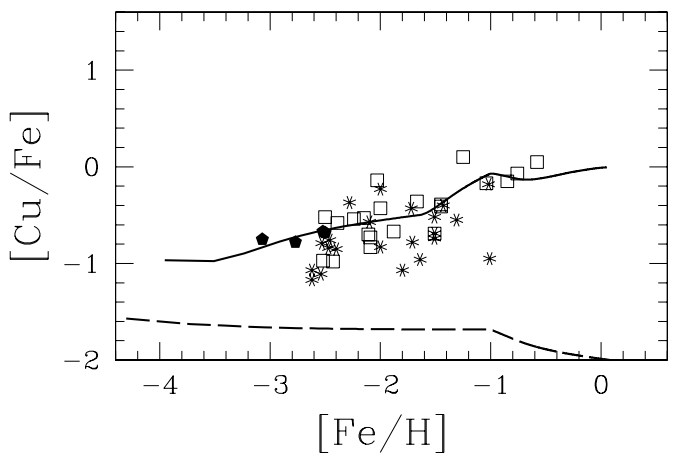

FIG. 16.—[Cu/Fe]-[Fe/H] relation. Observational data sources for halo stars are Sneden et al. (1991; *squares*); Primas et al. (2000; *asterisks*); and Honda et al. (2004; *pentagons*). [*See the electronic edition of the Journal for a color version of this figure.*]

3.2.5. *Potassium, Scandium, and Vanadium*

K, Sc, and V yields are overall very underabundant by ∼1 dex, compared with observations (Figs. 17, 18, and 19). For K, the NLTE effect is corrected by a constant shift of −0.35 (Cayrel et al. 2004). To solve these problems, UN05 have introduced a low-density model, in which the density is assumed to be reduced during explosive burning. This model enhances the α-rich freezeout and thus the Sc production. This is based on the idea that a relatively weak jet expands the interior of the progenitor before a strong jet forms a strong shock to explode the star. Alternatively, Fröhlich et al. (2006) showed that the delayed neutrino mechanism that leads to $Y_e > 0.5$ in the innermost region gives larger production of Sc, Ti and Zn. T. Yoshida et al. (2006, in preparation) have added neutrino processes to explosive nucleosynthesis

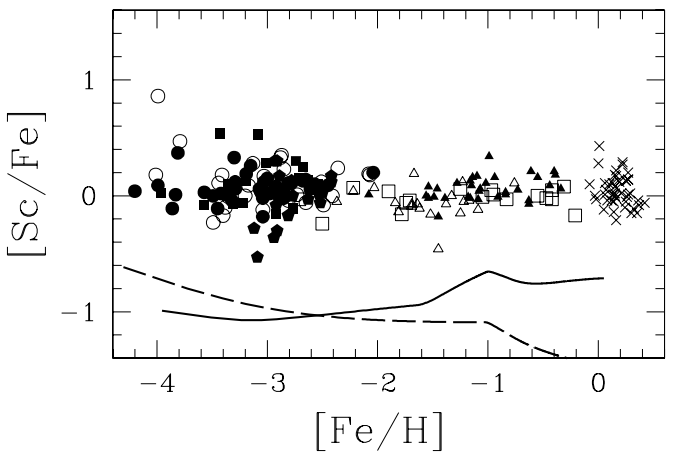

FIG. 18.—Same as Fig. 10, but for [Sc/Fe]-[Fe/H] relation. [*See the electronic edition of the Journal for a color version of this figure.*]

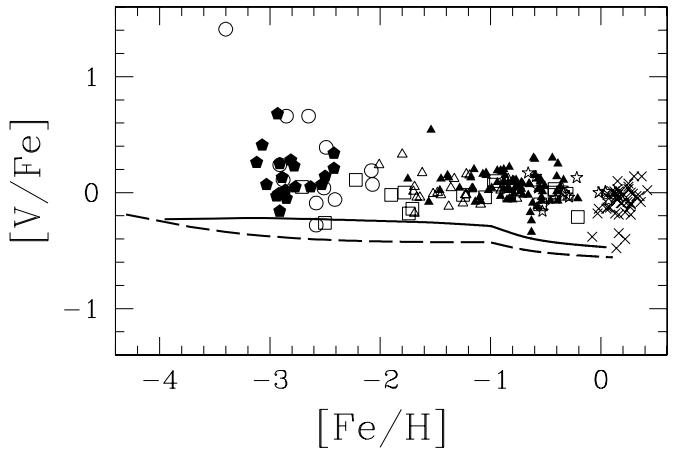

FIG. 19.—Same as Fig. 10, but for [V/Fe]-[Fe/H] relation. [*See the electronic edition of the Journal for a color version of this figure.*]

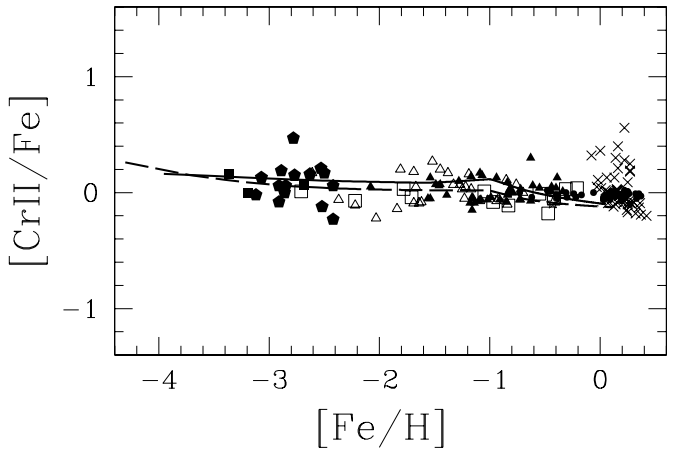

FIG. 21.—Same as Fig. 10, but for [Cr II/Fe]-[Fe/H] relation. [*See the electronic edition of the Journal for a color version of this figure.*]

of UN05, and found larger Sc, V, and Mn production by a factor of 10. Such additional physical processes would actually work, even for zero-metallicity stars.

3.2.6. *Chromium, Manganese, Cobalt, and Nickel*

McWilliam et al. (1995) and Ryan et al. (1996) found the decreasing trend of [(Cr, Mn)/Fe] and the increasing trend of [Co/Fe] toward lower metallicity. These trends have been first explained by Nakamura et al. (1999) by the stellar mass-dependent mass cut, because Co is synthesized by complete Si-burning in the deepest layer of the ejecta, while Cr and Mn form in the outer incomplete Si-burning layers. Then, UN05 found that a larger explosion energy enhances the amount of Co and decreases Cr and Mn and showed that these trends can be explained by the energy effect (1) if the interstellar medium is not mixed, so that the EMP stars are enriched only by a single supernova (Audouse & Silk 1995), and (2) if the hydrogen mass swept by supernovae ejecta is proportional to the explosion energy and the metallicity correlates well with the energy. However, C04 claimed that no relation is found in [Mn/Fe] after 0.4 dex correction for low metallicity.

In our chemical evolution model (Figs. 20–24), since we use the yields for typical SNe II and HNe, no such trends are seen. Instead, we focus on whether our mean values meet the observations at [Fe/H] ~ -2.5. As a whole, our yields are in better agreement with observations than N97 yields, although the $\sim$0.1 dex offsets still remain: $\sim$+0.2, -0.1, -0.1, and -0.1 dex offsets for Cr, Mn, Co, and Ni, respectively. However, these elements are much affected by the mixing-fallback process, the explosion energy, and the electron excess Y_e, so it would be possible to find a better set by fine-tuning the parameters under our model. We also note that there is an inconsistency of observed Cr abundances taken with Cr I and Cr II lines, and higher value of Cr II is favored for our model.

From [Fe/H] ~ -1, SNe Ia start to contribute, which results in the increasing [Mn/Fe] toward higher metallicity. This is confirmed both observationally and theoretically, and Mn can be a key element to discuss the SN Ia contribution, HN fraction, and IMF. Cr and Co are produced not only from SNe Ia but also from SNe II with [Cr, Co/Fe] ~ 0 at [Fe/H] $\gtrsim -1$. The observed [Ni/Fe] is $\sim$0 for all range of [Fe/H], and the Ni overabundance of SNe Ia can be reduced; the Ni yield depends on Y_e in the burning region, which is determined by electron capture and thus sensitive to the propagation speed of the burning front and the central density of the white dwarf (Nomoto et al. 1984; Iwamoto et al. 1999).

3.2.7. *Zinc*

The most important agreement of our yields lies in Zn, which is an important element for discussing the cosmic chemical enrichment and is observed in the damped Lyα systems without the dust depletion effect. The production of the isotopes of Zn depends on metallicity. At higher metallicity ($Z \geq 0.004$), ^{66}Zn and ^{68}Zn are synthesized by the neutron-capture processes during He and C burning. At lower metallicity, only ^{64}Zn is formed in the

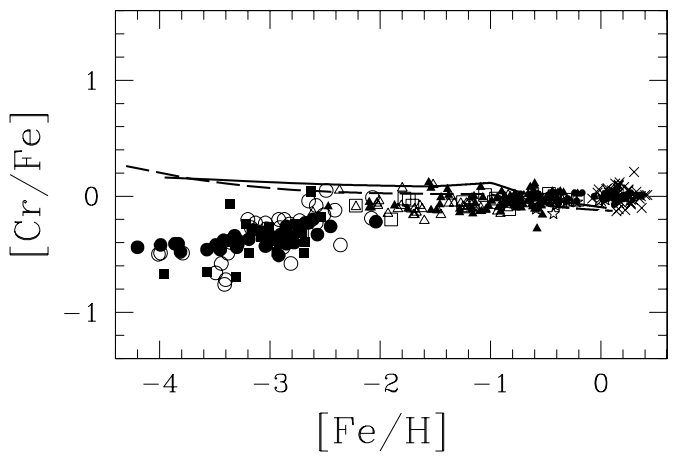

FIG. 20.—Same as Fig. 10, but for [Cr/Fe]-[Fe/H] relation. [*See the electronic edition of the Journal for a color version of this figure.*]

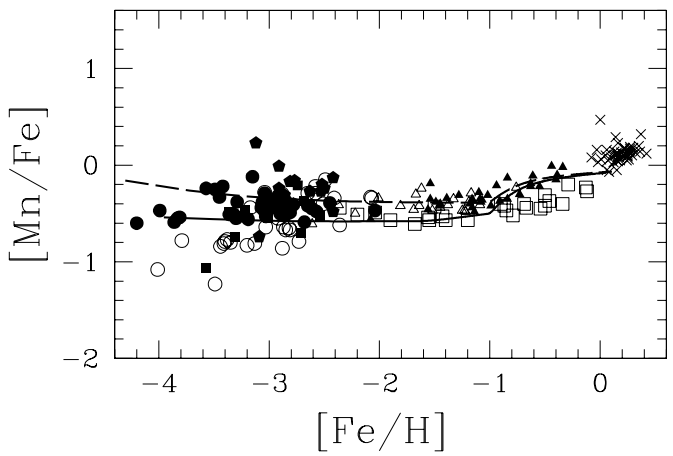

FIG. 22.—Same as Fig. 8, but for [Mn/Fe]-[Fe/H] relation.Open squares are halo stars from Gratton (1989). [*See the electronic edition of the Journal for a color version of this figure.*]

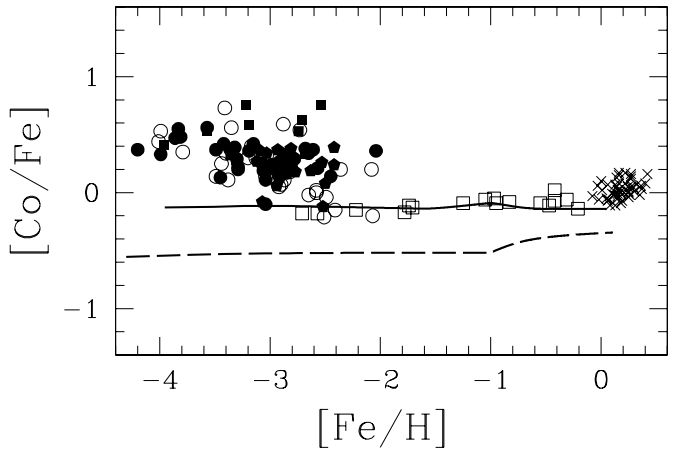

FIG. 23.—Same as Fig. 10, but for [Co/Fe]-[Fe/H] relation. [*See the electronic edition of the Journal for a color version of this figure.*]

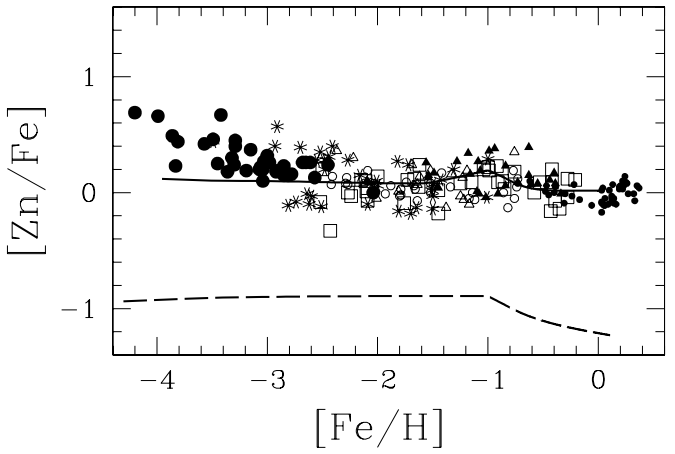

FIG. 25.—Same as Fig. 8, but for [Zn/Fe]-[Fe/H] relation. Open squares are halo stars from Sneden et al. (1991). Eight-pointed asterisks are halo stars from Primas et al. (2000). [*See the electronic edition of the Journal for a color version of this figure.*]

deep complete Si-burning region and needs to be mixed out into the ejecta in order for enough amount to be ejected. The ^{64}Zn can be enhanced only by the high-energy explosions of HNe (UN03, UN05). At $-2.5 \lesssim$ [Fe/H] $\lesssim -1.5$, [Zn/Fe] is constant $\sim$0.1, mildly increases to $\sim$0.2 from [Fe/H] ~ -1.5 due to the metallicity effect, and mildly decreases to $\sim$0 from [Fe/H] ~ -1 due to SNe Ia, which are all consistent with observations (Fig. 25).

Primas et al. (2000) found the increasing [Zn/Fe] trend toward lower metallicity at [Fe/H] $\lesssim -3$. UN05 explained this by the energy effect as well as other trends of iron-peak elements. Such a trend is not realized in our chemical evolution model. The contribution of pair-instability supernovae, which produce much more Fe and less [Zn/Fe], is not observed in EMP stars. Recently, Ohkubo et al. (2006) proposed that core-collapse very massive stars with $M \sim 500$–$1000\ M_\odot$ also produce large [Zn/Fe].

3.2.8. *Carbon and Nitrogen*

Since the enrichment from stellar winds and the contribution of low- and intermediate-mass stars are not included in our chemical evolution model, C and N are overall underabundant when compared to observed values. The major sources of C and N are AGB stars and/or Wolf-Rayet (WR) stars. Intermediate-mass stars (3–8 $M_\odot$) may not be favored, because no strong increase is observed in [C/Fe] from [Fe/H] ~ -2 to ~ -1 (Prantzos et al. 1994). The decrease from [Fe/H] ~ -1 in our model is due to the SN Ia contribution. Because no such decrease is observed, low-mass stars with $M < 2\ M_\odot$ may also contribute to C and N production.

With our yields, [C/Fe] and [N/Fe] are $\sim$0.4 dex smaller than observations at [Fe/H] $\sim$ 0, but larger than N97 yields (Figs. 26 and 27). The ejected ^{12}C mass is comparable to N97 yields, and the increase of [C/Fe] is caused by the difference in the Fe mass (i.e., the larger and smaller Fe mass than N97 are adopted for massive and low-mass SNe II, respectively). The ejected ^{14}N mass is 10 times larger than N97 yields, because a larger amount of convective mixing of H into the He-burning layer takes place in our progenitor stars. The N production in metal-free stars strongly depends on the detail treatment of the convective mixing and can be increased by more than a factor of 10 (Iwamoto et al. 2005).

In the observational data, there are many stars that show a large enhancement of carbon abundances ([C/Fe] $\gg$ 0), and some of them also shows a large enhancement of Mg. As already mentioned, [Zn/Fe] can put a constraint on the enrichment source. With our yield set, massive SNe II can increase [C/Fe] to $\sim$0.4, but [Zn/Fe] is much smaller than 0. HNe can increase [Zn/Fe], but [C/Fe] cannot be larger than 0. The stars with [C/Fe] > 0.4 suggest

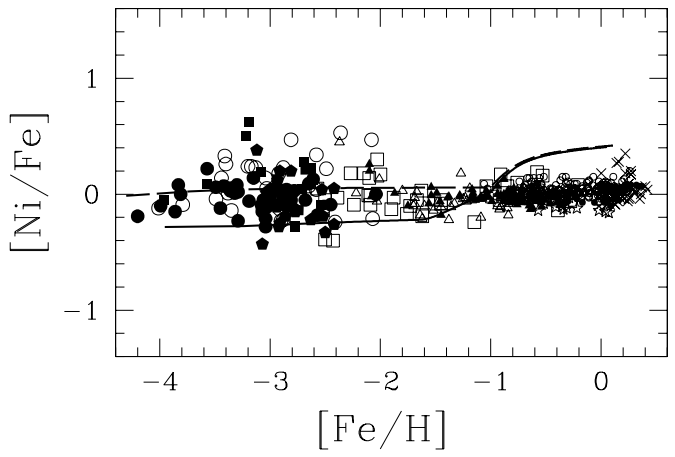

FIG. 24.—Same as Fig. 8, but for [Ni/Fe]-[Fe/H] relation. Open squares show halo stars from Sneden et al. (1991). [*See the electronic edition of the Journal for a color version of this figure.*]

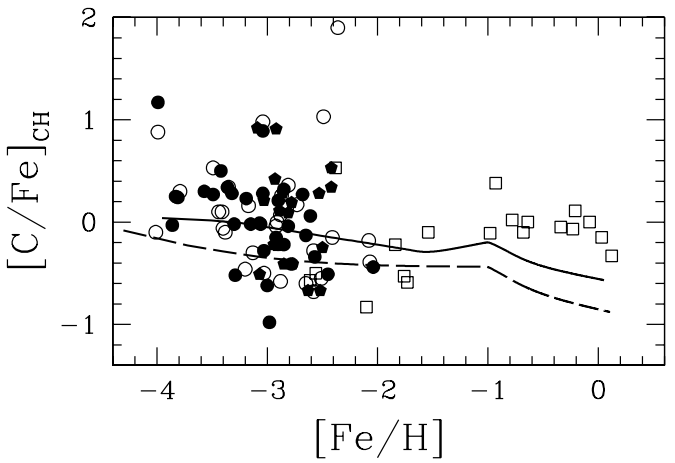

FIG. 26.—[C/Fe]-[Fe/H] relation for the model with our yields (*solid line*) and the K98 model with N97 yields (*dashed line*). Observational data source for disk stars is Carretta et al. (2000; *open diamonds*). Data source for halo stars are McWilliam et al. (1995; *large open circles*), Cayrel et al. (2004; *large filled circles*), and Honda et al. (2004; *filled pentagons*). [*See the electronic edition of the Journal for a color version of this figure.*]

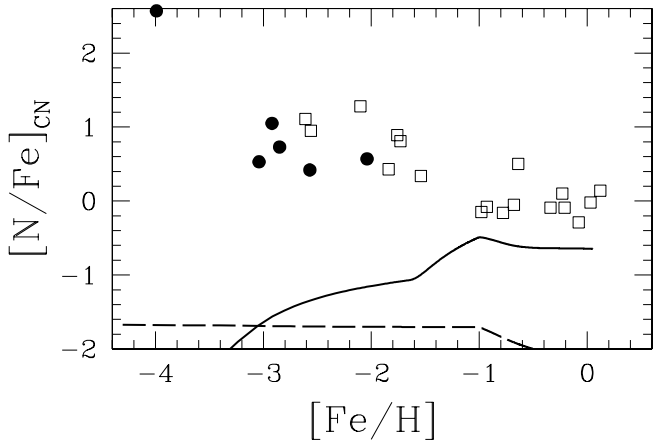

FIG. 27.—[N/Fe]-[Fe/H] relation for the model with our yields (*solid line*) and the K98 model with N97 yields (*dashed line*). Observational data source for disk stars is Carretta et al. (2000; *open diamonds*). Data source for halo stars is Cayrel et al. (2004; *large filled circles*). [*See the electronic edition of the Journal for a color version of this figure.*]

other enrichment sources, which could be (1) a single supernova (Umeda & Nomoto 2003; Iwamoto et al. 2005), namely, a faint supernova with $E_{51} < 1$), (2) a few supernovae (Limongi et al. 2003), or (3) external enrichment from a binary companion (e.g., Suda et al. 2004).

3.2.9. *Other Elements*

Figure 28 shows the [X/Fe]-[Fe/H] diagrams for the other elements as well. Neon and argon are α-elements with plateau values of [Ne/Fe] ~ 0.5 and [Ar/Fe] ~ 0.3 at [Fe/H] $\lesssim -1$ and can be tested with X-ray observations. Phosphorus, chlorine, and argon can be seen in the damped Lyα systems. Fluorine is an important element for examining the neutrino process.

4. CHEMICAL EVOLUTION OF HALO, BULGE, AND THICK DISK

4.1. *Galactic Halo Model*

Here, we apply our yields to chemical evolution models for the bulge and halo of the Milky Way galaxy. For the halo, the

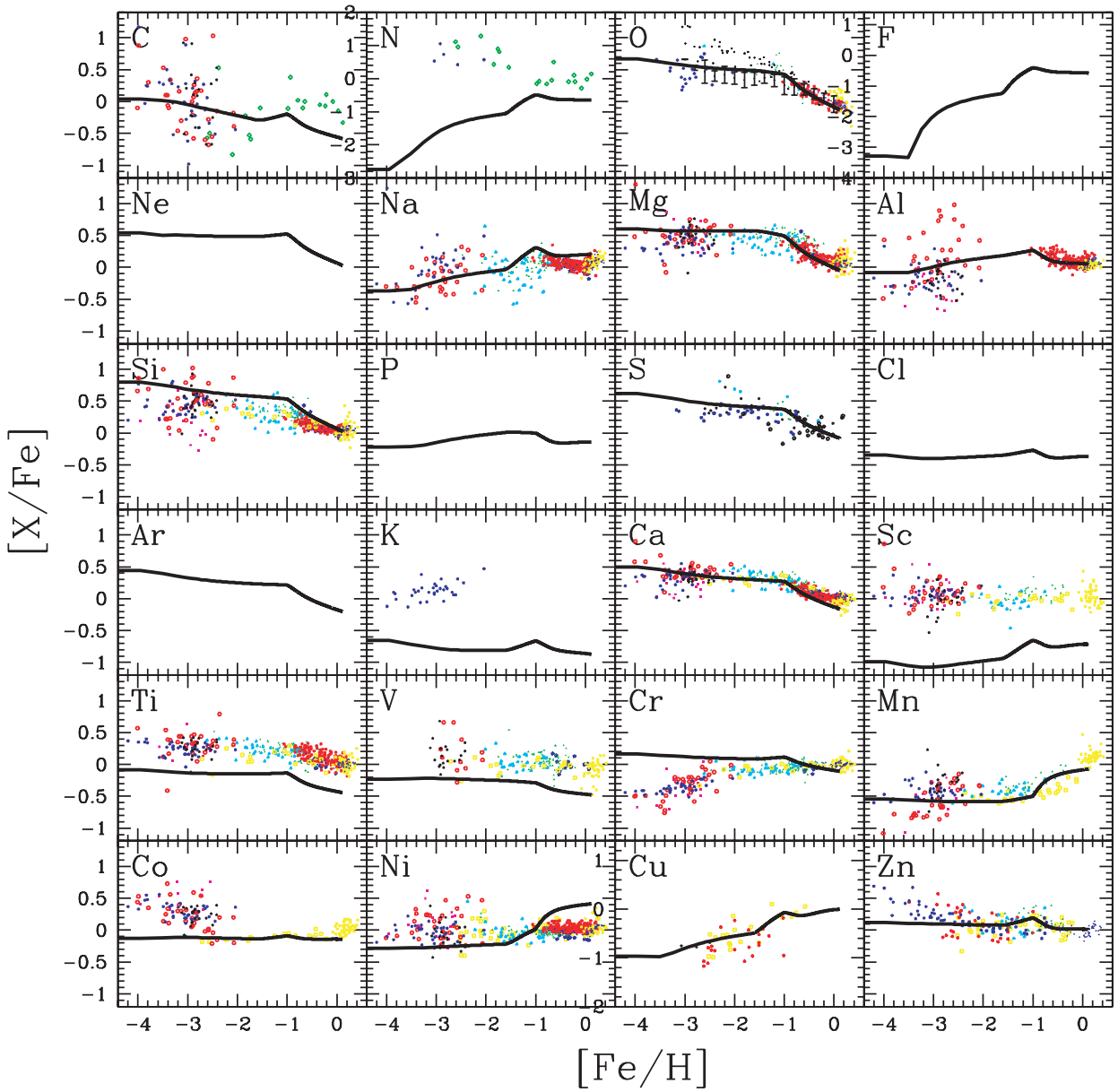

FIG. 28.—[X/Fe]-[Fe/H] relations. See Figs. 7–27 for the observational data sources.

TABLE 4

PARAMETERS OF CHEMICAL EVOLUTION MODELS; INFALL, STAR FORMATION, AND OUTFLOW TIMESCALES, AND THE GALACTIC WIND EPOCH

PARAMETERS	VALUES (Gyr)				
	τ_i	τ_s	τ_o	t_w	x
Solar neighborhood	5	2.2	...	...	1.35
Halo	...	8	1	...	1.35
Bulge, model (A)	1	1	...	...	1.35
Bulge, wind model (B)	5	0.5	...	3	1.35
Bulge, flat IMF model	5	0.5	...	2	1.10
Thick disk, disk-like model (A)	5	2.2	...	6	1.35
Thick disk, closed-box model (B)	...	0.5	...	...	1.35
Thick disk, infall model (C)	5	1	...	3	1.35

NOTE.—The term x denotes the slope of the initial mass function.

MDF of field stars selected with *Hipparcos* kinematics shows a peak at low [Fe/H] ~ -1.6 (Chiba & Yoshii 1998) and has no metal-rich component that is seen in the MDF of globular clusters (Zinn 1985). This suggests that the efficiencies of star formation and chemical enrichment are very low in the halo. We use a closed-box model that allows the outflow of material. The driving source of the outflow should be the feedback from supernovae. Thus, the outflow rate is assumed to be $R_{\rm out} \equiv (1/\tau_o) f_g$, which is proportional to the SFR [$\psi \equiv (1/\tau_s) f_g$; see K00 for the other formulation]. Timescales of $\tau_s = 8$ Gyr and $\tau_o = 1$ Gyr are adopted to meet the MDF. The adopted parameters in our chemical evolution models are summarized in Table 4.

Figure 29*a* shows the SFR, Figure 29*b* shows the age-metallicity relation, Figure 29*c* shows the MDF, and Figure 29*d* shows the [O/Fe]-[Fe/H] relation. The solid and dashed lines show the cases with and without the metallicity effect of SNe Ia, respectively. The metallicity increases quickly to [Fe/H] ~ -1.5 at $t \sim 0.9$ Gyr, and then the outflow becomes effective and chemical enrichment takes place slowly. If we do not include the SN Ia metallicity effect, [Fe/H] keeps on increasing, which results in the double

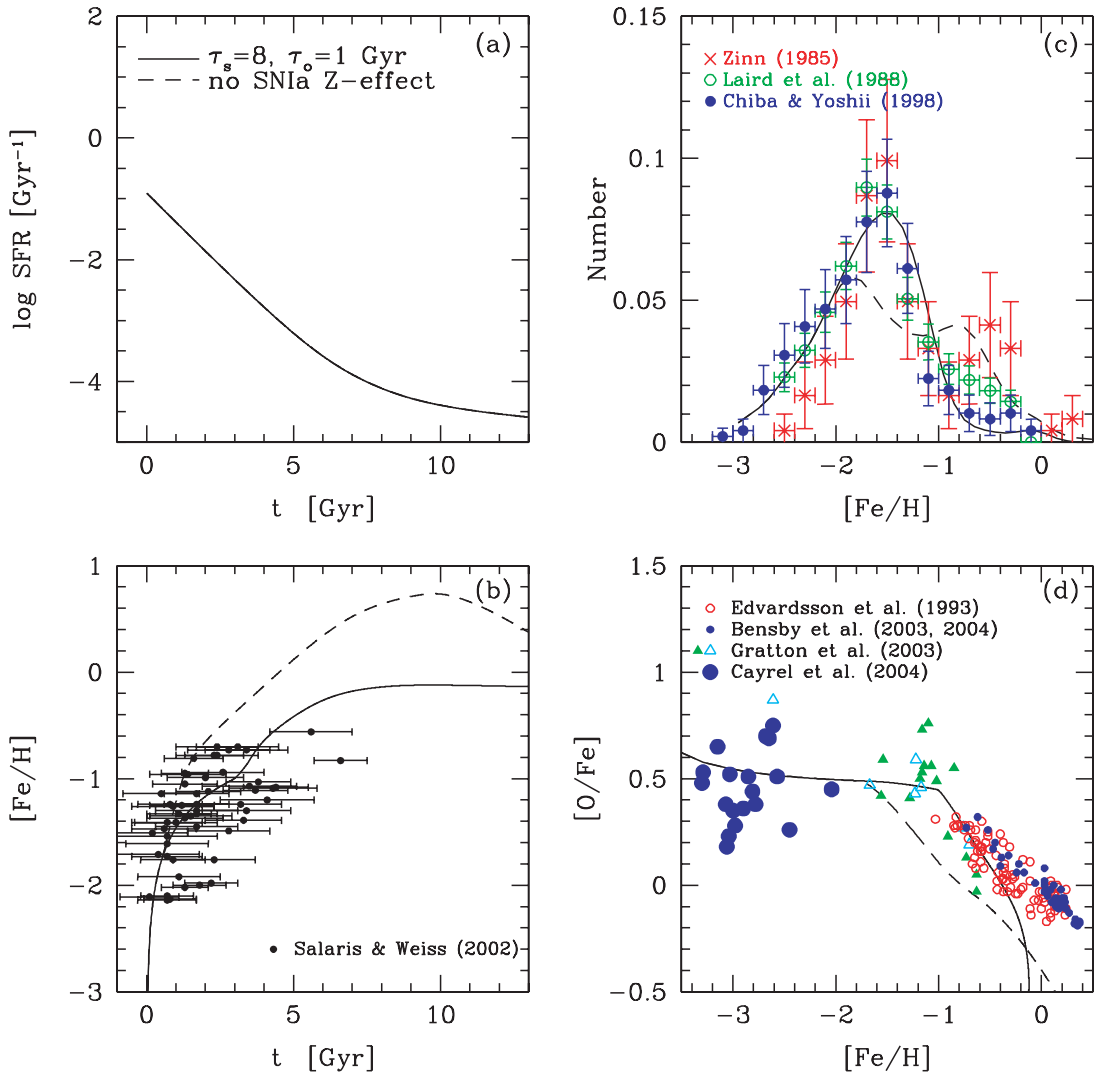

FIG. 29.—Chemical evolution of the Galactic halo: (*a*) Star formation rate, (*b*) Age-metallicity relation, (*c*) Metallicity distribution function, and (*d*) [O/Fe]-[Fe/H] relation. The solid and short-dashed lines are for the outflow model with and without the SN Ia metallicity effect, respectively. Observational data sources are as follows. (*b*) *filled circles*: Salaris & Weiss (2002); (*c*) *crosses*: Zinn (1985); *open circles*: Laird et al. (1988); *filled circles*: Chiba & Yoshii (1998); and (*d*) *small open circles*: Edvardsson et al. (1993); *small filled circles*: thin disk stars in Bensby et al. (2004a); *filled and open triangles*: Gratton et al. (2003); *large filled circles*: Cayrel et al. (2004).

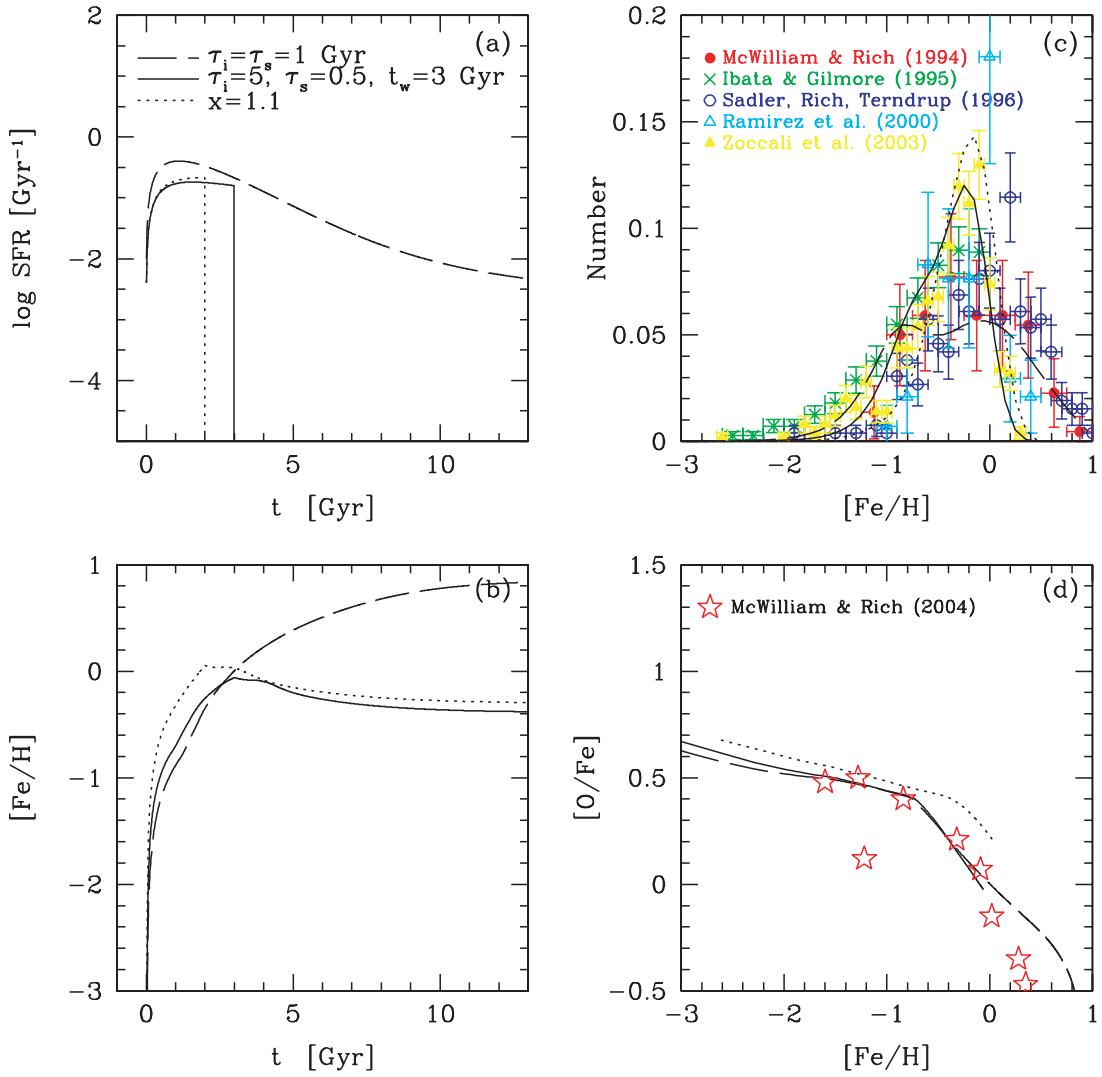

FIG. 30.—Same as Fig. 29, but for the Galactic bulge. The dashed and solid lines are for the wind models to give broad and narrow metallicity distribution functions, respectively. The dotted line is for the model with a flatter IMF to give constant [O/Fe]. Observational data sources are as follows. (c) *filled circles*: McWilliam & Rich (1994); *crosses*: Ibata & Gilmore (1995); *open circles*: Sadler et al. (1996); *open triangles*, Ramírez et al. (2000); *filled triangles*: Zoccali et al. (2003); and (*d*) *stars*: McWilliam & Rich (2004).

peaks in the MDF (Fig. 29*c*). Without the metallicity effect, [α/Fe] starts to decrease at [Fe/H] ~ -1.7, which is earlier than observed (Fig. 29*d*). Since our SN Ia progenitor scenario requires the companion mass range of $\sim$1–3 $M_\odot$, the SN Ia lifetime spans over 0.5–20 Gyr. It is difficult to delay the onset of the decrease in [α/Fe] without the metallicity effect (K98).

4.2. *Galactic Bulge Model*

For the bulge, observational results of the MDF are controversial (Fig. 30*c*). McWilliam & Rich (1994) showed a broad MDF that extends to [Fe/H] $\sim$ 1. However, a narrow MDF was found recently with a subsolar peak and a sharp cutoff at [Fe/H] $\sim$ 0 (Zoccali et al. 2003). We thus construct several models to meet each observation.

Model A.—For the McWilliam & Rich (1994) MDF, a simple infall model ($R_{\rm in} \equiv (1/\tau_i)\exp(-t/\tau_i)$) with a short star formation timescale ($\tau_s = \tau_i = 1$) gives a good agreement (Fig. 30, *dashed line*). With our model A, the SFR is peaked at $\sim$1 Gyr, and the star formation continues until the present, producing a lot of low-[α/Fe] stars in the bulge.

Model B.—On the other hand, to reproduce the Zoccali et al. (2003) MDF, star formation needs to be terminated somehow at $t_w = 3$ Gyr (Fig. 30, *solid line*), possibly by supernova-induced galactic winds or by the feedback from the active galactic nuclei. To meet this MDF, $\tau_s = 0.5$ and $\tau_i = 5$ Gyr are adopted. With our model B, [Fe/H] does not increase after $t \sim 3$ Gyr, and [α/Fe] cannot be lower than 0.

The short timescale of chemical enrichment is imprinted in the [α/Fe]-[Fe/H] diagram (Fig. 30*d*), namely in the decrease of [α/Fe] toward higher [Fe/H] than -1 (Matteucci & Brocato 1990). However, McWilliam & Rich (2004) claimed that the abundance patterns of bulge stars look peculiar, and the evolutions of [O/Fe] and [(Mg, Si)/Fe] are different. Both our models show the [α/Fe] decrease from [Fe/H] ~ -0.7, which is consistent with the observed O trends. However, Mg observation does not show such decrease, which may suggest that the chemical enrichment timescale is much shorter. For example, with a flatter IMF model of $x = 1.1$, [α/Fe] is almost constant until [Fe/H] ~ -0.3 (Fig. 30, *dotted line*). (Since a larger amount of metals are ejected for $x = 1.1$ than for the Salpeter IMF, the time duration of

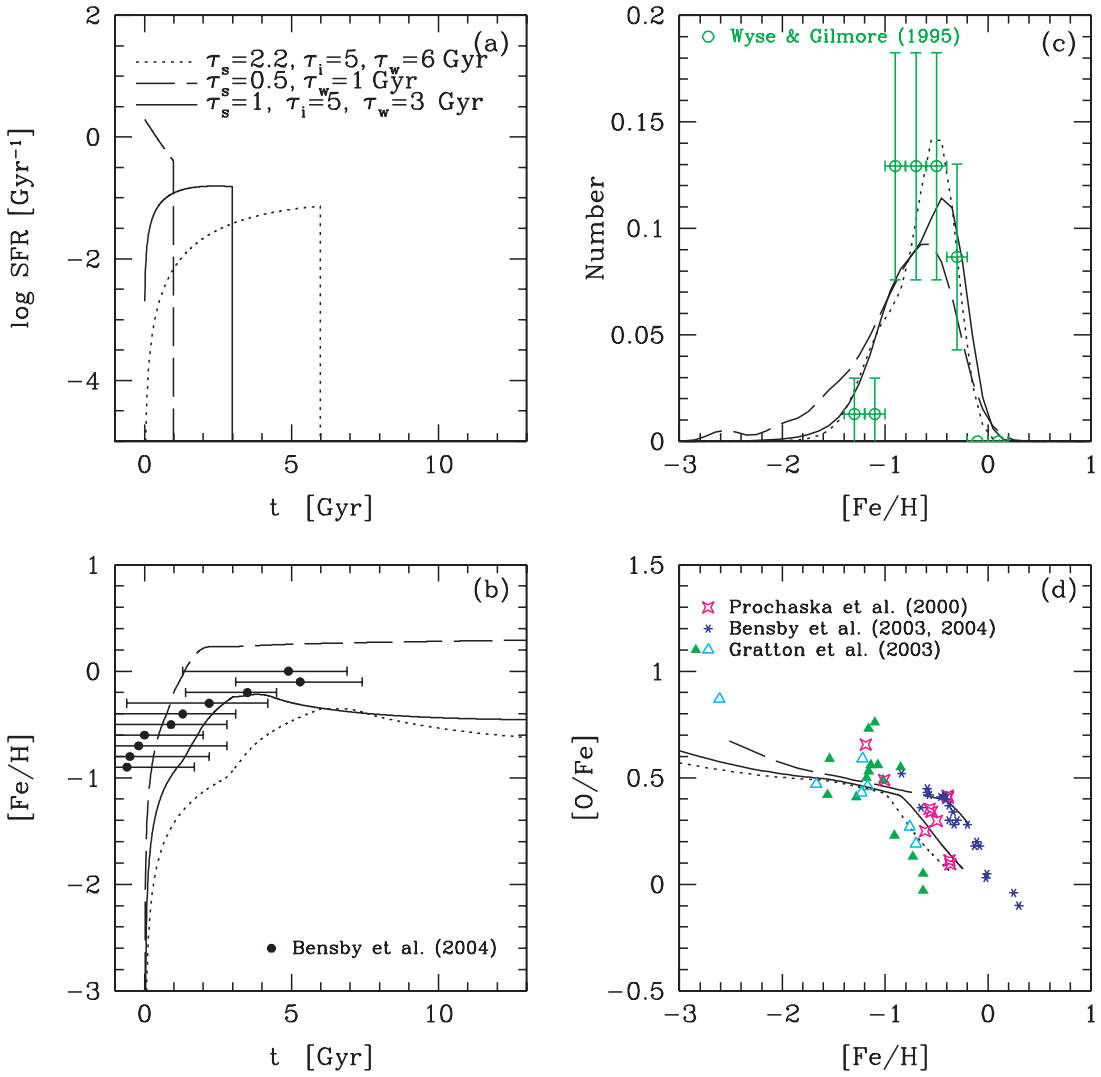

FIG. 31.—Same as Fig. 29, but for the Galactic thick disk. The dotted line is for the same model as the solar neighborhood, but with a truncated SFR. The dashed and solid lines are for the closed-box and infall models with short star formation timescales. Observational data sources are as follows. (*b*) *filled circles*, Bensby et al. (2004b); (*c*) *open circles*: Wyse & Gilmore (1995); and (*d*) *four-pointed stars*: Prochaska et al. (2000); *filled and open triangles*: dissipative and accretion components, respectively, in Gratton et al. (2003); *asterisks*: thick disk stars in Bensby et al. (2004a).

chemical enrichment should be shorter, i.e., $t_w = 2$ Gyr, in order to meet the MDF.) The resulting MDF is shifted to higher metallicity and the number of metal-poor stars with [Fe/H] $\lesssim -1$ is as small as in the observation by Ramírez et al. (2000). In these bulge models, the chemical enrichment timescale is so short that [Fe/H] reaches -1.1 at $t \sim 0.4$ Gyr, and no difference is realized for the cases with and without the SN Ia metallicity effect.

4.3. *Thick Disk*

Several formation scenarios of the Galactic thick disk have been debated for the following observational features: (1) the lack of vertical gradients of metallicity, (2) the existence of SN Ia contribution, (3) the larger [α/Fe] than in thin disk stars, (4) the older age than the thin disk, and (5) the lack of very metal-poor G-dwarfs (e.g., Gilmore et al. 1995; Feltzing 2004).

Here, we construct several models for the thick disk as well as the Galactic halo and bulge. Although we use the one-zone model, we do not assume that the thick disk is formed monolithically, and violent heating and satellite accretion scenarios are not excluded. Because of the lack of very metal-rich and very young stars in thick disk, we assume that star formation is truncated at $t = t_w$ (Fig. 31*a*). With these SFRs, the available MDF can be reproduced (Fig. 31*c*). However, the age-metallicity (Fig. 31*b*) and [O/Fe]-[Fe/H] (Fig. 31*d*) relations obtained from these models are different, with which we can put a constraint on the star formation history as follows.

Model A.—If the thick disk is formed as well as the thin disk, we can adopt the same SFR as the solar neighborhood model in §3.1, but with the cutoff at 6 Gyr (Fig. 31, *dotted line*). It is assumed that the stars formed in the solar neighborhood model at $t > 6$ Gyr and $t \leq 6$ correspond to the thin and thick disk stars, respectively. In this scenario chemical enrichment takes place slowly in infalling materials. Our model A predicts that the relations of the age-metallicity and [α/Fe]-[Fe/H] are the same as in the thin disk, which seems to be inconsistent with the available observations.

Model B.—The closed-box model (Fig. 31, *dashed line*) is not viable because of the G-dwarf problem, i.e., the lack of very metal-poor stars in the MDF. In our model B the peak metallicity of the observed MDF requires such a short timescale of star formation as 0.5 Gyr, which results in the strong initial starburst, a rapid increase of [Fe/H], and much larger [α/Fe] at [Fe/H] $\gtrsim -1$.

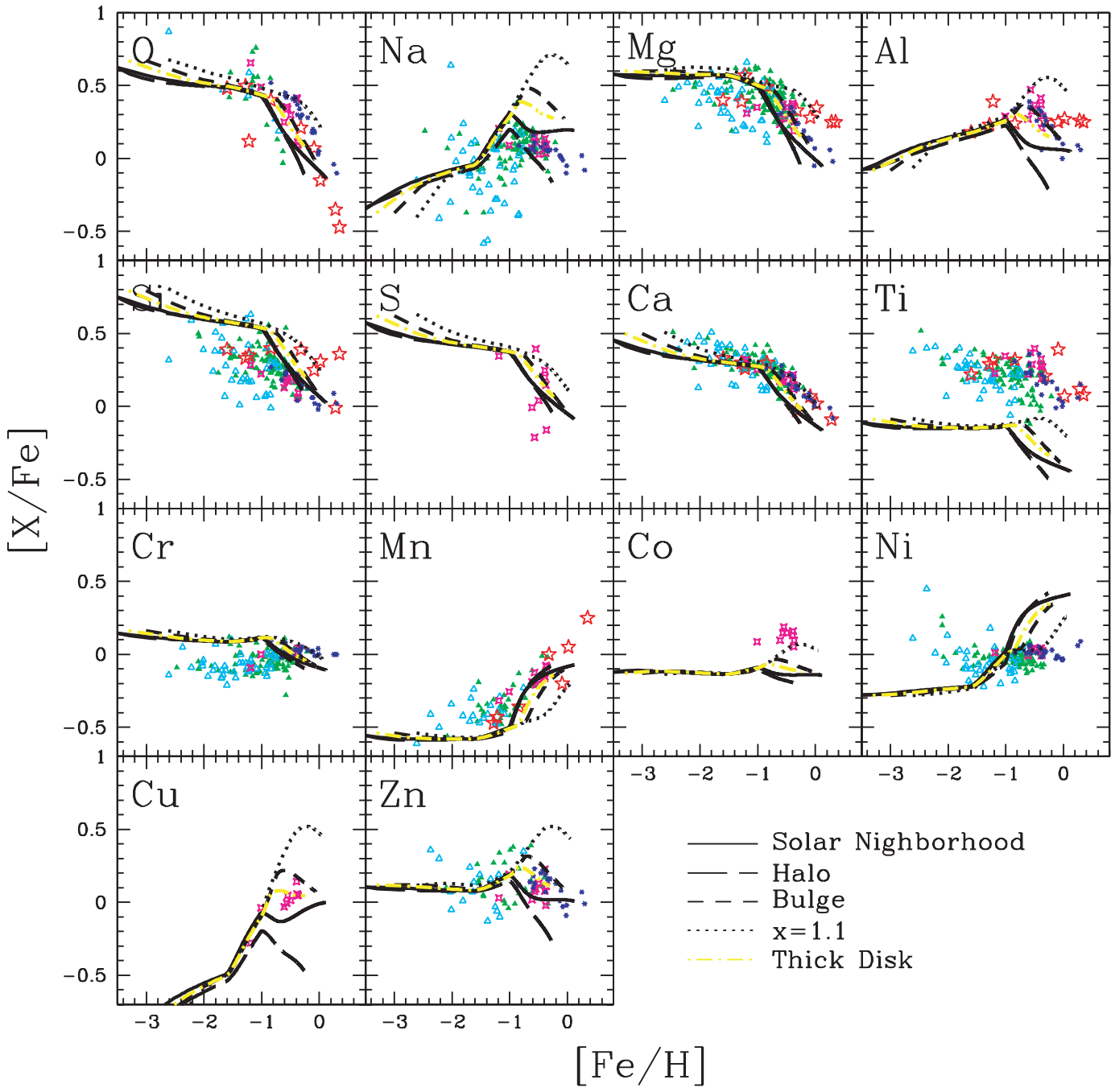

FIG. 32.—[X/Fe]-[Fe/H] relations for the disk (*solid line*), halo (*long-dashed line*), and bulge (*short-dashed line*), bulge with a flatter IMF (*dotted line*), and thick disk (*dot-dashed line*) models. Here, we take the solar neighborhood model (solid line in Fig. 6) for the disk, the outflow model for the halo (solid line in Fig. 29), the bulge models with the Salpeter IMF (solid line in Fig. 30) and the flat IMF (dotted line in Fig. 30), and the infall model for the thick disk (dotted line in Fig. 31). Observational data sources are as follows. For thick disk stars, *four-pointed stars*: Prochaska et al. (2000); *filled and open triangles*: dissipative and accretion components, respectively, in Gratton et al. (2003); *small asterisks*: Bensby et al. (2004a). Large stars are bulge stars from McWilliam & Rich (2004).

Model C.—The infall model with short star formation timescale (Fig. 31, *solid line*) can meet the observed MDF, and still give larger $[\alpha/\mathrm{Fe}]$ at $[\mathrm{Fe/H}] \gtrsim -1$ than the thin disk model, which is as large as in Prochaska et al. (2000). This scenario may be quite possible. Our model C predicts that the age-metallicity relation is different from the thin disk, as shown in Bensby et al. (2004b), and that the duration of star formation is as short as ~3 Gyr.

4.4. *Discussion*

In Figure 32 we compare the [X/Fe]-[Fe/H] relations for the Galactic disk (*solid line*), halo (*long-dashed line*), bulge (*short-dashed line*), bulge with a flat IMF (*dotted line*), and thick disk models (*dot-dashed line*). Observational data of thick disk stars are shown (Prochaska et al. 2000; Bensby et al. 2003; Gratton et al. 2003), except for the large stars are for bulge stars (McWilliam & Rich 2004). Here, we take the solar neighborhood model (Fig. 6, *solid line*) for the disk, the outflow model for the halo (Fig. 29, *solid line*), the bulge models B with the Salpeter IMF (Fig. 30, *solid line*) and the flat IMF (Fig. 30, *dotted line*), and the infall model C for the thick disk (Fig. 31, *solid line*). We note that these models are constructed based on the observations of the limited regions (solar neighborhood and Baade's window), and the radial dependencies

on star formation and chemical enrichment histories are neglected. Since in all models the same stellar yields are adopted and the initial metallicity is set to be primordial, differences among model predictions are due to differences in the SFR, the IMF, and the SN Ia contribution.

Since the metallicity effect on SNe Ia is included for all models, all models give similar results at $[\mathrm{Fe/H}] \lesssim -1$, where SNe Ia do not contribute. The plateau values of $[\alpha/\mathrm{Fe}]$ at $-2 \lesssim [\mathrm{Fe/H}] \lesssim -1$ depend on the IMF, because $[\alpha/\mathrm{Fe}]$ is larger for larger stellar mass. The flat IMF model gives 0.1 dex larger $[\alpha/\mathrm{Fe}]$ than the Salpeter IMF. The increasing trends of $[\alpha/\mathrm{Fe}]$ and decreasing trends of $[(\mathrm{Na, Al, Cu})/\mathrm{Fe}]$ toward lower metallicity are, respectively, originated from the mass and metallicity dependences. The slope of these trends depends on the SFRs, namely, the chemical enrichment timescale, which is short in our bulge models. Therefore, the slope is steep in our bulge models.

From $[\mathrm{Fe/H}] \sim -1$, $[\alpha/\mathrm{Fe}]$ decreases because of the SN Ia contribution. While the decreasing point of $[\alpha/\mathrm{Fe}]$ is simply determined by the SN Ia metallicity effect in the disk and halo, but it is determined by the SN Ia lifetime in the bulge where the chemical enrichment timescale is short enough. In such systems as bulge, we can safely discuss the formation timescale from the $[\alpha/\mathrm{Fe}]$ decreasing point. For faster chemical enrichment, $[\alpha/\mathrm{Fe}]$ starts decreasing at larger [Fe/H]. In our bulge model with Salpeter IMF, $[\alpha/\mathrm{Fe}]$ decreases from $[\mathrm{Fe/H}] \sim -0.7$, while it decreases from $[\mathrm{Fe/H}] \sim -0.4$ with the flat IMF model.

Among α-elements, McWilliam & Rich (2004) showed different trends for the bulge (Fig. 32, *stars*). The observed O trend is well reproduced with the Salpeter IMF model, while the flat IMF model is favored from the constant Mg/Fe. As noted before, it is difficult to explain the different evolution of O and Mg with our models. Some uninvolved physics such as strong stellar winds might be important. For Si, observational data show a large scatter and is consistent with both models. S and Ca can be produced also by SNe Ia to some extent, and thus, the observed Ca trend is consistent with both models.

At the same [Fe/H], iron-peak abundance ratios also change, and the [Mn/Fe] ratio increases quickly, because more Mn is produced by SNe Ia than Fe, relative to the solar abundance (i.e., $[\mathrm{Mn/Fe}] > 0$). The odd-Z abundance ratios $[(\mathrm{Al, Na, Cu})/\mathrm{Fe}]$ increase to be supersolar with a peak at $[\mathrm{Fe/H}] \sim -0.4$ because of the yield metallicity dependence and the SNe Ia contribution. [Zn/Fe] may put a constraint on the IMF, because Zn yield depends strongly on the mass and Zn is mainly produced from HNe and metal-rich massive SNe. With the flat IMF model, larger enhancement of [Zn/Fe] is predicted at $[\mathrm{Fe/H}] \gtrsim -1$ than with the Salpeter IMF. This does not depend on our assumption of the constant hypernova efficiency ϵ_{HN}, because massive SNe produce Zn as much as HNe at $Z \geq 0.004$.

The formation timescale of the system can be constrained from the elemental abundance ratios and the metallicity distribution function. However, since observational results are still controversial, we summarize our predictions focusing on a part of the observational results. If there is not many supersolar metal stars in the bulge like the Zoccali et al. (2003) MDF, star formation should be somehow truncated, and the duration of star formation should be $\sim$3 Gyr. Even if no such truncation is included, the star formation timescale should be as short as $\sim$1 Gyr, and most stars should be as old as $\sim$10 Gyr. On the other hand, the decrease in $[(\mathrm{O, Ca})/\mathrm{Fe}]$ and the increase in [Mn/Fe] by SNe Ia require that star formation continues longer than $\sim$1 Gyr. The flat $[(\mathrm{Mg, Si})/\mathrm{Fe}]$ may suggest that the IMF is flatter than the Salpeter IMF and that the chemical enrichment timescale is much shorter. In this case, the duration of star formation should be shorter ($\sim$2 Gyr) than the Salpeter IMF case, in order to reproduce the same MDF. It is important to confirm the different trends of O and Mg with large sample, and Zn observation is also interesting.

For thick disk stars, similar observational features are seen. Prochaska et al. (2000) showed the abundance patterns of thick disk stars (Fig. 32, *four-pointed stars*). They found that $[(\mathrm{O, Si, Ca})/\mathrm{Fe}]$ decrease with increasing [Fe/H], while $[(\mathrm{Mg, Ti})/\mathrm{Fe}]$ are constant, which are similar to the bulge stars except for Si. Bensby et al. (2004a) also showed that the abundance patterns of the thin (*circles*) and thick (*asterisks*) disk are different, and $[(\mathrm{O, Mg, Al})/\mathrm{Fe}]$ and [Zn/Fe] of the thick disk are larger than those of the thin disk. In the thick disk models, constructed to meet the narrow MDF by Wyse & Gilmore (1995), star formation and chemical enrichment take place slightly slower than in our bulge model. The resulting [X/Fe]-[Fe/H] relations are similar to those of the bulge model but with a slightly earlier decrease of $[\alpha/\mathrm{Fe}]$ from $[\mathrm{Fe/H}] \sim -0.8$, which is roughly consistent with observations (small points except for large stars). Therefore, we would conclude that the thick disk is as old as the bulge, and the formation timescale is as short as $\sim$1–3 Gyr.

5. CONCLUSIONS

We calculate the evolution of heavy-element abundances from C to Zn in the solar neighborhood, adopting our new nucleosynthesis yields. Our new yields are based on the new developments in the observational/theoretical studies of supernovae and extremely metal-poor stars in the Galactic halo. We use the light-curve and spectra fitting of individual supernova to estimate the mass of the progenitor, explosion energy, and produced ^{56}Ni mass.

The elemental abundance ratios are in good agreement with observations. Figure 33 provides a summary of our new yield table set. The solid and long-dashed lines show the abundance patterns in our chemical evolution model for the solar neighborhood at $[\mathrm{Fe/H}] = 0$ and -1.1, respectively, which should correspond to the solar abundance $[\mathrm{X/Fe}] = 0$ and the IMF-weighted SN II yield without a SN Ia contribution, respectively. The metallicity and energy dependencies of the yields are demonstrated by the short-dashed and dotted lines, which show the IMF-weighted yield with $Z = 0$ and the HN yield with $M = 20\ M_{\odot}$, $E_{51} = 10$, $Z = 0$, respectively.

1. The solar abundance (i.e., $[\mathrm{X/Fe}] = 0$) is basically well reproduced with our chemical evolution model at $[\mathrm{Fe/H}] = 0$ (Fig. 33, *solid line*). Some of the discrepancies between our model and observations may be explained as follows.(i) The underabundances of C and N may suggest that AGB stars and Wolf-Rayet star winds are the dominant sources of these elements. (ii) F, K, Sc, Ti, and V are underabundant, which cannot be increased by changing our parameters such as metallicity and energy. A jetlike explosion (Maeda & Nomoto 2003) can efficiently increase Ti and Zn abundances, and a low-density model (UN05) or neutrino process (Fröhlich et al. 2006; Wanajo 2006; T. Yoshida et al. 2006, in preparation) may increase Sc abundance. (iii) Ni overproduction by SNe Ia can be reduced (Iwamoto et al. 1999).

2. The observed plateau values at $-1.5 \lesssim [\mathrm{Fe/H}] \lesssim -1$ (Fig. 33, *dots*; Sneden et al. 1991; Melendez & Barbuy 2002; Gratton et al. 2003) are in good agreement with our model at $[\mathrm{Fe/H}] = -1.1$ (*long-dashed line*), where SNe Ia do not contribute. Only Ti, Sc and V are underabundant by 0.4, 0.6, and 0.2 dex, respectively, relative to Fe.

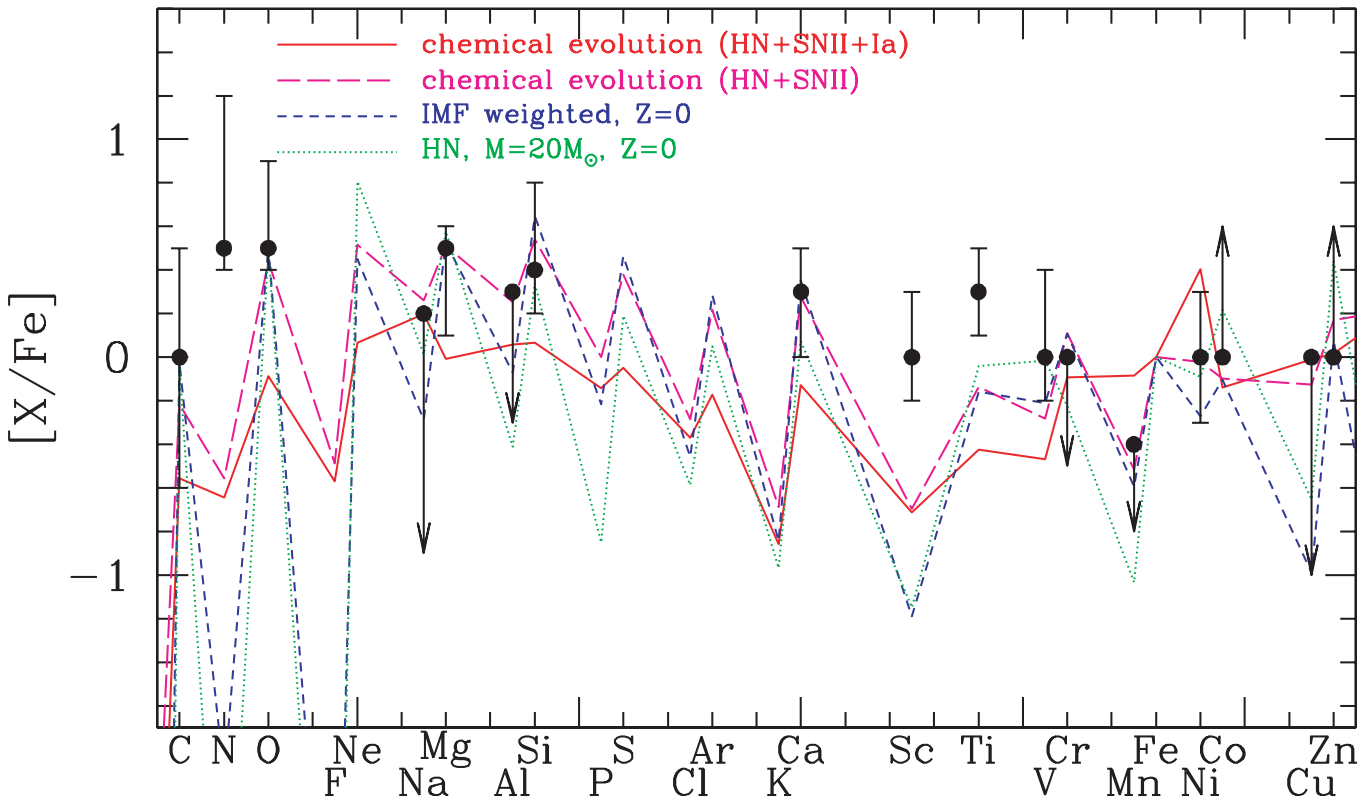

FIG. 33.—Solid and long-dashed lines show the abundance patterns with our chemical evolution model at [Fe/H] = 0 and −1.1, respectively, which correspond to the solar abundance [X/Fe] = 0 and the IMF-weighted SN II yield without a SN Ia contribution, respectively. The dots, error bars, and arrows show the observations for the plateau value at $-1.5 \lesssim$ [Fe/H] $\lesssim -1$ (Sneden et al. 1991; Melendez & Barbuy 2002; Gratton et al. 2003), the scatter at $-3.5 \lesssim$ [Fe/H] $\lesssim -2.5$, and the trend toward [Fe/H] ~ -4 (McWilliam et al. 1995; Ryan et al. 1996; Cayrel et al. 2004; Honda et al. 2004), respectively. The short-dashed and dotted lines show the IMF-weighted yield with $Z = 0$ and the HN yield with $M = 20\ M_\odot$, $E_{51} = 10, Z = 0$, respectively.

3. The observed scatter at $-3.5 \lesssim$ [Fe/H] $\lesssim -2.5$ (Fig. 33, *error bars*) and the observed trends toward [Fe/H] ~ -4 (*arrows*; McWilliam et al. 1995; Ryan et al. 1996; Cayrel et al. 2004; Honda et al. 2004) may be due to *inhomogeneous* enrichment and could be explained with the variations of the properties of individual supernovae, such as energy and metallicity (UN05).

4. The metallicity effect is seen in our IMF-weighted yield of metal-free stars (Fig. 33, *short-dashed line*), where the abundance ratios of the odd-Z elements [(Na, Al, Mn, Cu, . . .)/Fe] are smaller than those of the even-Z elements by ∼0.6 dex. The observed trends (*arrows*) are well reproduced with this metallicity effect in our chemical evolution model.

5. The energy effect is seen in our HN yield for $M = 20\ M_\odot$, $E_{51} = 10$, and $Z = 0$ (Fig. 33, *dotted line*), where the abundance ratios of iron-peak elements [(Cr, Mn, Co, Zn)/Fe] are different from normal SNe II. The observed trends (*arrows*) could be explained with the variation of the explosion energy of individual supernovae.

6. O, Mg, Si, S, Ca, and Ti depend on the mass of the progenitor star and is larger for massive SNe II. For HNe, however, because the iron yield is as large as the yields of α-elements, [α/Fe] is almost constant. This may account for the observed small scatter of [α/Fe] in the solar neighborhood, being independent of the mixing process of interstellar medium. The small [α/Fe] (O, Mg, Si, S, Ca, and Ti) in some anomalous stars is due to 1) SNe Ia, 2) relatively large Fe production from low-mass SNe II with $M = 13$–$15\ M_\odot$, 3) large Fe production from HNe, or 4) the SN I.5 explosion of some AGB stars (see §3.2). The large [α/Fe] is due to 1) small Fe production from SNe II with $E_{51} \leq 1$ or 2) large fallback mass for HNe. From Zn and iron-peak elements, we can distinguish the enrichment source of such stars; HNe produce large [(Zn, Co)/Fe], and SNe Ia and I.5 produce relatively large [Mn/Fe].

This work has been supported in part by the grants-in-aid for Scientific Research (17030005, 17033002, 18104003, and 18540231) and the 21st Century COE Program (QUEST) from the Japan Society for the Promotion of Science (JSPS) and the Ministry of Education, Culture, Sports, Science, and Technology (MEXT) of Japan. C. K., N. T., and T. O. thank the JSPS for a financial support. We would also like to thank K. Maeda and M. Shirouzu for fruitful discussions.

REFERENCES

Anders, E., & Grevesse, N. 1989, Geochim. Cosmochim. Acta, 53, 197
Aoki, W., Norris, J. E., Ryan, S. G., Beers, T. C., Christlieb, N., Tsangarides, S., & Ando, H. 2004, ApJ, 608, 971
Arnett, W. D. 1996, Supernovae and Nucleosynthesis (Princeton: Princeton Univ. Press)
Asplund, M. 2005, ARA&A, 43, 481
Audouse, J., & Silk, J. 1995, ApJ, 451, L49
Beers, T., & Christlieb, N. 2005, ARA&A, 43, 531
Bensby, T., Feltzing, S., & Lundström, I. 2003, A&A, 410, 527
———. 2004a, A&A, 415, 155
———. 2004b, A&A, 421, 969
Boesgaard, A. M., King, J. R., Deliyannis, C. P., & Vogt, S. S. 1999, AJ, 117, 492
Carretta, E., Gratton, R. G., & Sneden, C. 2000, A&A, 356, 238

Caughlan, G. R., & Fowler, W. A. 1988, At. Data & Nucl. Data Tables, 40, 283
Cayrel, R., et al. 2004, A&A, 416, 1117 (C04)
Chen, Y. Q., Nissen, P. E., Zhao, G., & Asplund, M. 2002, A&A, 390, 225
Chiappini, C., Matteuci, F., & Gratton, R. G. 1997, ApJ, 477, 765
Chiba, M., & Yoshii, Y. 1998, AJ, 115, 168
Ciardi, B., Ferrara, A., & White, S. D. M. 2003, MNRAS, 344, L7
Colella, P., & Woodward, P. R. 1984, J. Comput. Phys., 54, 174
de Jager, C., Nieuwenhuijzen, H., & van der Hucht, K. A. 1988, A&AS, 72, 259
Edvardsson, B., Andersen, J., Gustafsson, B., Lambert, D. L., Nissen, P. E., & Tomkin, J. 1993, A&A, 275, 101
Feltzing, S. 2004, in Chemical Abundances and Mixing in Stars in the Milky Way and Its Satelites, ed. S. Randlich & L. Pasquini (Berlin: Springer)
Feltzing, S., & Gustafsson, B. 1998, BAAS, 129, 237
Fenner, Y., & Gibson, B. K. 2003, Publ. Astron. Soc. Australia, 20, 189
Filippenko, A. V. 1997, ARA&A, 35, 309
Fowler, W. A. 1984, Rev. Mod. Phys., 56, 149
Frebel, A., et al. 2005, Nature, 434, 871
Fröhlich, C., Martínez-Pinedo, G., Liebendörfer, M., Thielemann, F.-K., Bravo, E., Hix, W. R., Langanke, K., & Zinner, N. T. 2006, Phys. Rev. Lett., 96, 142502
Galama, T. J., et al. 1998, Nature, 395, 670
Gilmore, G. Wyse, R. F. G., & Jones, J. B. 1995, AJ, 109, 1095
Gratton, R. G. 1989, A&A, 208, 171
Gratton, R. G., & Sneden, C. 1991, A&A, 241, 501
Gratton, R. G., et al. 2003, A&A, 404, 187
Hachisu, I., Kato, M., & Nomoto, K. 1996, ApJ, 470, L97
———. 1999a, ApJ, 522, 487
Hachisu, I., Kato, M., Nomoto, K., & Umeda, H. 1999b, ApJ, 519, 314
Hix, W. R., & Thielemann, F.-K. 1996, ApJ, 460, 869
Honda, S., et al. 2004, ApJ, 607, 474
Ibata, R. A., & Gilmore, G. F. 1995, MNRAS, 275, 605
Israelian, G., García-López, R. J., & Rebolo, R. 1998, ApJ, 507, 805
Israelian, G., & Reboro, R. 2001, ApJ, 557, L43
Israelian, G., Reboro, R., Garcia-Lopez, R. J., Bonifacio, P., Molaro, P., Basri, G., & Shchukina, N. 2001, ApJ, 551, 833
Iwamoto, K., Brachwitz, F., Nomoto, K., Kishimoto, N., Umeda, H., Hix, W. R., & Thielemann, F.-K. 1999, ApJS, 125, 439
Iwamoto, N., Umeda, H., Tominaga, N., Nomoto, K., & Maeda, K. 2005, Science, 309, 451
Iwamoto, K., et al. 1998, Nature, 395, 672
Janka, H.-Th., Buras, R., & Rampp, M. 2003, Nucl. Phys. A, 718, 269
Kobayashi, C., Tsujimoto, T., & Nomoto, K. 2000, ApJ, 539, 26 (K00)
Kobayashi, C., Tsujimoto, T., Nomoto, K., Hachisu, I., & Kato, M. 1998, ApJ, 503, L155 (K98)
Kodama, T., & Arimoto, N. 1997, A&A, 320, 41
Kudritzki, R. P., Pauldrach, A., Puls, J., & Abbott, D. C. 1989, A&A, 219, 205
Laird, J. B., Rupen, M. P., Carney, B. W., & Latham, D. W. 1988, AJ, 96, 1908
Liebendörfer, M., Mezzacappa, A., Messer, O. E. B., Martinez-Pinedo, G., Hix, W. R., & Thielemann, F.-K. 2003, Nucl. Phys. A, 719, 144
Limongi, M., & Chieffi, A. 2003, ApJ, 592, 404
Limongi, M., Chieffi, A., & Bonifacio, P. 2003, ApJ, 594, L123
Maeda, K., & Nomoto, K. 2003, ApJ, 598, 1163
Matteucci, F. 1997, ASP Conf. Ser. 126, From Quantum Fluctuations to Cosmological Structures, ed. D. Valls-Gabaud et al. (San Francisco: ASP), 495
———. 2001, The Chemical Evolution of the Galaxy (Dordrecht: Kluwer)
Matteucci, F., & Brocato, E. 1990, ApJ, 365, 539
Matteucci, F., & Recchi, S. 2001, ApJ, 558, 351
McWilliam, A., Preston, G. W., Sneden, C., & Searle, L. 1995, AJ, 109, 2757
McWilliam, A., & Rich, R. M. 1994, ApJS, 91, 749
———. 2004, in Origin of Evolution of the Elements, ed. A. McWilliam & M. Rauch (Pasadena: Carnegie Obs.), http://www.ociw.edu/ociw/symposia/series/symposium4/proceedings.html
Melendez, J., & Barbuy, B. 2002, ApJ, 575, 474
Nakamura, T., Umeda, H., Nomoto, K., Thielemann, F.-K., & Burrows, A. 1999, ApJ, 517, 193
Nissen, P. E., Chen, Y. Q., Asplund, M., & Pettini, M 2004, A&A, 415, 993
Nissen, P. E., Primas, F., Asplund, M., & Lambert, D. L. 2002, A&A, 390, 235
Nissen, P. E., & Schuster, W. J. 1997, A&A, 326, 751
Nomoto, K., & Hashimoto, M. 1988, Phys. Rep., 163, 13
Nomoto, K., Maeda, K., Mazzali, P., Umeda, H., Deng, J., & Iwamoto, K. 2004, in Stellar Collapse, ed. C. L. Fryer (Dordrecht; Kluwer), 277
Nomoto, K., Thielemann, F.-K., & Yokoi, K. 1984, ApJ, 286, 644
Nomoto, K., Tominaga, N., Umeda, H., Kobayashi, C, & Maeda, K. 2006, Nucl. Phys. A, 777, 424
Nomoto, K., Uenishi, T., Kobayashi, C., Umeda, H., Ohkubo, T., Hachisu, I., & Kato, M. 2003, in From Twilight to Highlight: The Physics of Supernovae, ed. W. Hillebrandt & B. Leibundgut (Berlin: Springer), 115
Nomoto, K., Yamaoka, H., Shigeyama, T., Kumagai, S., & Tsujimoto, T. 1994, in Supernovae, ed. S. A. Bludman et al. (Amsterdam: North Holland), 199
Nomoto, K., et al. 1997a, Nucl. Phys. A, 616, 79 (N97)
———. 1997b, Nucl. Phys. A, 621, 467
Nordström, B., et al. 2004, A&A, 418, 989
Ohkubo, T., Umeda, H., Maeda, K., Nomoto, K., Suzuki, T., Tsuruta, S., & Rees, M. J. 2006, ApJ, 645, 1352
Pagel, B. E. J. 1989, Rev. Mex. AA, 18, 161
———. 1997, Nucleosynthesis and Chemical Evolution of Galaxies (Cambridge: Cambridge Unv. Press)
Prantzos, N., Vangioni-Flam, E., & Chauveau, S. 1994, A&A, 285, 132
Primas, F., Reimers, D., Wisotzki, L., Reetz, J., Gehren, T., & Beers, T. C. 2000, in The First Stars, ed. A. Weiss, T. Abel, & V. Hill (Berlin: Springer), 51
Prochaska, J., Naumov, S. O., Carney, B. W., McWilliam, A., & Wolfe, A. M. 2000, AJ, 120, 2513
Ramírez, S. V., Stephens, A. W., Frogel, J. A., & DePoy, D. L. 2000, AJ, 120, 833
Ryan, S. G., Norris, J. E., & Beers, T. C. 1996, ApJ, 471, 254
Sadler, E. M., Rich, R. M., & Terndrup, D. M. 1996, AJ, 112, 171
Salaris, M., & Weiss, A. 2002, A&A, 388, 492
Sneden, C., Gratton, R. G., & Crocker, D. A. 1991, A&A, 246, 354
Spruit, H. C. 1992, A&A, 253, 131
Suda, T., Aikawa, M., Machida, M. N., Fujimoto, M. Y., & Iben, I., Jr. 2004, ApJ, 611, 476
Takada-Hidai, M., et al. 2002, ApJ, 573, 614
———. 2005, PASJ, 57, 347
Thomas, D., Maraston, C., & Bender, R. 2003, MNRAS, 343, 279
Tinsley, B. M. 1980, Fundam. Cosm. Phys., 5, 287
Tolstoy, E., Venn, K. A., Shetrone, M., Primas, F., Hill, V., Kaufer, A., & Szeifert, T. 2003, AJ, 125, 707
Tominaga, N., Umeda, H., & Nomoto, K. 2006, ApJ, submitted
Travaglio, C., Gallino, R., Arnone, E., Cowan, J., Jordan, F., & Sneden, C. 2004, ApJ, 601, 864
Tsujimoto, T. 2006, A&A, 447, 81
Tsujimoto, T., & Shigeyama, T. 2003, ApJ, 584, L87
Turatto, M., et al. 1998, ApJ, 498, L129
Tutukov, A. V., & Yungelson, L. R. 1994, MNRAS, 268, 871
Umeda, H., & Nomoto, K. 2002, ApJ, 565, 385
———. 2003, Nature, 422, 871 (UN03)
———. 2005, ApJ, 619, 427 (UN05)
Umeda, H., Nomoto, K., & Nakamura, T. 2000, in The First Stars, ed. A. Weiss, T. Abel, & V. Hill (Berlin: Springer), 150
Umeda, H., Nomoto, K., Yamaoka, H., & Wanajo, S. 1999, ApJ, 513, 861
Wanajo, S. 2006, ApJ, 647, 1323
Woosley, S. E., & Weaver, T. A. 1995, ApJS, 101, 181
Wyse, R. F. G., & Gilmore, G. 1995, AJ, 110, 2771
Yoshii, Y., Tsujimoto, T., & Nomoto, K. 1996, ApJ, 462, 266
Zinn, R. 1985, ApJ, 293, 424
Zoccali, M., et al. 2003, A&A, 399, 931